Alma Mater Studiorum – Università di Bologna

DOTTORATO DI RICERCA IN
Scienze Chimiche

Ciclo XXV

Settore Concorsuale di afferenza: **03/B1**
Settore Scientifico disciplinare: **CHIM/03**

MULTICOMPONENT NANODEVICES BASED ON MOLECULAR AND NANOCRYSTAL MOIETIES

Presentata da: **Tommaso Avellini**

Coordinatore Dottorato
Prof. Adriana Bigi

Relatore
Prof. Margherita Venturi

Esame finale anno 2013

"Science that abdicates its cultural values risks being perceived as an extension of technology, an instrument in the hands of political or economic power.

Humanity that disavows science risks falling into the hands of superstition."

Nicola Cabibbo

Contents

Overview

Nanoscience is an emerging and fast-growing field of science with the aim of manipulating nanometric objects with dimension below of 100 nm. Top down approach is currently used to build these type of architectures (e.g microchips). Photolithography is the principal technique employed in the construction of microchips bearing submicron-scale and nano-scale transistor. The miniaturization process cannot proceed indefinitely due to physical and technical limitations. Those limits are focusing the interest on the bottom-up approach and construction of nano-objects starting from "nano-bricks" like atoms, molecules or nanocrystals. Unlike atoms, molecules can be "fully programmable" and represent the best choice to build up nanostructures. In the past twenty years many examples of functional nano-devices able to perform simple action have been reported. Nanocrystals which are often considered simply nanostructured materials, can be active part in the development of those nano-devices, in combination with functional molecules.

The object of this dissertation is the photophysical and photochemical investigation of nano-objects bearing molecules and semiconductor nanocrystals as components.

The thesis is divided in four parts. *Part I (***Chapter 1**) introduces the basic concepts of nanotechnology focusing on the main limitations of traditional top-down approach for the construction of nano-scale objects. Bottom-up approach and supramolecular chemistry are shown as effective tools for the design of nanometer-scale devices. Concepts related to supramolecular chemistry and artificial machines are reported in the first part, while the second part concerns basic concepts on nanostructured materials and luminescence semiconductor nanocrystals and strategy for their surface functionalization.

Part II (**Chapter 2**) illustrates the techniques used to characterize and investigate the systems reported in this thesis. In this chapter are also reported the methodology for semiconductor nanocrystals synthesis.

Part III (**Chapter 3**) focuses on the characterization of a bistable rotaxane. This study, in collaboration with the group of Prof. J.F. Stoddart (Northwestern

University, Evanston, Illinois, USA) who made the synthesis of the compounds, shows the ability of this artificial machine to operate as bistable molecular-level memory under kinetic control.

Part IV (**Chapter 4-5**) describes the works related to the luminescence semiconductor nanocrystals. In particular, I focused the study on their surface properties.

In **Chapter 4** is reported the study on the effect of acid and base on *core* CdSe and *core-shell* CdSe-ZnS quantum dots. Spectroscopical and TEM investigations suggest that depletion of organic shell layer followed by aggregation of those nanocrystals might occur.

Chapter 5 illustrates the work carried out in the laboratory of Prof H. Mattoussi (Florida State University, Tallahassee, Florida, USA). In this period I worked on the surface functionalization of nanoparticles for biological applications, developing a novel method for the surface decoration with lipoic acid - based ligands involving the photoreduction of the di-thiolane moiety.

Chapter 1

Introduction

1.1 Nanotechnology

Nanotechnology can be defined as the ability to fabricate structures consisting of individual atoms, molecules and macromolecular building blocks in the nanometric size range (1-100nm).[1] This length definition is not mandatory and many objects with dimension of few hundred nanometers are often considered nano-object.[2] More generally nanotechnology is focusing on the utilization, manipulation and organization of nanoscale objects in order to perform specific functions.[3] Since its nature of multidisciplinary subject, nanotechnology can mean different things to different people that work in different field of science (e.g. chemistry, physics, engineer, biotechnology). Engineers define nanotechnology as toolbox providing nanometric-size building blocks, others say that is all about building things and others consider nanotechnology as a kind of revolution in the physical science. The common and focal point is probably the atomistic understanding and control that enable systematic development of complex nanosystems (e.g. nanoparticles for drug delivery)[4].

The birth of nanotechnology is commonly attributed to Richard Feynman and his famous speech "There's a plenty of the room at the bottom".[5,6] In 1959 at CalTech he hypothesized the possibility to build and manipulate nanodevices with atomic precision. More specifically Feynman speech concerned the possibility to write an enormous quantities of information in a reduced space (in 1/25000 inch square) or to build nano-machines able to mimic macroscopic devices. He was aware that in the nanometric size region all the characteristics of such devices are different respect to those of macroscopic devices. The fuel for those machines is coming from different chemical reactions and forces that are fundamentals in the macroscopic world (e.g. gravity and inertial force) became less important due to the reduced mass of the molecules.

The construction of micro-nano scale objects can be pursued following two types of approaches [3,7–10]

- *Top-down approach*, consisting in the miniaturization of macrostructures or materials until the achievement of the micro-structure.
- *Bottom-up approach*, consisting in the building of a nano or micro-structures using nano-object as fundamental bricks.

The miniaturization of the components for the construction of useful devices is usually achieved using the first approach, especially in the field of integrated electronic and personal computer. Evolution of calculating machines and personal computer is a good example of miniaturization and top-down approach.[11]

The first freely programmable computer was the Z3, invented by Konrad Zuse in 1941. This machine used 2600 telephone relays as functional units.[12] Few years later Americans developed ENIAC, the first electronic general-purpose computer. This computer combined the speed of the electronics with the ability to be programmed for many complex problems. The machines contained 18,000 vacuum tubes for a total weight of 30 tons. The major engineering problem was the avoiding of tubes burn-out.[13] The introduction of transistor instead vacuum tube enabled the construction of smaller machines and in 1970 Intel introduces the first microprocessor (Intel 4004). This microprocessor had in a single device (2,300 transistor) a computing power similar to ENIAC.[14,15] Modern personal computer has a microprocessor with billion of transistors in few centimeter square of surface. For example microprocessor *Intel core i7* has

2.27 billion of transistors in 434 square millimeter and an half pitch of 22 nm. In Table 1.1 are reported the principal characteristics for the four type of computer reported above.

Year	1941	1944	1970	2010
Model	Z3	ENIAC	Intel 4004	Intel Core i7
Functional units	Relays	Vacuum tubes	Transistors	Transistors
Number of units	2,600	18,000	2,300	2,700,000,000
Clock rate	5-10Hz	5kHz	740kHz	2.27 GHz

Table1.1: Evolution of the characteristics of four type of calculating machines

Modern microprocessors are usually built using lithography techniques.[16–18] Photolithography is used to pattern chips shining UV light trough a mask. The mask bears slits arranged in the motif that has to be reproduced on the chip. Lenses below the stencil reduce the patter to one-quarter of its original size and then project the picture on a silicon wafer coated with a polymer called photoresist. Chemicals are used to removed the polymer exposed or not to UV light in order to obtain a positive or a negative imagine of the mask on the silicon wafer. Silicon part of the wafer are carved and the spaces filled with metals, insulators or semiconductor in order to make transistors.[16] In general the shorter the wavelength of the light used, the smaller the features that can be transferred on the silicon wafer. Physical limits of this technique do not allow the construction of nanostructured materials below a certain value. This is due to the Abbe's principle[1] which states that the resolution of an optical instruments is $\lambda/2$ where λ is the wavelength used. If in photolithography technique a 248 nm light is used, the maximum resolution is around 120 nm. Deep UV light can exploit but at some stages (below 157 nm) no materials are transparent and lenses must be replaced with reflactive mirrors with increasing cost. This poses a limitation to the use of photolithography, and *top-down* approach, for the construction of nanometric architectures.

Bottom-up approach is a promising strategy to build-up structures starting from nano or subnano objects (atoms or molecules)[3]. Chemists, that are able to manipulate atoms and molecules, are in the ideal position to contribute for the development of nanoscience and nanotechnology.

The simplest objects can be manipulated are the atoms. This small entity has no specific intrinsic function, which arise from ensembles of such objects. Punctual manipulation of atoms or very simple molecules can be performed using scanning microscopy techniques at low temperature and ultra-high vacuum[19] (e.g. AFM and STM). Atoms are extremely reactive and such reactivity cannot be "programmed".

Clusters or even better nanoparticles and nanocrystals have reduced reactivity that enables easy manipulation. The surface can be engineered with simple molecules to allow the formation of superlattice of bare or different nanoparticles.[20–22] These materials with new characteristics emerging at the nanoscale, not present in the parent bulk material, could find application in many field (e.g. catalysis[23]).

Molecules are much more useful and convenient building blocks than atoms, to construct nanoscale devices.[24] The main foundations of this idea are report below[25]:

- Molecules are stable species
- Nature starts from molecules and not from atoms to construct a variety of nanodevices
- Most laboratory processes are dealing with molecules
- Molecules exhibit proper shape and properties which can be manipulate using different inputs
- Molecules can be connected or self-assemble in order to make large structures

This last point reflects the basic principles of the *supramolecular chemistry*,[26] that will be explained in the next paragraph.

1.2 Supramolecular Chemistry

"Supramolecular chemistry may be defined as *chemistry beyond the molecule*, bearing on the organized entities of higher complexity that result from the association of two or more chemical species held together by intermolecular forces".[26] This is the most classical and most accepted definition of supramolecular chemistry reported by J.M. Lehn, Nobel Prize in Chemistry in 1987 with C.J. Pedersen and D.J. Cram "for their development and use of molecules with structure-specific interactions of high selectivity".[27]
Supramolecular chemistry shifts the interest from molecules to assemblies of molecules. If we follow literary the Lehn's definition, when moieties of a multicomponent system are linked together via covalent bond, it cannot be defined supramolecular system but molecule. This has to be taken into account when molecular-level devices and machines are composed of units held together with chemical bond of different nature. For example a pseudorotaxane[28] where the two components are linked together via non-covalent interaction, is a supramolecualr system, while a rotaxane in which the ring and axle component cannot be disassembled without breaking a covalent bond, should be called a molecule. This simple example shows that while the classical definition "*chemistry beyond the molecule"* is useful in general, in order to distinguish what is a molecule and what is a supramolecular system, a distinction based on the interaction between the components should be evaluate.[25]

The single component of a supramolecule has specific features or functions that are maintained in the multicomponent systems. In other terms, the molecular component remain discernible in the assembly. This concept can be better explained using, as an example, a system under photochemical stimulation consisting of two units **A~B** where **~** indicate the type of bond between **A** and **B**. (Figure 1.1). When light absorption causes excitation that is localized on either **A** or **B**, or an electron transfers from **A** to **B** (or viceversa), the multicomponent system can be defined a supramolecular system. Conversely, when the excitation energy is delocalized on the entire multicomponent system, the species is considered a large molecule. Similarly reduction and oxidation processes are localized on one of its units in a supramolecular systems, while is delocalized on the entire system in case of a large molecule

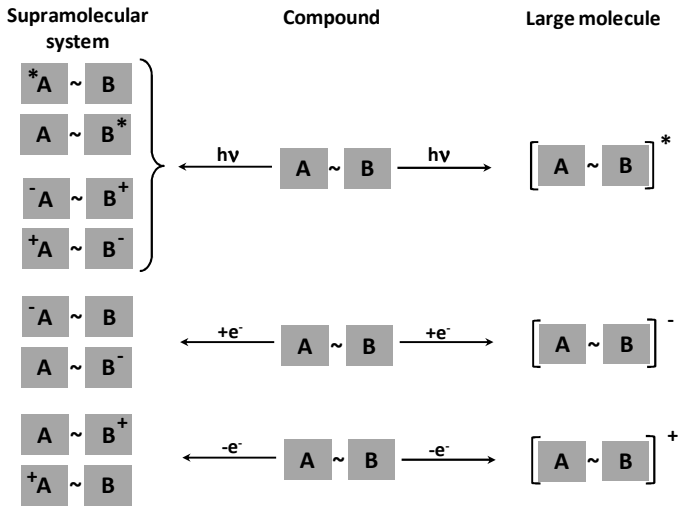

Figure 1.1 Differences between a supramolecular system and a large molecule based on the effect caused by light excitation and red-ox stimulation. Molecular components of a supramolecular system maintain their features in the assembly while the molecular components of large molecule lose their properties in the assembly.

The main concept that belongs to supramolecular chemistry is the *molecular recognition* defined as "the ability of a molecule to recognize and associate with another molecule based on the presence of complementary chemical functionalities".[25] The *molecular information* stored in the interacting species enables the *recognition*. The instructed components can recognized each other and *self-assemble*.

Self-assembly is a well-know concept in Nature. This concept originated with studies on tobacco mosaic virus and ribonuclease.[29]
Tobacco mosaic virus is composed of a single RNA string encased in a protein cylinder. This cylinder is formed of thousands identical protein monomers. Each components can be isolated by dissociation of the virus. The isolated compounds could re-forming the intact virus in vitro. The reconstitution experiments showed that all the information necessary to reach the final nano-assembly, the mosaic tobacco virus, can be found in the constituent parts.

From these experiments the virtue of self-assembly emerged:

- *Information*. Reduction of genetic information is achieved using one or few repeating unit.
- *Control*. Control of assembly and disassembly using multiple bond of relatively low energy, changing environmental conditions
- *Error-checking*. The information are contained in the components. Defective subunits are descared.
- *Efficiency*. Large structure can be constructed more efficiently by assembling of subunits rather than by direct construction

Self assembly offers considerable opportunities to synthetic chemists. These concepts were successfully used to construct a series of supramolecular assemblies, like molecular devices and machines, that are the object of the next section.

1.3 Molecular Devices and Machines

A device can be defined as an assembly of simple components. Each component can performed simple actions. When those components are assembled together in a proper way, new and more complex functions arise.

In a similar way, a molecular device can be defined as an assembly of a discrete number of molecular components designed to achieve a specific function.[25] Each molecular component performs single acts while the supramolecular system performs complex actions arising from the cooperation of each molecular component.

A molecular machine is a type of nanodevice in which the molecular components can display changes in their relative positions as result of the application of an external stimulus. Similarly to macroscopic systems, nano-scale devices are characterized by several features:

1. the kind of fuel (energy) to activate the machine and make it work
2. the movements performed by their molecular components
3. monitoring and control of the movement
4. the possibility to repeat the operation several times
5. the timescale needed to complete an entire working cycle
6. the type of function performed

1 ENERGY SUPPLY

As macroscopic machines, nanomachines need energy in order to perform their functions. The energy can be of three different type: chemical, electrical and light.

Chemical Energy

Natural molecular machines present in plant, use the chemical energy of a phosphate bond to perform their functions.[30] For example, the chemical pump for Na^+ and K^+, called *(Na^+-K^+)ATPase*, located in the plasma membrane of animal cell, consumes one molecule of ATP in order to translocate Na^+ from the

inner to the outer of the cell and K^+ from outer to inner of the cell. This type of motor "burns" one molecule of fuel each steps.[31] Addition of fresh reactant allows the motor to work for another additional step while the products are removed.

Similarly to those, artificial molecular level machines need addition of fresh reactant at any steps of the working cycle.[32] After every operation steps, waste products are released. For example in the case of an acid-driven molecular machine, a single cycle of operation implies the use of an acid first and then a base in order to reset the system at the initial state. The consequence of that operation is the accumulation of the acid-base waste products. Accumulation of products will compromise the operation of the machine unless they are removed from the system, as happens in both natural machines and in the macroscopic internal combustion engines.

The need to remove waste products poses noticeable limitations in the design and construction of artificial molecular machines based on chemical energy.[33]

Electrical Energy

Electrical potential can be used to cause redox reactions in supramolecular systems in solution. By playing with a reversible redox couple, it is possible to generate the product applying a potential. Reversing the potential, it is possible to return to the reactant, to cause a switching process without formation of waste products.[34] Electrochemical inputs, instead chemical redox one, can be switched on/off easily and rapidly. Electrochemical techniques can be used also to monitoring the state of the system. Furthermore, electrodes are one of the best ways of interfacing the molecular-level systems with the macroscopic world.

Light Energy

Plants use sunlight in order to sustain the machinery of life.[31] In these sophisticated systems, light is used to produced a chemical fuel, the ATP, used as propellant for all the natural machines.

Light can directly used in order to involve photochemical reactions, which cause a large nuclear movements. An example of this type of photochemical reactions, is the photoinduced isomerization of a molecule containing -C=C- and -N=N- double bonds from its stable *trans* to metastable *cis* form. The initial conformation can be restored by a spontaneous or light-induced reaction.[35] This

photoreaction has been used to construct molecular machines driven by light energy inputs.[36,37] In supramolecular systems photoinduced electron-tranfer reactions can cause large-scale displacement of molecular components.[38]
Big advantage of light-stimulate systems is the possibility to perform endless sequence of cycles without generating waste products. Light energy has other big advantages:

- light can be switched on/off easily and rapidly
- special light sources (e.g. lasers) allow short time and reduced space control
- using light, the machine does not need to be touched in order to supply energy; the only requirement is the transparency of the media to the light used.
- photons can be used also to "read" the state of the system and monitor the operation of the machine

2 MOTIONS

Various type of movements can be performed. The most important are linear movements (e.g. ring along a wire),[39] rotary motions,[40,41] changes in molecular structure (e.g allosteric processes),[42] assembly-disassembly (e.g. of host-guest species),[43] translocation of components (e.g. metal ions)[44] and contraction and extension.[45]

3 CONTROL AND MONITORING

The control and monitoring of the machine can be carried out if changes in the position of the moving component causes readable changes in properties of the systems. Any kind of chemical and physical techniques can be useful. The state of the system is controlled most frequently using spectroscopic technique (NMR, UV-Vis absorption and luminescence). Electrochemical techniques can be use in systems based on donor-acceptor interaction. Information on the rate constants are usually obtained using conventional kinetic techniques (slow processes), stopped flow and electrochemistry (relatively rapid process) and flash spectroscopy (fast processes).

4 RESET

Since machine must work by repeating cycles, reset is an important requirement. Chemical reactions involved in the movements of the component parts must be reversible. Photoinduced isomerization reactions, acid-base reactions and electron transfer reactions (red-ox) are used to accomplish this purpose.

5 TIMESCALE

The operation timescale of molecular machines is very variable and depends on the type of structural rearrangements take place. This can vary from picoseconds (for moving of small portion of molecules) to hours (in the case of remarkable rearrangements of the systems).

6 FUNCTIONS

The functions that can be performed exploiting the movements of the component parts are various. Mechanical movements in such machines correspond to a transition between two stable structures (states) that can be exploited as memory logic devices. Mechanical movement can be also used as it is, in order to move objects, even macroscopic one.[41,46,47]

1.3.1 ROTAXANE

Rotaxane is a mechanically interlocked molecular system (supramolecular system) consisting of a dumbbell-shaped component and a ring component.[28,39] The linear component is threaded in the ring one and the disassembly of the supramolecular system is avoided by the presence of two bulky groups (stoppers) at both sides. If properly synthesized, a rotaxane can be considered a molecular machine.

The template-direct synthesis of rotaxanes is based on the self-assembled principles used to obtain pseudorotaxanes.

1. Dumbbell and macrocycle should have a proper structure in order to give a self assembling architecture. Shape and size of both units should be complementary.
2. The units have to contain information that allow self-recognition and self-assembly, namely complementary functional groups/interactions.

Common type of interactions between the components of a rotaxane are: electron donor/acceptor, hydrogen bonding, hydrophobic/hydrophilic, π–π stacking, coulombic forces and metal-ligand forces. Mixture of those interactions might be present.

Usually these interactions can be highlighted due to the changing of some properties of the system (e.g. spectroscopic and/or redox). For example, charge transfer (CT) interaction often introduces a low-energy excited state with the appearance of a new band in the electronic absorption spectra. This interaction can also cause a change in the electrochemical properties.

The formation of an interaction between two suitable components, in order to form a rotaxane, can be carried out following three main ways (Figure 1.2).

1. Threading of a molecule through a ring and capping the end(s) of the thread.
2. Slipping of a preformed ring over the stoppers of a preformed dumbbell into a thermodynamically favourable site on the rod part of the dumbbell.
3. Clipping of an U-type component onto a suitable dumbbell followed by closure to form a ring.

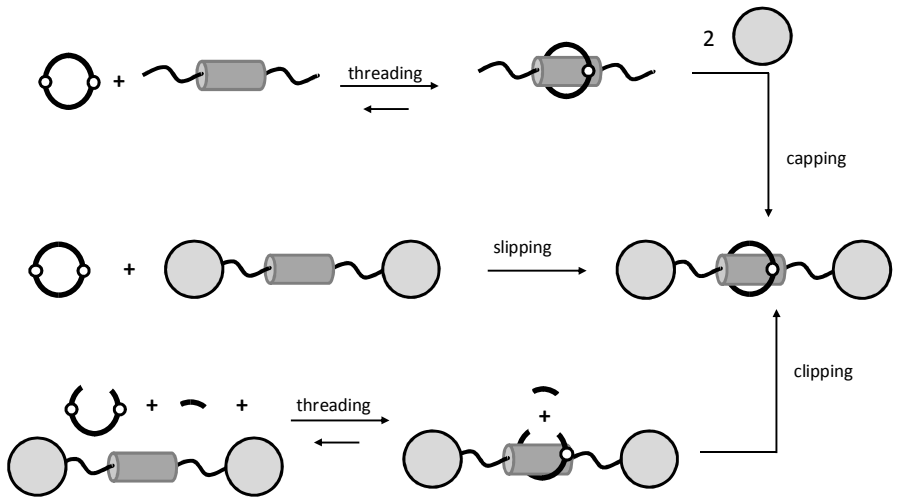

Figure 1.2 Synthesis routes to obtain rotaxanes. White circles on the ring indicate sites of interaction between the axle and the dumbbell

The ring unit of a rotaxane can perform a rotary motion around the axle molecule or linear motions along the dumbbell component. If two identical recognition sites are present along the axle, with which the ring can interact, the system presents two identical energy minima of the same probability to be occupied (Figure 1.3a).[48] Over a certain temperature the ring can be freely oscillated from one site to the other and the movement is governed just by thermal fluctuation.

Much more interesting is the case when the dumbbell molecule contains two different stations.[49] For each of those stations, the ring has different affinity (Figure 1.3b). In this case the system presents two different energy minima. At the equilibrium just one site is preferentially occupied by the interaction with the microcycle. With an appropriate stimulus, the interaction can be destabilized and the energy minima raised or removed and consequently the ring shuttles on the second site. Using a second and opposite input, the system is reset. The nature of the inputs depends on the nature of interaction between the ring and the recognition site on the dumbbell.

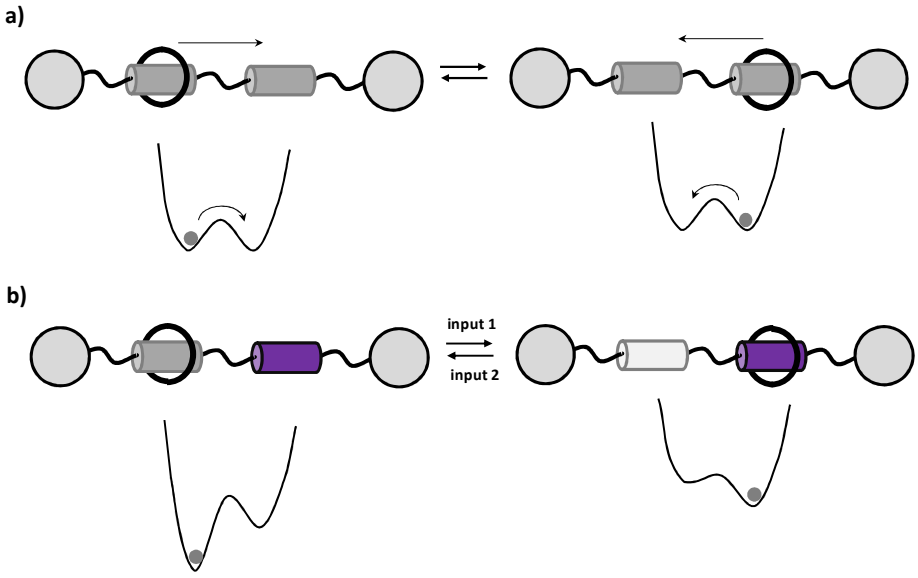

Figure 1.3 Schematic representation of a general rotaxane bearing two recognition sites for the ring and energy profile of the possible states. (a) Rotaxane with two identical recognition sites on the dumbbell molecule; the system is represented by two identical energy minima. (b) Rotaxane with different recognition sites with different affinity for the macrocycle; the system is represented by two different energy minima.

As already said, the movements in this systems between two stable states can be exploited in principle to develop binary logic systems at the molecular scale level. This was the purpose of part of this thesis where the performance of a bistable mechanically interlocked molecular system is reported (Chapter 3).

1.4 Nanostructured Materials: Semiconductor Nanocrystal Quantum Dots

In the field of nanotechnology nanostructured materials like nanoparticles-nanocrystals, nanowires, carbon nanotubes, etc. become very often active part in the development of new nanohybrids constituted of those units and functional molecules. These systems are developed using the concept related to the supramolecular chemistry (i.e. self-assembly).

A nanostructured material is a material bearing at least one dimension in the nanoscale size range.[1] At this regime physical and electronical properties of such materials are dependent by the dimension of the latter. This means that materials with the same chemical composition but different size, have different physical and electronical properties.[50]

The electronic structure of a "bulk" conductor, insulator or semiconductor material, can be described using the band theory.[51] An electronic band is defined as a combination of atomic orbitals that constituted the material. This band can be visualized as dense series of molecular orbitals, generated by linear combination of atomic orbitals. A conductor material has a band that is partially filled and partially empty regardless of temperature. The consequence is an high conductivity of such material. In the case of semiconductor and insulator materials, no partially filled band is present. The highest energy filled band is called *valence band* and the lowest energy empty band is called *conduction band*. The energy separation between the two bands is defined *energy band gap*. The difference between an insulator and a semiconductor is concerning the entity of such band gap. In the case of a semiconductor, at ambient temperature, electrons have enough energy to be promoted in the conduction band. However the number of charge carriers are less than those in conductor material.

Photons can be used to excite electrons from valence band to the conduction band. The consequence is the formation of a couple hole-electron, located in the valence band and in the conduction band respectively, called *exciton*. Electron and hole relax to the band edge where they can recombine with emission of a photon of the same energy of the semiconductor band gap. This process is called *band edge luminescence* (Figure 1.4)

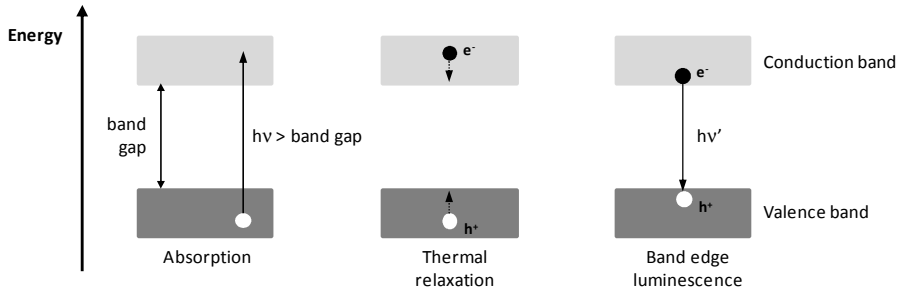

Figure1.4 Scheme representing band-edge luminescence of a semiconducting material.

Since the energy of the emitted photon depends on the energy band gap, the emission wavelength can be modulated by modulating the energy band gap (e.g. changing the material).

In the case of nanostructured materials, as anticipated above, the electronic properties are dependent on the size of the materials. In these systems the motion of the electrons, determining the electronic properties, follows the quanto-mechanical model of a *particle in a box*:[52] the electronic properties are strictly correlated with the size of the material. The quantum-confinement of the electronic wave-function, due to the reduced dimension of the material/box, generates a discretization of the electronic levels, leaving the *continuum* present in bulk materials.[53] Decreasing of nanocrystals size causes an increasing in the band-gap energy and consequently variation in the electronic properties. In the case of a semiconductor nanocrystal the main effect of increasing band-gap energy is an ipsochromic shift of the emission spectra. (Figura 1.5)

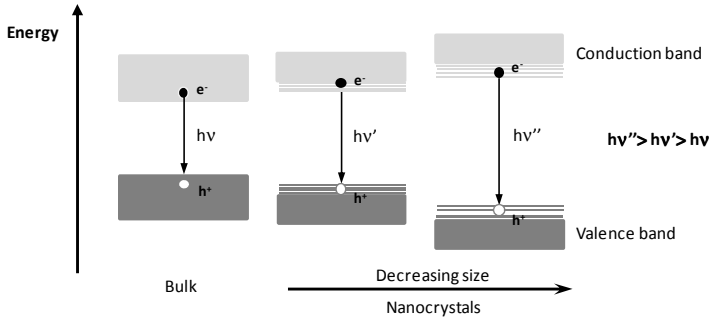

Figure 1.5 Effect of the quantum confinement on the emission energy of bulk and nanostructured semiconductor materials.

Luminescence Semiconductor Nanocrystal Quantum Dots (QDs) are emerging nanostructured semiconductor materials with unique photophysical properties that are not observed in their parent-bulk material.[53,54] These particular photophysical properties can be summarized as following:

- Tunable emission wavelength adjusting the size of the nanocrystals.[55] This characteristic is unique and it is due to the quantic confinement of the exciton wavefunction. The full width at half maximum (FWHM) of the Gaussian-shaped emission spectra is around 30 nm.[56]
- Broad band absorption spectra with high absorption cross section and high luminescence quantum yield. This last feature enables the measurements of luminescence signal at extremely dilute condition.[57]
- Longer fluorescence lifetime (20-30 ns)[58] instead classical fluorophores.
- High photostability[59] that allows application in which long irradiation time is required (e.g. in vivo imaging).[60]

The electronic features of those nanocrystals are due to the discretization of the energetic levels as reported above. The emission process in semiconductor nanocrystals is due, as already shown for bulk materials, to the recombination of a couple hole-electron (exciton) generated upon the absorption of a photon (Figura 1.4). For nanoparticles with diameter smaller than 10 nm, the Bohr radius associated to the exciton is bigger than the nanocrystal diameter. These conditions define the *strong confinement regime*[52] in which both charge carriers are quatitized. Under this condition the properties can be modulated by changing the diameter of the nanocrystal. In particular, the energy band gap increases by decreasing the size of the QDs and this implies that emission energy increases, decreasing the NC's size (Figure 1.5).
The preparation of semiconductor nanocrystals can be pursued following three main ways

1. Molecular Beam Epitaxy (MBE)[61] in which the nanocrystal growths on a surface using special precursors in vapour phase.
2. Lithographic technique[62]
3. Chemical methods

Chemical methods, also called 'wet' methods, allow the precise size and shape control, as well as high monodispersity and high photoluminescence quantum yield. All these features are unmatched using the other two methods. Solution based synthesis of nearly free-defects colloidal QDs is relatively inexpensive, facile and scalable with an impurity tolerance far exceeding to that required for epitaxial growth. Moreover size control in MBE is difficult.[63]

In the past two decades CdS, CdSe, CdTe, InAs and InP core colloidal nanocrystals, having these characteristics, have been successfully synthesized.[54,64–66] Despite all those nanocrystals have these particular electronic features, CdSe based nanocrystals are the most studied nanoparticles due to the remarkable resistance to chemical and photodegradation and high two photon action cross section.[59,60,67,68]

Highly luminescent, with narrow emission profile, and nearly monodisperse CdSe nanocrystal QDs were usually synthesized reacting organometallic precursors at high temperature in strongly-coordinating solvents.[69] In 1993 Bawendi and co-workers developed a method to synthesize high quality CdSe nanocrystals using organometallic precursors.[64] The mentioned method involves pyrolisis of Cd and Se organometallic source (dimethyl cadmium, $CdMe_2$, and trioctylphosphine selenide, TOPSe, respectively) at 300 °C in trioctylphosphine oxide, TOPO, as high boiling point solvent. The preparation of the precursors is usually carried out in an air-free environment dry-box by mixing desired amount of Cd and Se precursors in trioctylphosphine, TOP, as solvent. This method represents a clear break with previous works where ionic precursors were used as Cd and Se source in water or other polar solvents. The use of TOP-Se and $CdMe_2$ as organometallic precursors was inspired by a work carried out in late 1980s in Bell Laboratories in which $Se(TMS)_2$ and Cd^{2+} were reacted in inverse micelles at room temperature to yield CdSe nanoclusters.[70]

Concerning the cadmium precursor used in the hot injection method, $CdMe_2$ is toxic and pyrophoric substance and it must be handled under inert atmosphere.[71] Successive works involving the synthesis of CdSe QDs *via* hot injection technique, focused on the substitution of $CdMe_2$ with other cadmium sources. In early 2000s Peng and co-workers published a series of papers on the synthesis of quantum dots using other cadmium sources. Cadmium oxide, cadmium acetate, cadmium carbonate mixed with various fatty acid, amine or phosphonic acid

were used for the synthesis of high quality CdSe and other II-VI semiconductor nanocrystals.[72,73] Moreover in these papers authors show the possibility to use non-coordinating and less expensive solvents instead the use of alkyl phosphine. The nanocrystals used in this thesis were synthesized following the Peng's method with minor modifications.

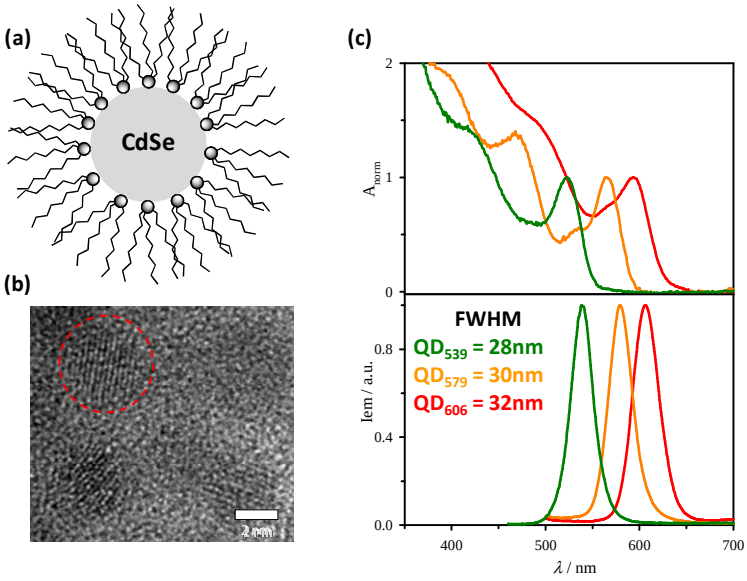

Figure 1.6 CdSe core nanocrystals. (a) Representation of CdSe core with hydrophobic ligands on the surface. (b) HRTEM picture shows single CdSe nanocrystallite. (c) Normalized absorption and emission spectra of a series of CdSe of different diameter: 2.6 nm for QD_{539}, 3.4 nm for QD_{579} and 4.3 nm for QD_{606}.

The surface of as prepared quantum dots is covered with a monolayer of organic ligands (TOPO, TOP, amine, fatty acid or phosphonic acid). These ligands passivate the surface avoiding aggregation. Despite the presence of these ligands, the surface can be easily altered and defects might appear.[74] Surface defects can act as trap states for both electron and hole with decreasing of the photophysical and luminescence properties. In order to increase the chemical stability and the photophysical properties, the nanocrystal can be covered with another semiconductor material of wider band gap forming a *core-shell* architecture. In this way both charge carriers generated in the CdSe *core* are constrained due to the higher potential barrier of the outer ZnS *shell*. CdSe-ZnS core-shell nanocrystals are much more stable against photo-oxidation and post synthetic surface modifications.

The overcoating of CdSe QDs was reported the first time by Guyot-Sionnest and co-workers in 1996.[75] The method involve the use of highly reactive organometallic reagents (diethyl zinc, $ZnEt_2$, and hexamethylsilathiane, $S(TMS)_2$). Precursors are loaded in the reaction solution containing bare-CdSe core in one single step. Using this method and further developments,[76] it is possible to obtain CdSe-ZnS QDs with high luminescence quantum yield and photostability.

In 2003 Peng and co-workers reported another overcoating method involving the use of less reactive and air-stable precursors like zinc stearate and elemental sulfur.[77] Using the Single Ion Layer Absorpion and Reaction (SILAR) technique is possible to growth a precise number of shell monolayers. The Zn and S precursors are alternatively loaded into the reaction solution containing the CdSe *core* until obtaining a *shell* of a desired thickness. This strategy allows also the preparation of multi-shell nanocrystals in which the nanocrystal is covered with a shell constituted of different semiconductor materials.[78]

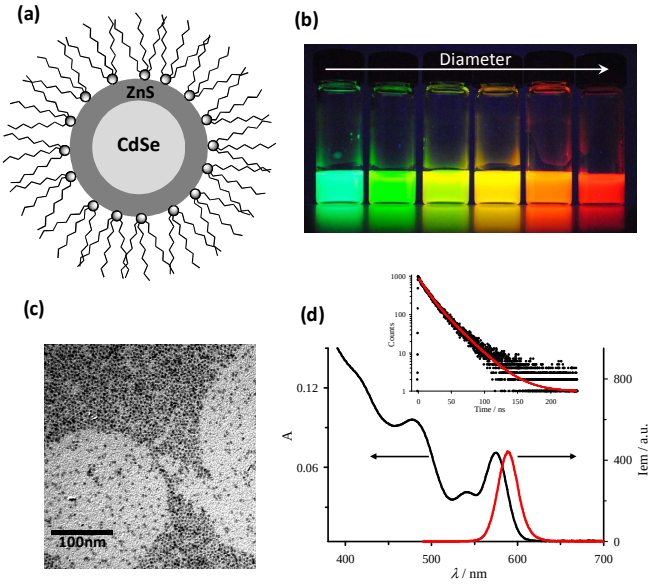

Figure 1.7.(a) Representation of CdSe-ZnS *core-shell* semiconductor nanocrystals covered with hydrophobic ligands. (b) Picture showing a series of different emitting CdSe-ZnS *core-shell* QDs. Arrow indicates the increasing of the core diameter. (c) TEM picture of 6.6 nm CdSe-ZnS QDs. (d) Absorption (black line) and emission (red line) spectra of CdSe-ZnS reported in TEM picture. Inset picture is the fluorescence decay profile and the red line represents the data-fitting according to a bi-exponential decay equation.

Detailed procedure concerning the synthesis of CdSe *core* and CdSe-ZnS *core-shell* are reported in Chapter 2.

Applications of luminescence quantum dots are ranging from electronic (e.g. LED production[79]) to solar cells[80,81] and biological fields, with the development of luminescence platforms for imaging and sensing.[82] Recently Sony commercialized a LED-TV where the conventional back light was substituted with blue-LED coupled with green and red emitting quantum dots.[83,84]
For biological applications and sensing, surface functionalization is a critical and required step. Next paragraph focuses on the strategy of surface functionalization of semiconductor nanocrystals.

1.4.1 SURFACE FUNCTIONALIZATION OF LUMINESCENCE SEMICONDUCTOR NANOCRYSTALS

The synthetic methodologies reported in the past paragraph for both *core* and *core-shell* nanocrystals, provide materials that are covered with a monolayer of organic ligands (TOPO, TOP, amine, fatty acid or phosphonic acid). These molecules confer hydrophobicity to the QDs with solubility of the latter in apolar organic solvents like chloroform, toluene or hexane. The dynamic nature of the binding of these ligands to the nanoparticle surface[85] allows the exchange of native ligands with other molecules. Post-synthetic surface modifications are carried out basically for two main reasons:

1. To make the QD's surface hydrophilic and biocompatible.
2. To introduce functional molecules on the QDs surface in order to perform specific function (e.g sensing[86]).

In the following paragraph are reported the principal procedures of post-synthetic surface modifications with few examples concerning the object of this thesis.

1.4.1.1 WATER SOLUBLE QUANTUM DOTS

One of the most promising application of colloidal semiconductor nanocrystals concerns the use of those nanoparticles as fluorescence platform for biological applications. Water compatibility of QDs is a key-point to achieve this purpose. Post synthetic modification must provide a stable material under different biological conditions.[82,87] (e.g. broad pH range, concentration of electrolyte, etc) The surface can be made water-compatible following two main strategies.[88]

1) *Ligand Exchange*. Native ligands are substituted with capping agents that combine an anchoring group for the metal surface and an hydrophilic part.

2) *Particle Encapsulation*. The hydrophobic particles are encapsulated using amphiphilic molecules or polymers.

In Figure 1.8 is reported a general scheme of the two functionalization strategies.

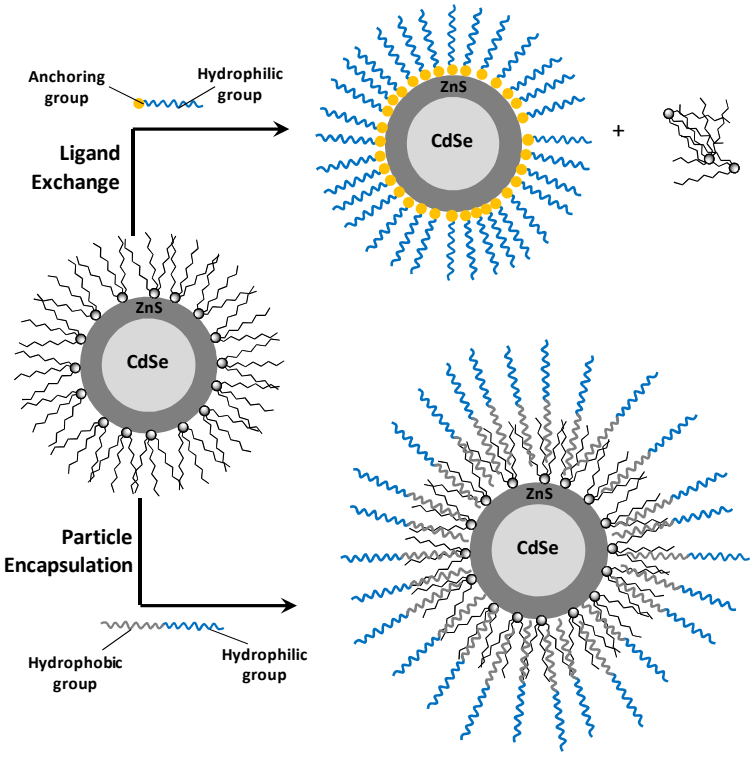

Figure 1.8 Schematic representation of the two main strategies to obtain water soluble quantum dots.

The *ligand exchange* procedure allows the preparation of nanocrystals with compact organic shell (i.e. small hydrodinamic radius) but the overall luminescence quantum yield is drastically reduced. Suitable anchoring groups for the ZnS shell are moieties that have certain affinity for the Zn or S atoms of the surface. For this purpose, imidazole[89] and thiols are the best choice. Many examples in literature reported ligands bearing thiol as anchoring group. The simplest molecule that satisfies the requirements reported above, is the mercapoacetic acid. This acid has a thiol group as anchoring group and a carboxylic acid conferring hydrophylicity to the system. The ligand was successfully used in 1998 by Nie and coworkers to solubilized QD in water and biological media.[90] The presence of a carboxylic acid requires deprotonation of the acid and formation of a carboxylate in order to solubilize the nanohybrid. This can be achieved storing QD with the new ligand in phosphate buffer (pH=7.4). QDs covered with this kind of ligand, and more generally all types of ligand that bearing carboxylic acid as hydrophilic group, are unstable under acidic condition where they aggregate and precipitate from solution. Another problem of monothiolated ligands is the low stability of this type of coating and the tendency to leave the QD's surface with consequent aggregation of the nanoparticles. Other types of monothiolated ligands are mercapotundecanoic acid[91] or small amino acid like cysteine in which the hydrophilic group is in a zwitterionic form at working conditions.[92]

In order to increase the stability of the coating, molecules containing a bis thiol can be used. The reduced form of the lipoic acid (LA), the di-hydro lipoic acid (DHLA) was successfully used to obtain a much more stable coating.[57] Reduction of LA is usually performed using $NaBH_4$. QDs coated using DHLA are stable for several months in basic buffer.[93] In Figure 1.9 are reported the chemical formula of the mono and bis thiolated compounds described above

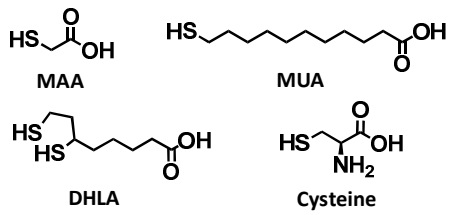

Figure 1.9 Thiolated ligands for QDs. In clockwise order, mercapto acetic acid (MAA), mercapto undecanoic acid (MUA), cysteine and di-hydro lipoic acid (DHLA)

The presence of carboxylic acid poses several limitations in the pH range of utilization of such hydrophilic QDs.[94]

Further improvements of the DHLA coating system came from Mattoussi and coworkers in 2005. They introduced a new class of ligands for semiconductor nanocrystals (and also gold nanoparticles) where the DHLA anchoring group is coupled with a poly ethylene glycol polymer chain (PEG) as hydrophilic group.[95] This coating provides a stabile QDs water dispersion in a broad pH range (from 5.8 to 8.0). Successive improvements ameliorated the colloidal stability with increased pH range from 3 to 13.[94,96] The synthesis of LA-PEG ligands is based on the DCC (*N,N'*-Dicyclohexylcarbodiimide) coupling reaction of lipoic acid with PEG molecule (Figure 1.10). The introduction of an amide bond instead an ester one, requires a premodification of polyethylene glycol with introduction of a terminal amine group. A minimum number of ethylene oxide monomers (about 8) is required in order to obtain QDs soluble in water. Minor modifications on the reaction scheme synthesis allow the introduction of functional terminated groups on the PEG chain.

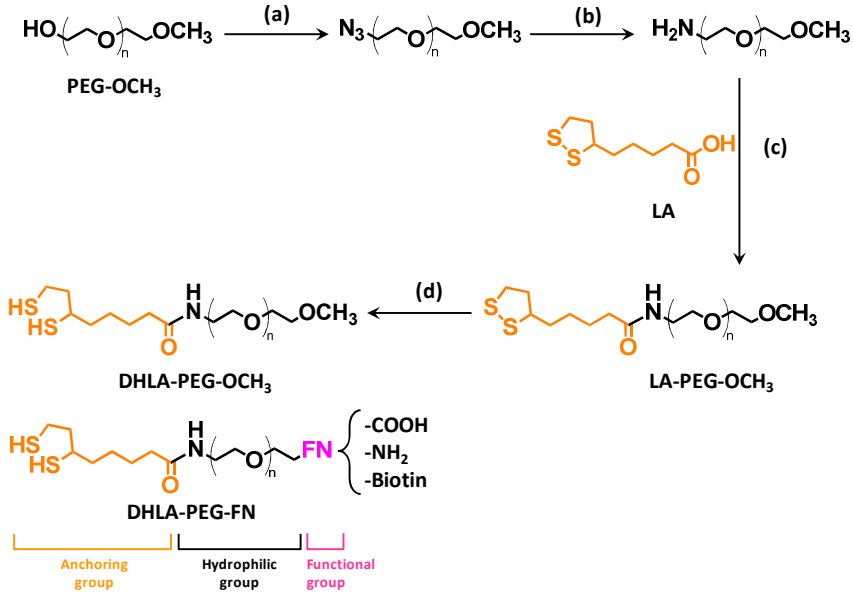

Figure 1.10 Chemical formula and synthetic scheme of LA-PEG ligands. (a) (i) CH_3SO_2Cl, Et_3N, THF; (ii) H_2O, NaN_3, $NaHCO_3$, (b) PPh_3, H_2O, THF, (c) DCC, DMAP, CH_2Cl_2, (d) $NaBH_4$, MeOH, H_2O.

The generality of the cap exchange method enables the introduction of functional groups (-COOH, $-NH_2$ and biotin) on the QDs surface without any modification in the cap exchange reaction.[97] Since all of those ligands have same anchoring and hydrophilic groups, the cap-exchange driving force for both functional and "inert" (-OH or $-OCH_3$ terminated) molecule is the same. As consequence, the fraction of functional groups present on the QD surface is the same of the solution used for the cap exchange.
Part of this thesis will focus on the use of those bidentate ligands (DHLA and DHLA-PEG) as hydrophilic ligands for semiconductor nanocrystals.
Increasing the number of anchoring groups, the stability of water dispersion increases. Examples of tridentate[98] , tetradentate[99] and multidentate polymeric ligands[100] based on thiols and PEG chains were recently reported in literature. PEG chain can be substituted using other hydrophilic groups, like zwitterions, in order to obtain compact ligands for biological application.[101–103]

Polymers containing phosphine oxide as anchoring group and polyethylene glycol as hydrophilic part were used to solubilized QDs and other various nanoparticles in water.[104]

The *particle encapsulation* strategy allows the preparation of nanocrystals with almost unchanged photophysical properties (e.g. luminescence quantum yield). Despite optimal photophysical properties, encapsulated particles have an increased hydrodynamic radius that can preclude their utilization in Forster resonance energy transfer application or biological imaging.[82] Amphipilic polymers[105,106] or phospholipids[107] were successfully used.

Another type of coating, that is a mixture of both ligand exchange and particle encapsulation, is based on the exchange of the native ligand with mercapto propylsilanols[108] and successive silanization of these units that allow the formation of a robust silica shell dispersible in water and buffer media. Further addition of siloxane precursors produce a much more thick shell with the aim of a better water compatibility.
Peptides can also be used to cover the surface of semiconductor nanocrystals and promote the solubilization in water and buffer media.[109]

1.4.1.2 SURFACE DECORATION OF QUANTUM DOTS WITH FUNCTIONAL UNITS

Introduction of functionalities (e.g. peptides, metal complexes, bioactive molecules, etc.) on the surface of those water soluble QDs can be achieved via covalent attachment on the ligand shell,[110–113] self assembling on the nanocrystal surface using, for example, histidine-rich peptides[114–116] or self assembling on the ligand shell *via* cationic-anionic interaction.[117]

Some of those nanohydrids were successfully tested as pH sensors. As an example, in 2006 Bawendi and co-workers reported the functionalization of an hydrophilic core-shell QDs with a squaraine dye with the aim of develop a ratiometric pH sensor. The FRET between QD and the dye is modulated by the environment since the absorption profile of the squaraine is a function of pH.[110]

Another interesting example involves the self assembling of a DHLA-PEG coated quantum dots and dopamine-peptide for the construction of a pH sensible nanohybrid[115] (Figure 1.11).

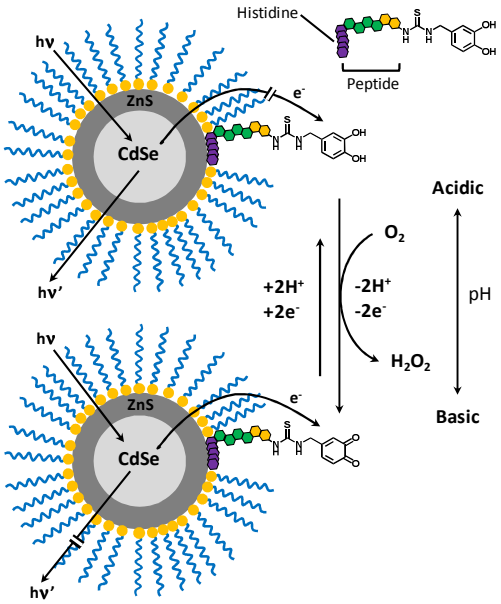

Figure 1.11 Schematic representation of hydrophilic QD-dopamine nanohybrid as pH sensor

Dopamine is a well-know neurotransmitter existing in two different forms, depending on the pH. At low pH reduced-hydroxiquinone is the preminent form.

Hydroxiquinone is a poor electron acceptor and the quenching of the QDs does not take place. At basic pH reduced-hydroxiquinone is oxidized to quinone due to the presence of oxygen in the media. Dopamine-quinone is a strong electron-acceptor and can quench the QD luminescence by electron transfer. This nanohybrid was successfully used to sense *in vitro* the cytoplasmatic pH.

Also hydrophobic QDs can be functionalized with molecules in order to sense some analytes. CdSe-ZnS QDs were capped with the imidazole-pyrene ligand (Figure 1.12) to yield a ratiometric luminescence oxygen sensor.[118] Emission signals originating from pyrene (378 nm) and QD (632 nm) are fully independent. While pyrene is quenched by O_2, QD luminescence is not. This observation enables a ratiometric determination of dissolved oxygen.

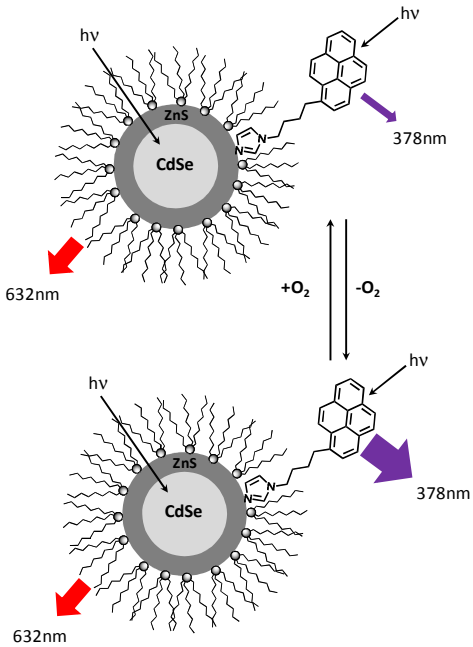

Figure 1.12 Schematic representation of the QD-Pyrene system as ratiometric oxygen sensor

QDs can be functionalized with molecules in order to modulate the luminescence using an external stimulus, e.g. photochemically.[86] Recently CdSe-ZnS QDs coated with an hydrophilic polymer were functionalized with a photo-cleavable 2-nitrobenzyl group with the aim of photoswitching the luminescence

of the QD.[112] Enhancing of the QD's luminescence was observed after photolysis of the nitrobenzyl group, in both solution and *in vitro*.

References and Notes

(1) Borisenko, V. B.; Ossicini, S. *What is What in the Nanoworld*; Wiley-VCH Verlag: Weinheim, 2004.
(2) Grieneisen, M. L.; Zhang, M. *Small* **2011**, *7*, 2836–2839.
(3) Balzani, V. *Small* **2005**, *1*, 278–283.
(4) Theis, T.; Parr, D.; Binks, P.; Ying, J.; Drexler, K. E.; Schepers, E.; Mullis, K.; Bai, C.; Boland, J. J.; Langer, R.; Dobson, P.; Rao, C. N. R.; Ferrari, M. *Nat. Nanotech.* **2006**, *1*, 8–10.
(5) Feynman, R. P. *Eng. Sci.* **1960**, *23*, 22–36.
(6) Feynman, R. There's a plenty of room at the bottom http://www.its.caltech.edu/~feynman/plenty.html.
(7) Mijatovic, D.; Eijkel, J. C. T.; Van den Berg, A. *Lab Chip* **2005**, *5*, 492–500.
(8) Mizuta, H.; Oda, S. *Microelectron. J.* **2008**, *39*, 171–176.
(9) Palma, C.-A.; Samorì, P. *Nat. Chem.* **2011**, *3*, 431–436.
(10) Lu, W.; Lieber, C. M. *Nat. Mater.* **2007**, *6*, 841–850.
(11) History of computer http://inventors.about.com/library/blcoindex.htm.
(12) Zuse Z3 http://www.computermuseum.li/Testpage/Z3-Computer-1939.htm.
(13) Eniac http://ftp.arl.mil/~mike/comphist/eniac-story.html.
(14) Faggin, F.; Shima, M.; Hoff, M. E.; Freeney, H.; Mazor, S. *Solid State Circuit Magazine, IEEE* **2009**, *1*, 55–60.
(15) 4004 Intel Processor http://inventors.about.com/od/mstartinventions/a/microprocessor.htm.
(16) Service, R. F. *Science* **2001**, *293*, 785–786.
(17) Totzeck, M.; Ulrich, W.; Göhnermeier, A.; Kaiser, W. *Nat. Photonics* **2007**, *1*, 629–631.
(18) Perry, J. W. *Science* **2009**, *324*, 892–893.
(19) Hla, S.-W.; Meyer, G.; Rieder, K.-H. *ChemPhysChem* **2001**, *2*, 361–366.
(20) Shevchenko, E. V; Talapin, D. V; Kotov, N. a; O'Brien, S.; Murray, C. B. *Nature* **2006**, *439*, 55–59.
(21) Macfarlane, R. J.; Lee, B.; Jones, M. R.; Harris, N.; Schatz, G. C.; Mirkin, C. a *Science* **2011**, *334*, 204–208.
(22) De Graaf, J.; Manna, L. *Science* **2012**, *337*, 417–418.
(23) Kang, Y.; Ye, X.; Chen, J.; Qi, L.; Diaz, R. E.; Doan-Nguyen, V.; Xing, G.; Kagan, C. R.; Li, J.; Gorte, R. J.; Stach, E. a; Murray, C. B. *J. Am. Chem. Soc.* **2013**, *135*, 1499–1505.
(24) Balzani, V.; Credi, A.; Venturi, M. *Chem. Eur. J.* **2002**, *8*, 5524–5532.
(25) Balzani, V.; Credi, A.; Venturi, M. *Molecular Devices and Machine - Concepts and Perspectives for the Nanoworld*; 2nd ed.; Wiley-VCH Verlag: Weinheim, 2008.
(26) Lehn, J.-M. *Angew. Chem. Int. Ed.* **1988**, *27*, 89–112.
(27) Nobel Prize Chemistry 1987 http://www.nobelprize.org/nobel_prizes/chemistry/laureates/1987/.

(28) Balzani, V.; Gomez-Lopez, M.; Stoddart, J. F. *Acc. Chem. Res.* **1998**, *31*, 405–414.
(29) Lindsey, J. S. *New J. Chem.* **1991**, *15*, 153–180.
(30) Magnasco, M. O. *Phys. Rev. Lett.* **1994**, *72*, 2656–2659.
(31) Voet, D.; Voet, J. J.; Pratt, C. W. *Fondamenti di Biochimica*; Zanichelli: Bologna, 2001.
(32) Badjic, J. D.; Balzani, V.; Credi, A.; Silvi, S.; Stoddart, J. F. *Science* **2004**, *303*, 1845–1849.
(33) Ballardini, R.; Balzani, V.; Credi, A.; Gandolfi, M. T.; Venturi, M. *Acc. Chem. Res.* **2001**, *34*, 445–455.
(34) Asakawa, M.; Ashton, P. R.; Balzani, V.; Credi, A.; Hamers, C.; Mattersteig, G.; Montalti, M.; Shipway, A. N.; Spencer, N.; Stoddart, J. F.; Tolley, M. S.; Venturi, M.; White, A. J. P.; Williams, D. J. *Angew. Chem. Int. Ed.* **1998**, *37*, 333–337.
(35) Durr, H.; Bouas-Laurent, H. *Photochromism, Molecules and Systems*; Elsevier Science Publishers B.V.: Amsterdam, 1990.
(36) Balzani, V.; Credi, A.; Marchioni, F.; Stoddart, J. F. *Chem. Comm.* **2001**, *2*, 1860–1861.
(37) Qu, D.-H.; Wang, Q.-C.; Tian, H. *Angew. Chem. Int. Ed.* **2005**, *44*, 5296–5299.
(38) Balzani, V.; Clemente-León, M.; Credi, A.; Ferrer, B.; Venturi, M.; Flood, A. H.; Stoddart, J. F. *Proc. Natl. Acad. Sci.* **2006**, *103*, 1178–1183.
(39) Balzani, V.; Credi, A.; Raymo, F.; Stoddart, J. *Angew. Chem. Int. Ed.* **2000**, *39*, 3348–3391.
(40) Feringa, B. L. *Acc. Chem. Res.* **2001**, *34*, 504–513.
(41) Eelkema, R.; Pollard, M. M.; Vicario, J.; Katsonis, N.; Ramon, B. S.; Bastiaansen, C. W. M.; Broer, D. J.; Feringa, B. L. *Nature* **2006**, *440*, 163.
(42) Kottas, G. S.; Clarke, L. I.; Horinek, D.; Michl, J. *Chem. Rev.* **2005**, *105*, 1281–1376.
(43) Balzani, V.; Credi, A.; Venturi, M. *Proc. Natl. Acad. Sci.* **2002**, *99*, 4814–4817.
(44) Amendola, V.; Fabbrizzi, L.; Mangano, C.; Pallavicini, P. *Acc. Chem. Res.* **2001**, *34*, 488–493.
(45) Collin, J.; Dietrich-buchecker, C.; Jimenez-molero, M. C.; Sauvage, J. *Acc. Chem. Res.* **2001**, *34*, 477–487.
(46) Berná, J.; Leigh, D. a; Lubomska, M.; Mendoza, S. M.; Pérez, E. M.; Rudolf, P.; Teobaldi, G.; Zerbetto, F. *Nat. Mater.* **2005**, *4*, 704–710.
(47) Liu, Y.; Flood, A. H.; Bonvallet, P. a; Vignon, S. a; Northrop, B. H.; Tseng, H.-R.; Jeppesen, J. O.; Huang, T. J.; Brough, B.; Baller, M.; Magonov, S.; Solares, S. D.; Goddard, W. a; Ho, C.-M.; Stoddart, J. F. *J. Am. Chem. Soc.* **2005**, *127*, 9745–9759.
(48) Anelli, P. L.; Spencer, N.; Stoddart, J. F. *J. Am. Chem. Soc.* **1991**, *113*, 5131–5133.
(49) Bissel, R. A.; Cordova, E.; Kaifer, A. E.; Stoddart, F. J. *Nature* **1994**, *369*, 133–137.
(50) Burda, C.; Chen, X.; Narayanan, R.; El-Sayed, M. a *Chem. Rev.* **2005**, *105*, 1025–1102.
(51) Atkins, P. W. *Chimica Fisica*; Zanichelli: Bologna, 1997.
(52) Efros, A. L.; Rosen, M. *Annu. Rev. Mater. Sci.* **2000**, *30*, 475–521.
(53) Alivisatos, A. P. *J. Phys. Chem.* **1996**, *3654*, 13226–13239.
(54) Talapin, D. V.; Lee, J.-S.; Kovalenko, M. V.; Shevchenko, E. V. *Chem. Rev.* **2010**, *110*, 389–458.
(55) Murray, C. B.; Kagan, C. R.; Bawendi, M. G. *Annu. Rev. Mater. Sci.* **2000**, *30*, 545–610.
(56) Rogach, A. L. *Semiconductor nanocrystal quantum dot*; Springer: Wien, 2008.
(57) Mattoussi, H.; Mauro, J. M.; Goldman, E. R.; Anderson, G. P.; Sundar, V. C.; Mikulec, F. V.; Bawendi, M. G. *J. Am. Chem. Soc.* **2000**, *122*, 12142–12150.
(58) Lounis, B.; Bechtel, H. A.; Gerion, D.; Alivisatos, A. P.; Moerner, W. E. *Chem. Phys. Lett.* **2000**, *329*, 399–404.

(59) Jaiswal, J. K.; Mattoussi, H.; Mauro, J. M.; Simon, S. M. *Nat. Biotechnol.* **2003**, *21*, 47–51.
(60) Larson, D. R.; Zipfel, W. R.; Williams, R. M.; Clark, S. W.; Bruchez, M. P.; Wise, F. W.; Webb, W. W. *Science* **2003**, *300*, 1434–1436.
(61) Xin, S. H.; Wang, P. D.; Yin, A.; Kim, C.; Dobrowolska, M.; Merz, J. L.; K., F. J. *Appl. Phys. Lett.* **1996**, *69*, 3884–3886.
(62) Bertino, M. F.; Gadipalli, R. R.; Martin, L. A.; Rich, L. E.; Yamilov, A.; Heckman, B. R.; Leventis, N.; Guha, S.; Katsoudas, J.; Divan, R.; Mancini, D. C. *Nanotechnology* **2007**, *18*, 1–6.
(63) Shirasaki, Y.; Supran, G. J.; Bawendi, M. G.; Bulović, V. *Nat. Photonics* **2013**, *7*, 13–23.
(64) Murray, C. B.; Noms, D. J.; Bawendi, M. G. *J. Am. Chem. Soc.* **1993**, *115*, 8706–8715.
(65) Guzelian, A. A.; Banin, U.; Kadavanich, A. V.; Peng, X.; Alivisatos, A. P. *Appl. Phys. Lett.* **1996**, *69*, 1432–1434.
(66) Micic, O. I.; Curtis, C. J.; Jones, K. M.; Sprague, J. R.; Nozik, A. J. *J. Phys. Chem.* **1994**, *98*, 4966–4969.
(67) Wu, X.; Liu, H.; Liu, J.; Haley, K. N.; Treadway, J. a; Larson, J. P.; Ge, N.; Peale, F.; Bruchez, M. P. *Nat. Biotechnol.* **2003**, *21*, 41–46.
(68) Clapp, A. R.; Pons, T.; Medintz, I. L.; Delehanty, J. B.; Melinger, J. S.; Tiefenbrunn, T.; Dawson, P. E.; Fisher, B. R.; O'Rourke, B.; Mattoussi, H. *Adv. Mater.* **2007**, *19*, 1921–1926.
(69) De Mello Donegá, C.; Liljeroth, P.; Vanmaekelbergh, D. *Small* **2005**, *1*, 1152–1162.
(70) Steigerwald, M. L.; Alivisatos, A. P.; Gibson, J. M.; Harris, T. D.; Kortan, R.; Muller, A. J.; Thayer, A. M.; Duncan, T. M.; Douglass, D. C.; Brus, L. E. *J. Am. Chem. Soc.* **1988**, *110*, 3046–3050.
(71) Material safety data sheet_Dimethyl Cadmium http://www.strem.com/catalog/v/48-5040/10/cadmium_506-82-1.
(72) Qu, L.; Peng, Z. A.; Peng, X. *Nano Lett.* **2001**, *1*, 333–337.
(73) Yu, W. W.; Peng, X. *Angew. Chem. Int. Ed.* **2002**, *41*, 2368–2371.
(74) Kuno, M.; Lee, J. K.; Dabbousi, B. O.; Mikulec, F. V.; Bawendi, M. G. *J. Chem. Phys.* **1997**, *106*, 9869–9882.
(75) Hines, M. a.; Guyot-Sionnest, P. *J. Phys. Chem.* **1996**, *100*, 468–471.
(76) Dabbousi, B. O.; Mikulec, F. V; Heine, J. R.; Mattoussi, H.; Ober, R.; Jensen, K. F.; Bawendi, M. G. *J. Phys. Chem. B* **1997**, *101*, 9463–9475.
(77) Li, J. J.; Wang, Y. A.; Guo, W.; Keay, J. C.; Mishima, T. D.; Johnson, M. B.; Peng, X. *J. Am. Chem. Soc.* **2003**, *125*, 12567–12575.
(78) Xie, R.; Kolb, U.; Li, J.; Basche, T.; Mews, A. *J. Am. Chem. Soc.* **2005**, *127*, 7480–7488.
(79) Kwak, J.; Bae, W. K.; Lee, D.; Park, I.; Lim, J.; Park, M.; Cho, H.; Woo, H.; Yoon, D. Y.; Char, K.; Lee, S.; Lee, C. *Nano Lett.* **2012**, *12*, 2362–2366.
(80) Kamat, P. V; Tvrdy, K.; Baker, D. R.; Radich, J. G. *Chem. Rev.* **2010**, *110*, 6664–6688.
(81) Sargent, H. *Nat. Photonics* **2012**, *6*, 133–135.
(82) Medintz, I. L.; Uyeda, H. T.; Goldman, E. R.; Mattoussi, H. *Nat. Mater.* **2005**, *4*, 435–446.
(83) Sony QD-LED TV http://www.technologyreview.com/news/509801/quantum-dots-get-commercial-debut-in-more-colorful-sony-tvs/.
(84) Bourzac, C. *Nature* **2013**, *493*, 283.
(85) Blaudeck, T.; Zenkevich, E. I.; Abdel-Mottaleb, M.; Szwaykowska, K.; Kowerko, D.; Cichos, F.; Von Borczyskowski, C. *ChemPhysChem* **2012**, *13*, 959–972.

(86) Credi, A. *New J. Chem.* **2012**, *36*, 1925–1930.
(87) Michalet, X.; Pinaud, F. F.; Bentolila, L. a; Tsay, J. M.; Doose, S.; Li, J. J.; Sundaresan, G.; Wu, a M.; Gambhir, S. S.; Weiss, S. *Science* **2005**, *307*, 538–544.
(88) Zrazhevskiy, P.; Sena, M.; Gao, X. *Chem. Soc. Rev.* **2010**, *39*, 4326–4354.
(89) Liu, W.; Greytak, A. B.; Lee, J.; Wong, C. R.; Park, J.; Marshall, L. F.; Jiang, W.; Curtin, P. N.; Ting, A. Y.; Nocera, D. G.; Fukumura, D.; Jain, R. K.; Bawendi, M. G. *J. Am. Chem. Soc.* **2010**, *132*, 472–483.
(90) Chan, W. C.; Nie, S. M. *Science* **1998**, *281*, 2016–2018.
(91) Chan, W.; Fisher, H.; Mardyani, S.; Jiang, W. US 7,151,047 B2 **2006**, 13.
(92) Liu, W.; Choi, H. S.; Zimmer, J. P.; Tanaka, E.; Frangioni, J. V; Bawendi, M. *J. Am. Chem. Soc.* **2007**, *129*, 14530–14531.
(93) Clapp, A. R.; Goldman, E. R.; Mattoussi, H. *Nat. Protoc.* **2006**, *1*, 1258–1266.
(94) Susumu, K.; Uyeda, H. T.; Medintz, I. L.; Pons, T.; Delehanty, J. B.; Mattoussi, H. *J. Am. Chem. Soc.* **2007**, *129*, 13987–13996.
(95) Uyeda, H. T.; Medintz, I. L.; Jaiswal, J. K.; Simon, S. M.; Mattoussi, H. *J. Am. Chem. Soc.* **2005**, *127*, 3870–3878.
(96) Mei, B. C.; Susumu, K.; Medintz, I. L.; Delehanty, J. B.; Mountziaris, T. J.; Mattoussi, H. *J. Mater. Chem.* **2008**, *18*, 4949–4958.
(97) Susumu, K.; Mei, B. C.; Mattoussi, H. *Nat. Protoc.* **2009**, *4*, 424–436.
(98) Thiry, M.; Boldt, K.; Nikolic, M. S.; Schulz, F.; Ijeh, M.; Panicker, A.; Vossmeyer, T.; Weller, H. *ACS Nano* **2011**, *5*, 4965–4973.
(99) Stewart, M. H.; Susumu, K.; Mei, B. C.; Medintz, I. L.; Delehanty, J. B.; Blanco-Canosa, J. B.; Dawson, P. E.; Mattoussi, H. *J. Am. Chem. Soc.* **2010**, *132*, 9804–9813.
(100) Palui, G.; Na, H. Bin; Mattoussi, H. *Langmuir* **2012**, *28*, 2761–2772.
(101) Muro, E.; Pons, T.; Lequeux, N.; Fragola, A.; Sanson, N.; Lenkei, Z.; Dubertret, B. *J. Am. Chem. Soc.* **2010**, *132*, 4556–4557.
(102) Susumu, K.; Oh, E.; Delehanty, J. B.; Blanco-Canosa, J. B.; Johnson, B. J.; Jain, V.; Hervey, W. J.; Algar, W. R.; Boeneman, K.; Dawson, P. E.; Medintz, I. L. *J. Am. Chem. Soc.* **2011**, *133*, 9480–9496.
(103) Zhan, N.; Palui, G.; Grise, H.; Tang, H.; Alabugin, I.; Mattoussi, H. *ACS Appl. Mater. Interfaces* **2013**, in press DOI:10.1021/am302788q.
(104) Kim, S.-W.; Kim, S.; Tracy, J. B.; Jasanoff, A.; Bawendi, M. G. *J. Am. Chem. Soc.* **2005**, *127*, 4556–4557.
(105) Gao, X.; Cui, Y.; Levenson, R. M.; Chung, L. W. K.; Nie, S. *Nat. Biotechnol.* **2004**, *22*, 969–976.
(106) Pellegrino, T.; Manna, L.; Kudera, S.; Liedl, T.; Koktysh, D.; Rogach, A. L.; Keller, S.; Ra, J.; Natile, G.; Parak, W. J. *Nano Lett.* **2004**, *4*, 703–707.
(107) Dubertret, B.; Skourides, P.; Norris, D. J.; Noireaux, V.; Brivanlou, A. H.; Libchaber, A. *Science* **2002**, *298*, 1759–1762.
(108) Gerion, D.; Pinaud, F.; Williams, S. C.; Parak, W. J.; Zanchet, D.; Weiss, S.; Alivisatos, a. P. *J. Phys. Chem. B* **2001**, *105*, 8861–8871.
(109) Pinaud, F.; King, D.; Moore, H.-P.; Weiss, S. *J. Am. Chem. Soc.* **2004**, *126*, 6115–6123.
(110) Snee, P. T.; Somers, R. C.; Nair, G.; Zimmer, J. P.; Bawendi, M. G.; Nocera, D. G. *J. Am. Chem. Soc.* **2006**, *128*, 13320–13321.
(111) Susumu, K.; Medintz, I. L.; Delehanty, J. B.; Boeneman, K.; Mattoussi, H. *J. Phys. Chem. C* **2010**, *114*, 13526–13531.

(112) Impellizzeri, S.; McCaughan, B.; Callan, J. F.; Raymo, F. M. *J. Am. Chem. Soc.* **2012**, *134*, 2276–2283.
(113) Ji, X.; Palui, G.; Avellini, T.; Na, H. Bin; Yi, C.; Knappenberger, K. L.; Mattoussi, H. *J. Am. Chem. Soc.* **2012**, *134*, 6006–6017.
(114) Boeneman, K.; Mei, B. C.; Dennis, A. M.; Bao, G.; Deschamps, J. R.; Mattoussi, H.; Medintz, I. L. *J. Am. Chem. Soc.* **2009**, *131*, 3828–3829.
(115) Medintz, I. L.; Stewart, M. H.; Trammell, S. A.; Susumu, K.; Delehanty, J. B.; Mei, B. C.; Melinger, J. S.; Blanco-canosa, J. B.; Dawson, P. E.; Mattoussi, H. *Nat. Mater.* **2010**, *9*, 676–684.
(116) Blanco-Canosa, J. B.; Medintz, I. L.; Farrell, D.; Mattoussi, H.; Dawson, P. E. *J. Am. Chem. Soc.* **2010**, *132*, 10027–10033.
(117) Yildiz, I.; Tomasulo, M.; Raymo, F. M. *Proc. Natl. Acad. Sci.* **2006**, *103*, 11457–11460.
(118) Amelia, M.; Lavie-Cambot, A.; McClenaghan, N. D.; Credi, A. *Chem. Comm.* **2011**, *47*, 325–327.

Chapter 2

Experimental techniques

2.1 Chemicals

All the studied supramolecular systems and molecular components have been prepared and characterized by the research groups reported in each chapter. Any reagent or model compound used occasionally was of the best purity commercially available.

The solvents were acetonitrile (Romil), chloroform (Merck Uvasol™) or dichloromethane (Merck Uvasol™) for the photochemical and photophysical experiments.

Cadmium oxide (CdO, 99.99%), diethyl zinc ($ZnEt_2$, 1M in *n*-eptane), hexamethyldisilathiane ($S(TMS)_2$, synthesis grade), trioctylphosphine (TOP, 90% technical grade), trioctylphosphine oxide (TOPO, 99% and 90% technical grade), hexadecylamine (HDA, 98%), octadecylamine (ODA, 99.0%), octadecene (ODE technical grade 90%), oleic acid (OlA, technical grade 90%), methanol (99.8% GC), chloroform (99.0% GC) and *n*-hexane (GC 95%) were purchased from Sigma Aldrich and used without further purification. Selenium powder (Se, 99.95%), stearic acid (StA, 98%), zinc oxide (99.99%) and

elemental sulfur (99.5%) were purchased from Alfa Aesar and used without further purification. All the reagents reported above were using for the synthesis of CdSe *core* and CdSe-ZnS *core-shell* quantum dots. Detailed synthesis are reported in the following paragraphs.
Solid samples were weighted with a Mattles AT261 balance (sensitivity 0.01mg, experimental error estimated <10%). The amount weighted were in no case smaller than 0.5mg.

2.2 Synthesis of Semiconductor Nanocrystals

CdSe *core* and CdSe-ZnS *core-shell* luminescence semiconductor nanocrystal quantum dots used in Chapter 4 were synthesized according to the procedure reported in literature with some modification.

2.2.1 SYNTHESIS OF CdSe "Core" QUANTUM DOTS

Quantum dots core CdSe were synthesized following the method developed by Peng and co-workers with minor modifications.[1–3] Briefly 25.7 mg of CdO (0.2 mmol) and 227.6 mg of StA (0.8 mmol) were placed in a 25 ml three-neck round bottom flask. The mixture was heated at 150°C under argon flow until the mixture become clear and colorless. The flask was allowed to cool down at room temperature and 1.5 g of HDA (or ODA), 0.5 g of TOPO 99% and 2 ml of ODE were added. The mixture was degassed at 120°C under reduced pressure and gently stirred for 2 hours followed by flushing with argon. Then the temperature was raised to the injection temperature (ranging from 260°C to 300°C). In an nitrogen filled dry box (MBraun Lab-Star, MB10), 160mg of selenium (2 mmol) were mixed with 2 ml of TOP in 8 ml glass vial equipped with septum. The selenium precursor was quickly injected using a proper plastic syringe equipped with 12 gauge metal needle. Growth temperature was set to a value 20-30°C lower than injection temperature. The mixture turned from colorless to light yellow, orange and dark red color. Aliquots of desired color/size were taken out and immediately quenched by dilution in chloroform. As an alternative, all the reaction batch was stopped at one desired size by removing the heating mantle. Fast cooling of the reaction mixture can be perform using a fan. Chloroform or hexane were added at 60°C to solubilize the nanocrystals preventing aggregation. QDs were precipitated twice adding an excess of methanol with the

purpose to remove as much excess of free ligands and unreacted precursors as possible. Finally the CdSe quantum dots, in form of fine powder, were dissolved in chloroform or hexane to obtain a concentrated solution (about 15μM). The exact concentration value was estimated from the wavelength of the exciton peak.[4]

2.2.2 SYNTHESIS OF CdSe-ZnS "Core-Shell" QUANTUM DOTS

CdSe-ZnS core-shell quantum dots were synthesized following two different methods. The first one is the Single Ion Layer Absorption and Reaction (SILAR) approach developed by Peng and co workers[3] and the second one is the one-time precursors injection developed the first time by Guyot-Sionnest and coworkers.[5] The purpose of using the first or the second method is based on the dimension of the CdSe core. For small QD (diameter < 3.4 nm) the one pot method is the best choice. This method involves the use of very reactive zinc and sulfur precursors ($ZnEt_2$ and $S(TMS)_2$) but the reaction can be carried out at relatively low temperature at which small CdSe nanocrystals are stable.
For big QDs (diameter > 3.4 nm) both methods can be used. The SILAR is the best choice due to the use of less reactive precursors (ZnO and elemental sulfur) and the possibility to afford a fine modulation of the zinc sulfide shell thickness. The reaction temperature in this case has to be high in order to activate the precursors.

The SILAR method is based on the alternative injection of Zn and S precursors in a solution containing CdSe nanocrystals for the growth of CdSe-ZnS core-shell nanocrystals. The amount of precursor is determined by number of surface atoms of a given size of core-shell quantum dots. Because there is about 10% lattice mismatch between CdSe and ZnS bulk crystals, the calculations were based on the wurtzite structure of CdSe nanocrystals. The average thickness of one monolayer of ZnS was taken as 0.31 nm. The first monolayer of ZnS shell would increase the diameter of a CdSe nanocrystal by 0.62 nm. In a typical experiment with 1.6×10^{-4} mmol of 3.4 nm core, 2.74×10^{-2} mmol of Zn and S precursors is needed for the first layer of shell, 3.67×10^{-2} mmol for the second layer and 4.72×10^{-2} mmol for the third layer.
Shell precursors were prepared in two different 20 ml scintillation vials equipped with rubber septa. Zn precursor was prepared by dissolving 0.325 g of ZnO,

0.904 g of OlA and 7.09 g of ODE at 250°C. S precursor was prepared by dissolving elemental Sulfur (12.8 mg) and ODE(7.88 g) at 150°C. During the heating step, both solutions were degassed under reduced pressure and air was replaced with argon. Before injection, the precursors were allowed to cool down at 80°C.

In a typical synthesis CdSe *core* QDs (1.6×10^{-4} mmol, 3.4 nm) dissolved in a minimum amount of chloroform or hexane, were mixed with 1.0 g of ODA, HDA or OlA and 10 g of ODE in a 100 ml three-neck round bottom flask. The mixture was carefully degassed under reduced pressure at 30°C in order to remove all the hexane or chloroform. Once vacuum stabilized, the solution was kept under reduced pressure for 1h and 30min. Additional heating at 120°C for 15 min was performed in order to remove all the traces of dissolved gasses and solvents (e.g. water). After, under argon flow the temperature was further increased at 230°C for the epitaxial growth of the shell. A certain amount of Zn precursor, calculated following the procedure reported above, was injected dropwise. More specifically, the rate of the addition was one drop every two seconds using a syringe equipped with a 22 gauge metal needle. After injection, the solution was maintained at 230°C for 20 minutes before the injection of the second precursor, in this case the S precursor. The operation was repeated until obtaining CdSe-ZnS *core-shell* quantum dots with the desired shell thickness. The reaction was monitored recording absorption and emission spectra of reaction aliquots. During the overcoating quantum dot's emission increased. Purification of the obtained CdSe-ZnS *core-shell* quantum dots were performed as reported above for the CdSe *core* quantum dots.

The one-time precursors injection reaction was reported the first time by Guyott-Sionnest in 1996 and further developed by Dabbousi *et al*. in 1997.[6] This method is based on the injection, in a single addition, of all the precursors required for a certain shell thickness. Diethyl zinc and hexamethyldisila-thiane were used as highly reactive zinc ad sulfur precursors. This method allow to overcoat small CdSe nanocrystals since the reaction temperature is relatively low. The amount of precursors were calculated as reported above for the SILAR method.

In a typical synthesis 13 g of TOPO 90% and 1.3 g of ODA were loaded in a 100 ml three-neck round bottom flask and degassed under reduce pressure at 120°C followed by flushing with argon. Temperature was decreased at 70°C and

hexane solution containing $1.6x\times10^{-4}$ mmol of 3.4 nm CdSe *core* QDs was added to the mixture. The solvent was removed under vacuum and the reaction vessel was further heated at 115°C for 15 minutes in order to remove water eventually presents in the hexane solution. Under argon flow the temperature was further increased at certain value, depending on the size.[6] In the case of 3.4 nm CdSe core the temperature was 150°C. A proper amount of Zn and S precursor (0.1M in TOP) prepared in a nitrogen filled dry box, was injected dropwise. The temperature was set at 150°C for 60 min and then dropped to 90°C for 3 hours in order to allow the aging of the shell on the CdSe *core*. Aliquots were taken out after each steps and absorption and emission spectra were recorded in order to check the quality of the material. Finally the solution was allowed to cool down and chloroform was added. Nanocrystals were purified three times via precipitation using excess of methanol. C*ore-shell* quantum dots were dissolved in minimum amount of chloroform obtaining a concentrated solution (about 15μM). The exact concentration value was estimated from the last maximum in the absorption spectra.[4]

Spectroscopical (absorption, steady state and time resolved emission) and morphological (TEM) characterization of the final material were carried out.

2.3 Electronic Absorption Spectra

All the experiments were carried out at room temperature on air equilibrated solutions of the samples contained in quartz cuvettes (optical path length of 1cm or 0.5cm). The concentration of the solutions was typically 10^{-7} to 10^{-4} M. Absorption spectra in the 190-1100nm range were recorded with Perkin Elmer λ45 spectrophotometer. Absorption spectra reported in Chapter 5 were recorded with Shimadzu UV-2450 spectrophotometer. Varian Cary 50 Bio instrument was used for the experiments at ambient temperature and in which the temperature of the cell holder was thermostated by using a circulating constant temperature bath maintained at required temperature. Occasionally a Perkin Elmer λ650 was used to record spectra in the 190-900nm wavelength range. The precision on the wavelength values was ± 1nm. Extinction coefficient values were determined using the Lambert-Beer law; the experimental error is estimated to be ±5%.
Spectrophotometric titrations were performed by adding with a microsyringe small aliquots (typically 5-20μL) of a concentrated solution (10^{-3} - 10^{-4}M) of titrating species to a known volume of a dilute solution of the titrated species in quartz cuvette.
Spectrophotometric kinetic experiments were performed using Varian Cary 50 Bio spectrophotomer and dilute solution of the compound (10^{-5} - 10^{-6} M). The obtained absorption variations were fitted by means of the SPECFIT software[7] using a suitable kinetic model.

2.4 Luminescence Spectra

Fluorescence emission spectra and excitation spectra in the 250-900nm range were recorded with a Perkin Elmer LS50 spectrofluorimeter equipped with a Hamamatsu R928 photomultiplier. The precision on the wavelength values was ± 2nm. Fluorescence emission spectra reported in Chapter 5 were recorded with Horiba Fluorolog-3 equipped with a TBX-PMT detector. Luminescence spectra were recorded at room temperature (ca 295K) on solutions of samples contained in quartz cuvettes (optical path length 1 cm). In order to compare the luminescence properties of different solutions, corrections on the observed luminescence intensity were made to take into account inner filter effects, geometrical factors (for solution of different absorbances at excitation wavelength), and reabsorption of the emitted light.[8]

2.4.1 LUMINESCENCE QUANTUM YIELD DETERMINATION

Luminescence quantum yields were determined on the solution samples at room temperature (ca. 295K) using a reference compound according to the optically dilute method described by Demas and Crosby.[9] The equation is given by the equation

$$\Phi_S = \Phi_R(A_S/A_R)(n_S/n_R)^2$$

where Φ, A and *n* indicate the luminescence quantum yield, the area subtended by the emission and the refractive index of the solvent used for the preparation of the solution, respectively; the subscripts S and R stand for the sample and reference, respectively. A_S and A_R must be obtained using the appropriate luminescence standard and under the same instrumental conditions; furthermore the sample and the reference must exhibit the same absorption at the excitation wavelength. Different standards were selected depending on the spectral region of interest.[10]

2.4.2 LUMINESCENCE LIFETIME MEASUREMENTS

Lifetime measurements in the range of 0.5ns – 30μs were performed at room temperature (ca 295K) with an Edinburgh Analytical Instruments time-correlated single photon counting equipment. A schematic view of this instrument is reported in Figure 1. The excitation source were a gas discharge lamp (model nF900, filled with nitrogen or deuterium, depending on excitation requirements) delivering pulses of 0.5ns width at a frequency comprised between 1 and 100 kHz, or a pulsed diode laser (406 nm Picoquant). The detector was a photomultiplier tube (Hamamatsu R928P) cooled -20°C and suitably amplified.

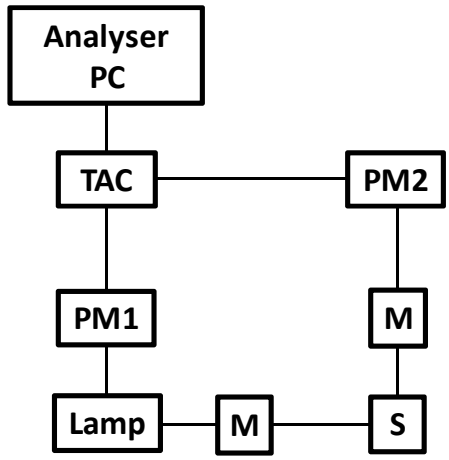

Figure 2.1 Experimental set-up of the single-photon counting equipment. The instrument is made of: a lamp, two monochromators (M) to select the excitation and emission wavelengths, a cell fopr the sample (S), two photomultipliers (PM), a time-to-amplitude converter (TAC) and an anayliser PC

This equipment is based on the TCSPC (time-correlated single-photon countin) technique. The solution of the sample, contained in a cell, is excited by a short pulse of light: the photons emitted by the sample are then revealed by the photomultiplier. The time delay between the excitation pulse and the causal detection of a single photon emitted by the sample as a consequence of the excitation is measured. This individual measured does not give the excited-state lifetime of the examined species, which is by definition a statical parameter. However, by repeating such procedure a large number of times, and by accumulating the signals in different channels according to their delay, it is possible to construct the luminescence decay curve. A multichannel analyzer (MCA) interfaced to a personal computer does this job. The fitting of a single exponential decays gives finally the lifetime value.

Data correlation and manipulation were carried out using EAI F900 software version 6.35. Emission lifetime were calculated using single exponential fitting function; a Levengberg-Marquardt algorithm with iterative reconvolution Edinburgh instruments F900 software was used. The reduced χ^2 and residual plots were used to judge the quality of the fits. The experiments error on lifetime values was estimated to be ± 5%.

2.5 Photochemical Experiments

Photochemical experiments were performed in a spectrophotometric quartz cuvette (1 cm path length) using an Hanau Q400 medium pressure Hg lamp (150 W) coupled with a proper interference filter as light source.

The photochemical experiments describe in Chapter 5 were performed using a photoreactor (Model LZC-4 V, Luzchem Research, Inc., Ottawa, Canada) equipped with 14 UVA lamps with maximum emission wavelength centered at 350nm (4.5 W/cm^2). Reaction vessels were glass scintillation vials with a transmittance of 90% at 310nm and >95% at 350nm.

2.5.1 PHOTOCHEMICAL QUANTUM YIELD DETERMINATION

Photochemical quantum yield was determined on the solution samples at room temperature (ca. 295K) using a chemical actinometer as reference compound. The chemical actinometer was potassium ferrioxalate. The potassium ferrioxalate is the most reliable and practical actinometer for UV and visible light up to 500nm proposed the first time by Hatchard and Parker.[10,11] Under light excitation the potassium ferrioxalate decomposed according to the following equations

$$Fe(C_2O_4)_3^{3-} \xrightarrow{h\nu} Fe^{2+} + C_2O_4^{\cdot-} + 2\,C_2O_4^{2-}$$

$$Fe(C_2O_4)_3^{3-} + C_2O_4^{\cdot-} \rightarrow Fe^{2+} + 2\,CO_2 + 3\,C_2O_4^{2-}$$

The amount of Fe^{2+} formed during the irradiation is monitored by conversion to the colored tris-phenantroline complex with ε = 11100 M^{-1}cm^{-1} at 510 nm. The original Fe^{3+} are not appreciable complexed by phenantroline and the complex does not absorb at 510nm.
The number of incident photons are given by

$$q_{p,in} = \frac{\Delta A(510nm)}{I \times \varepsilon(510nm)} \times \frac{V1 \times V3}{V2} \times \frac{N_A}{\Phi \times t}$$

If the light is not totally absorbed, the equation has to be modified according to the following equation

$$q_{p,in} = \frac{\Delta A(510nm)}{I \times \varepsilon(510nm)} \times \frac{V1 \times V3}{V2} \times \frac{N_A}{\Phi \times t \times (f_{as})_m}$$

where ΔA(510nm) is the optical difference in absorbance between the irradiated solution and that taken at dark, l is the optical path length of the irradiation cell, ε (510 nm) is that of the complex $Fe(phen)_3^{2+}$, V1 is the irradiated volume, V2 is the aliquot of the irradiated solution taken for the determination of the Fe^{2+}, V3 is the final volume after complexation with phenantroline (all in mL), Φ is the yield for the actinometer at a specific irradiation wavelength, t is the irradiation time, N_A is the Avogadro's number and f_{as} is the mean fraction of the light absorbed by the ferrioxalate solution. If the reaction vessel is a common spectrophotometric quartz cell with 1 cm path length containing 3ml of 0.012M ferrioxalate solution, a "micro" version of the same actinometer can be followed.[12] After irradiation, 0.5ml of buffered phenantroline is added to the cell and the absorbance at 510nm measured immediately. In this conditions the previous equation can be simplified

$$q_{p,in} = \frac{\Delta A(510nm)}{t} \times Y \times N_A$$

where Y is a factor containing the yield of the actinometer at a specific irradiation wavelength, the ε of the complex $Fe(phen)_3^{2+}$ at 510nm and the ratio of the volume shown in the previous equation.

The general equation for the photochemical quantum yield is reported below

$$\Phi_P = \frac{\Delta C \times V}{q_{p,in} \times (1 \times 10^{-Am}) \times f \times t}$$

where ΔC is the photoproduct concentration generated during the irradiation experiment and calculated by the ratio $\Delta A/\Delta\varepsilon$, V is the volume of the irradiated solution, $q_{p,in}$ is the intensity of the light source reported in Nhν/min, Am is the mean absorbance between irradiated and not irradiated solution at the irradiation wavelength and t is the irradiation time. The factor f is the fraction of absorbed light and is given by

$$f = \frac{\varepsilon_R \times [R]}{\varepsilon_P \times [P] + \varepsilon_R \times [R]}$$

This factor takes into account the partial absorption of the incident light by the photoproduct. The term ε_P is the molar absorptivity of the photoproduct, ε_R is the absorptivity of the reagent (both value at the irradiation wavelength) and [R] and

[P] are the molar concentration of the reagent and product respectively. The optical path length was omitted since is of 1cm.

2.6 Other Techniques

Transmission Electron Microscope (TEM). A Philips CM 100 transmission electron microscope operating at 80 kV was used for the morphological characterization of quantum dots and for the aggregation study reported in Chapter 4. For the TEM investigation a Formvar® resin film supported on conventional copper microgrids, was dried under vacuum after deposition of a drop of quantum dots solution in hexane.

Fourier Transform Infrared Spectroscopy (FTIR). FTIR-spectra reported in Chapter 5 were recorded with a Perkin Elmer Spectrum 100FT-IR spectrometer.

Gel electrophoresis experiment. The gel electrophoresis experiments reported in Chapter 5 were carried as following. The QDs dispersions in water were diluted in a 20% glycerol, 1X TBE (Tris borate EDTA) and loaded into 1% agarose gel media. The gel experiments were run at 7.5 V/cm using TBE (pH = 8.3) as running buffer for ~ 20min. The image was captured using an High Performance Transilluminator (UVP, Upland, CA) equipped with digital camera.

The *^{1}H NMR* spectra reported in Chapter 5 were collected using a 600 MHz spectrometer (Bruker SpectroSpin 600 MHz).

References and Notes

(1) Peng, Z. a; Peng, X. *J. Am. Chem. Soc.* **2001**, *123*, 183–184.
(2) Yu, W. W.; Peng, X. *Angew. Chem. Int. Ed.* **2002**, *41*, 2368–2371.
(3) Li, J. J.; Wang, Y. A.; Guo, W.; Keay, J. C.; Mishima, T. D.; Johnson, M. B.; Peng, X. *J. Am. Chem. Soc.* **2003**, *125*, 12567–12575.
(4) Yu, W. W.; Qu, L.; Guo, W.; Peng, X. *Chem. Mater.* **2003**, *125*, 2854–2860.
(5) Hines, M. a.; Guyot-Sionnest, P. *J. Phys. Chem.* **1996**, *100*, 468–471.
(6) Dabbousi, B. O.; Mikulec, F. V; Heine, J. R.; Mattoussi, H.; Ober, R.; Jensen, K. F.; Bawendi, M. G. *J. Phys. Chem. B* **1997**, *101*, 9463–9475.
(7) Binstead, R. A. SPECFIT, Spectrum Software Associates, Chapel Hill, NC (USA) **1996**.
(8) Credi, A.; Prodi, L. *Spectrochimica Acta A* **1998**, *54*, 159–170.
(9) Demas, J. N.; Crosby, G. A. *J. Phys. Chem.* **1971**, *75*, 991–1024.

(10) Montalti, M.; Credi, A.; Prodi, L.; Gandolfi, M. T. *Handbook of Photochemistry - Third Edition*; CRC Press: Boca Raton, FL (USA), 2006.
(11) Hatchard, C. G.; Parker, C. a. *Proc. R. Soc. A* **1956**, *235*, 518–536.
(12) Fisher, E. *EPA Newsletters* **1984**, *21*, 33–34.

Chapter 3

Photoinduced memory effect in redox controllable molecular switches

3.1 Introduction

A molecular switch can be defined as any kind of molecule-level systems capable of interconvertion between two or more different states in response to an external stimulus.[1,2] This kind of systems can be in principle used for storing information[3,4] or control the electron flow in metal junction.[5,6] A distinction can be made based on the type of switching process.[7] Molecular device in which the molecule responds to an external stimulus by switching to different thermodynamic states, is under thermodynamic control; the molecule remains in this state, until the stimulus is removed. Molecular device in which the two states are separated by a kinetic barrier, is under kinetic control. That type of switching is common in systems responding to photonic stimulation.[6,8] Kinetic control can operate for different time periods (from picoseconds to years) and the exit from the trapping state can be reached with a second different photonic stimulus.[1]

Mechanically interlocked molecules[9–11] in the form of bi or multi-stable rotaxanes in which the ring component can be switched between different co-conformations in response to external stimuli, are artificial molecular switches.[3,12,13] These systems can find application for the development of responsive surface,[14,15] molecules based muscle and actuators,[16–19] nanovalves for controlled drug delivery,[20,21] molecular electronics[4] and nanoreactors.[22] The operation of these systems is based on the switching mechanism between thermodynamic stable states and there are many example in literature.[23,24] The fulfillment of useful functions from these systems will be possible only if also the rate of the mechanical movements of the ring between the states can be controlled. This approach was recently used to implement ratchet-type mechanism,[25] essential building blocks for the development of molecular motors,[26,27] and is of relevance for the development of sequential logic devices such as flip-flop memories.[28,29] Adjust the shuttling kinetics by modulating the energy barriers using an external stimulus is a necessary step in the development of those systems.[30]

In this study we reported the operation of a molecular switch in the form of a [2]rotaxane. In this molecular level machine, the ring can be shuttling along the dumbbell-shape molecule under redox control and thus can be switched thermodynamically between two states, and the energy barriers between these two states can be controlled kinetically using a photochemical stimulus.

The design of the [2]rotaxanes reported in Figure 3.1 is based on well-studied architectures[31,32] in which the ring component is a cyclobis(paraquat-*p*-phenylene) ($CBPQT^{4+}$) and a dumbbell-shaped molecule containing three functional units: 1) a tetrathiafulvalene (TTF), 2) a dioxynaphtalene moiety (DNP) and 3) an azobenzene unit (AZO) located in between the TTF and DNP units. AZO unit can be reversibly and efficiently switched between its *trans* and *cis* configurations by photochemical stimuli.[33] The rotaxanes have different substituents on azobenzene unit: *trans*-$\mathbf{2}^{4+}$ has methyl groups (3,5,3',5'-tetramethylazobenzene) while *trans*-$\mathbf{4}^{4+}$ has fluorine atoms (3,5,3',5'-tetrafluorineazobenzene). Dumbbell-shaped molecules (*trans*-**1** and *trans*-**3**) have also been studied.

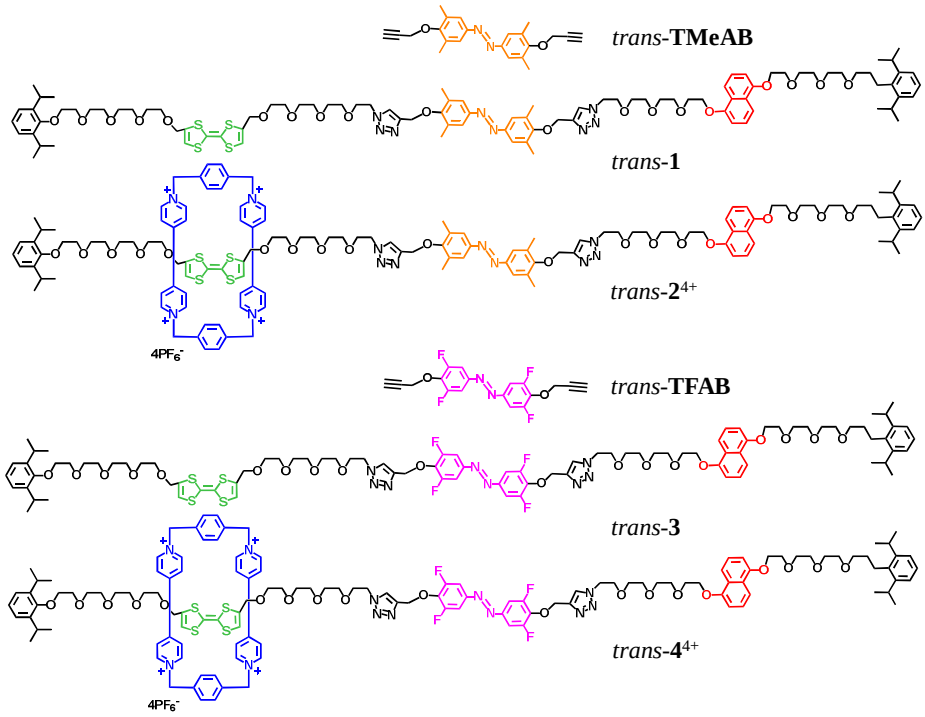

Figure 3.1: Structural formulae of tetramethylated azobenzene (*trans*-**TMeAB**), dumbbell (*trans*-**1**) and rotaxane (*trans*-**2**$^{4+}$) and tetrafluorinated azobenzene (*trans*-**TFAB**), dumbbell (*trans*-**3**) and rotaxane (*trans*-**4**$^{4+}$).

The behaviour of rotaxanes *trans*-**2**$^{4+}$ and *trans*-**4**$^{4+}$ can be briefly summarized as follows (for detailed description se next paragraphs). Initially the CBPQT is positioned on the TTF unit since this is more π-electron-rich than DNP one (*State A*). After oxidation of TTF unit to its radical cation (TTF$^{\bullet+}$) form, CBPQT^{4+} ring shuttles from TTF to the DNP recognition site, across the *trans*-AZO, due to the Coulombic repulsion between the ring and the oxidized TTF unit. Upon reduction of the TTF$^{\bullet+}$ unit to its neutral state, the ring resides on the DNP unit for some time before back-shuttling to TTF recognition site. The lifetime of this metastable state (*State B*) can be controlled by isomerization of the AZO unit from its *trans* to *cis* configuration. This process, which brings a large geometrical change, is capable of affecting substantially the free-energy barrier for the shuttling of the CBPQT^{4+} ring along the dumbbell molecules.[34] In the *cis* configuration AZO unit poses a much larger stearic hindrance to the shuttling of the ring than *trans* azobenzene (Figure 3.2). The system is an example of a flash memory where the information (ring position) written with an

oxidative stimulus (oxidation TTF) is locked using a photochemical input (photoisomerization AZO unit) and remains written even when the stimulus is removed (reduction of $TTF^{\bullet+}$) until the AZO unit is in the *cis* form.

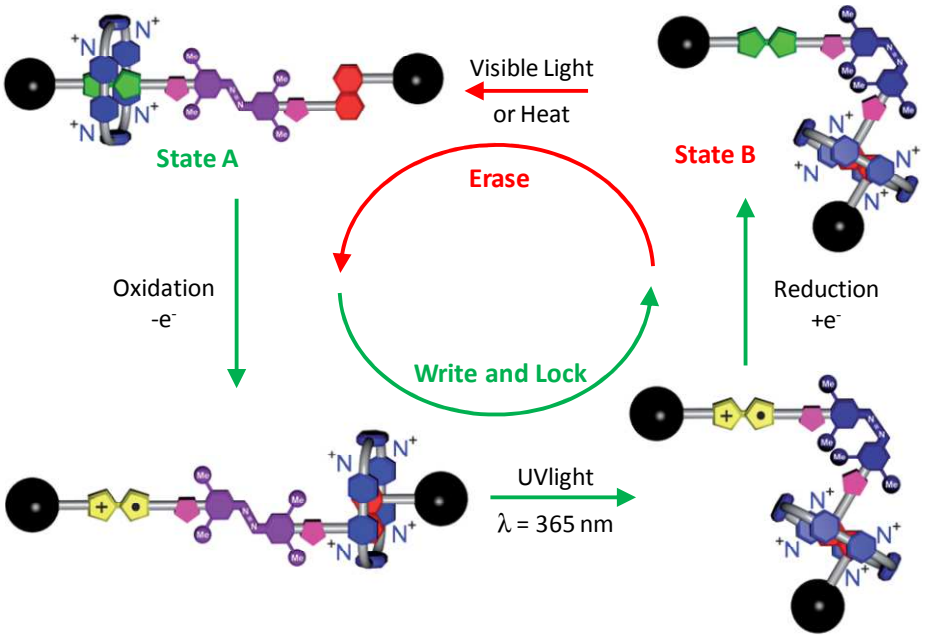

Figure 3.2: General scheme of chemically and photochemically triggered memory switching cycle[35] of the rotaxane *trans*-$\mathbf{2}^{4+}$.

This work was performed in collaboration with the group of Prof. J.F. Stoddart, Nortwestern University, Evanston, Illinois (USA), who made the synthesis of the studied compounds.

3.2 Results and Discussion

3.2.1 ELECTRONIC ABSORPTION SPECTRA

The photophysical and photochemical characterization of the compounds was carried out in air-equilibrated MeCN. The absorption spectra of *trans*-**1**, *trans*-**2**$^{4+}$, *trans*-**3** and *trans*-**4**$^{4+}$ and model compounds *trans*-**TMeAB** and *trans*-**TFAB** are shown in Figure 3.3. Photophysical and photochemical data are gathered in Table 3.1.

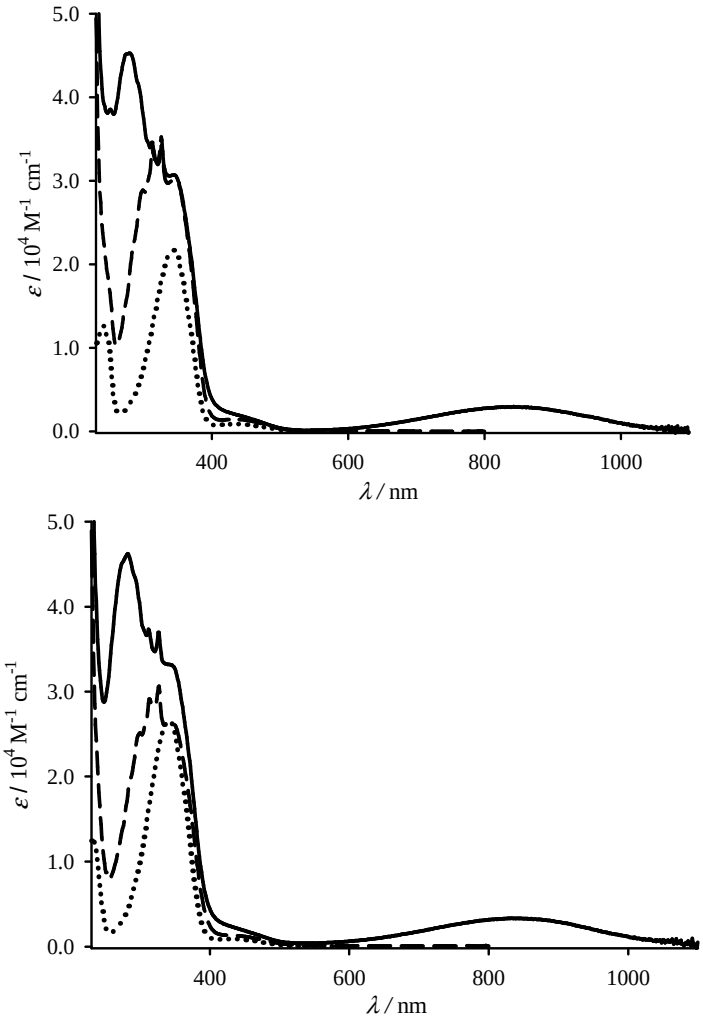

Figure 3.3:Top, absorption spectra of *trans*-**TMeAB** (•••), *trans*-**1**(- - -), and *trans*-**2**$^{4+}$(—). Bottom, absorption spectra of *trans*-**TFAB** (•••), *trans*-**3** (- - -), and *trans*-**4**$^{4+}$(—).

The absorption spectra of model compounds *trans*-**TMeAB** and *trans*-**TFAB** show the typical absorption band of azobenzene around 347 nm (π–π* band) and 436 nm (*n*-π* band).Typical π–π* and *n*–π* bands can be recognize in the absorption spectra of the two dumbbell compounds *trans*-**1** and *trans*-**3**. The two spiky peaks at 313 nm and 326 nm are due to the vibronic structure of the binaphtyl absorption.

In the absorption spectra of the two rotaxanes *trans*-$\mathbf{2}^{4+}$ and *trans*-$\mathbf{4}^{4+}$, all the features of the dumbbell molecules are presents, while the band at 280 nm is due to the bipyridinium dication units ($BIPY^{2+}$) of the $CBPQT^{4+}$ and the broad band with maximum at 850 nm (*trans*-$\mathbf{2}^{4+}$) and 837 nm (*trans*-$\mathbf{4}^{4+}$) is attributable to the charge transfer complex between the TTF unit and BPY units of the ring. This latter finding also evidences that the ring encircles the TTF unit in agreement with its electron donor properties better than DNP.

3.2.2 PHOTOISOMERIZATION OF AZOBENZENE UNIT

Photochemical isomerization of azobenzene units present in all the dumbbells, rotaxanes and model compounds were performed using the 365 nm or 436 nm wavelength of a medium pressure Hg vapor lamp, selected using an appropriate interference filter.

Irradiation of *trans*-$\mathbf{2}^{4+}$ with 365 nm causes the *trans*-*cis* photoisomerization of the TMeAB unit with a quantum yield of 0.14, comparable with the one obtained for the *trans*-**1**. The yield is slightly lower than the one obtained for the *trans*-**TMeAB**. In the case of *trans*-$\mathbf{4}^{4+}$ the quantum yield is 0.17 and comparable with those obtained for both *trans*-**3** and *trans*-**TFAB**. Upon exhaustive irradiation, more than 90% of the *trans* form can be converted to the *cis* form. This photoreaction affects neither the CT band centered at 850 nm ($\mathbf{2}^{4+}$) and 837 nm ($\mathbf{4}^{4+}$) and the DNP sharp features at around 320 nm. The first order rate constant for the thermal *cis*-*trans* back isomerization of the AZO unit is 7.5×10^{-6} s^{-1} for *cis*-$\mathbf{2}^{4+}$ and 9×10^{-6} s^{-1} for *cis*-$\mathbf{4}^{4+}$. All these values are of the same order of magnitude of those obtained for the dumbbell molecules (*cis*-**1** and *cis*-**3**) and the model compounds (*cis*-**TMeAB** and *cis*-**TFAB**). These observations also indicate that the presence of the $CBPQT^{4+}$ ring does not influence the isomerization of the AZO gate and the *trans*-*cis* conversion of the photoisomerizable unit does not have an impact on the distribution of the $CBPQT^{4+}$ ring between the TTF and DNP recognition sites in both rotaxanes.

The spectroscopic parameters of the *trans* and *cis* form of all the compounds, the photochemical quantum yield and the kinetic constants for thermal isomerization are reported in Table 3.1.

	Absorption		Photochemical isomerization	Thermal isomerization
	λ (nm)	ε (M^{-1} cm^{-1})	Φ	$k_{c\rightarrow t}$ (s^{-1})
trans-**TMeAB**	347 436	21600 860	0.33[a]	—
cis-**TMeAB**[b]	295 440	5300 1500	0.66[c]	4.1×10^{-6}
trans-**1**	299 313 326	28900 33700 35200	0.18[a]	—
cis-**1**[b]	296 312 325 438	27500 25400 18200 2600	*d*	6.0×10^{-6}
trans-$\mathbf{2}^{4+}$	281 313 326 350 440 850	45500 35000 34500 30400 2500 3100	0.14[a]	—
cis-$\mathbf{2}^{4+}$ [b]	272 326 440 850	47500 20300 3300 3000	*d*	7.5×10^{-6}
trans-**TFAB**	343 437	21700 870	0.19[a]	—
cis-**TFAB** [b]	294 434	5700 1740	0.44[c]	2.9×10^{-6}
trans-**3**	299 313 326 345	26300 30400 31900 27300	0.14[a]	—
cis-**3** [b]	295 312 325 435	24600 22500 16400 2300	*d*	6.97×10^{-6}
trans-$\mathbf{4}^{4+}$	282 312 326 350 445 837	33700 27200 26900 23500 1570 2400	0.17 [a]	—
cis-$\mathbf{4}^{4+}$	280 325 430 837	34400 14800 2400 2400	*d*	9×10^{-6}

Table 3.1:Photophysical and photochemical parameters for the investigated compounds in air-equilibrated acetonitrile. [a]*trans*→*cis* photoisomerization quantum yield; λ_{irr} = 365nm. [b]Data referred to the photostationary state obtained upon exhaustive 365nm-irradaition and containing >90% of the *cis* isomer. [c]*cis*→*trans* photoisomerization quantum yield; λ_{irr} = 436nm. [d]Not performed

3.2.3 SHUTTLING OF CBPQT^{4+} RING ALONG THE AXLE

Mono-oxidation of the TTF unit to its radical cation TTF$^{\bullet+}$ was performed using 1eq of $Fe(ClO_4)_3$. Upon chemical oxidation of *trans*-**2**$^{4+}$ and *trans*-**4**$^{4+}$, *trans*-**2**$^{5+}$ and *trans*-**4**$^{5+}$ are generated quantitatively. In Figure 3.5 are reported the absorption variations of *trans*-**2**$^{4+}$ and *trans*-**4**^{4} upon addition of $Fe(ClO_4)_3$. The typical TTF$^{\bullet+}$ bands with maximum at 447 nm and 600 nm appear. The charge transfer band between TTF and CBPQT^{4+} disappears due to the destabilization of the charge transfer interaction between TTF$^{\bullet+}$ and the two BIPY^{2+} unit of the CBPQT^{4+}. Moreover the sharp DNP peaks around 320 nm are no longer present, an observation which indicates that the CBPQT^{4+} ring moves to the DNP recognition site upon mono-oxidation of the tetrathiafulvane unit site on account of the Coulombic repulsion between the ring and the oxidized TTF unit, as reported for similar systems.[31,32,36] The general scheme of rotaxane oxidation and shuttling is reported in Figure 3.4.

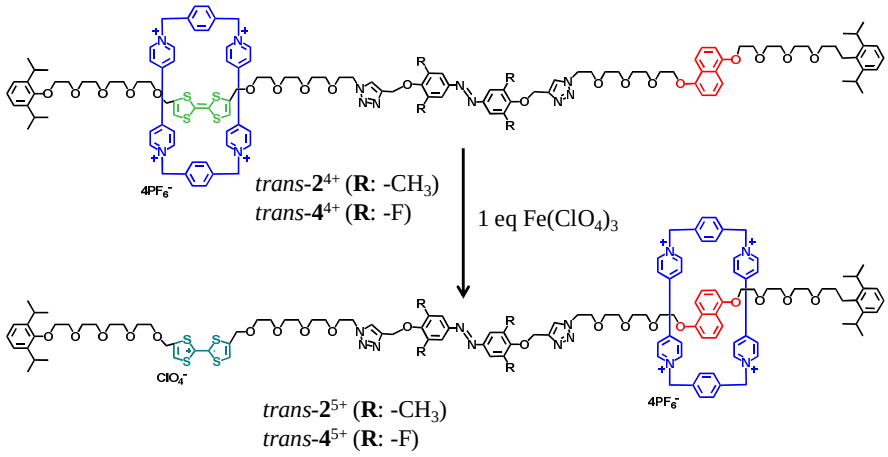

Figure 3.4 Reaction scheme of rotaxane oxidation and shuttling upon addition of 1 equivalent of $Fe(ClO_4)_3$

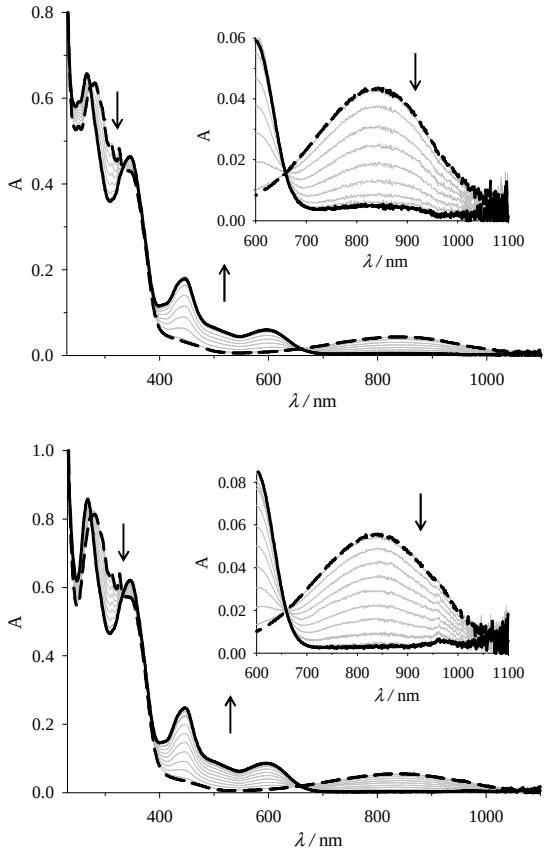

Figure 3.5 Top, absorption variations upon addition of 1eq of $Fe(ClO_4)_3$ to a 2.5 ml 11μM solution of *trans*-$\mathbf{2}^{4+}$ (- - -) to obtain *trans*-$\mathbf{2}^{5+}$(—). Bottom, absorption variations upon addition of 1eq of $Fe(ClO_4)_3$ to a 2.3 ml 21 μM solution of *trans*-$\mathbf{4}^{4+}$ (- - -) to obtain *trans*-$\mathbf{4}^{5+}$(—). In both figures, inset picture shows theTTF-$CBPQT^{4+}$ charge transfer band region.

The oxidation of TTF unit in dumbbell models *trans*-**1** and *trans*-**3** shows the typical $TTF^{\bullet+}$ bands with maximum at 447 nm and 600 nm (Figure 3.6). No effect was observed in the vibronic peak of DNP unit since no ring containing $BIPY^{2+}$ units is present. This observation is indicative of the charge transfer complex between $CBPQT^{4+}$ and DNP, consequence of ring shuttling from $TTF^{\bullet+}$ to DNP in *trans*-$\mathbf{2}^{4+}$ and *trans*-$\mathbf{4}^{4+}$. In the case of *trans*-**3**, the oxidation of TTF unit causes the increasing of a not addressable band at around 750nm. This band is reversible with the reduction and it is not present in the *trans*-$\mathbf{4}^{4+}$.

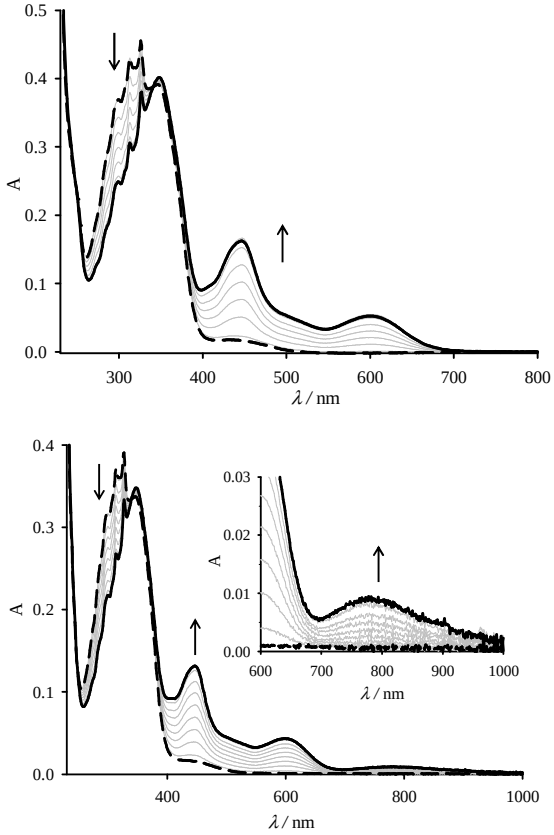

Figure 3.6 Top, absorption variations upon addition of 1eq of $Fe(ClO_4)_3$ to a 2.5 ml 11.3μM solution of *trans*-**1**(- - -) to obtain *trans*-**1**$^{1+}$(—). Bottom, absorption variations upon addition of 1eq of $Fe(ClO_4)_3$ to a 2.25 ml 13.6μM solution of *trans*-**3** (- - -) to obtain *trans*-**3**$^{1+}$(—); inset picture shows the region of the not-addressed band arising during TTF mono-oxidation.

The reduction of $TTF^{\bullet+}$ was performed using decamethyl ferrocene ($Me_{10}Fc$). The reduction is quantitative and fast. In *trans*-**2**$^{4+}$ the intensity of the charge transfer band between TTF and $BIPY^{2+}$ is completely restored while in the case of *trans*-**4**$^{4+}$ there is a slight difference between the intensity before and after the oxidation/reduction cycle. The DNP features are fully restored after the reduction step. These two observations confirm the back shuttling of the $CBPQT^{4+}$ ring from the DNP unit to the TTF one. The product of $Me_{10}Fc$ oxidation has two absorption band at 280 nm and 320 nm with relatively high epsilon values (ε_{280}=16360 $M^{-1}cm^{-1}$ and ε_{320}=10680 $M^{-1}cm^{-1}$) and small band at 790 nm (ε=540 $M^{-1}cm^{-1}$). The contribution of decamethyl ferrocinium ($Me_{10}Fc^{+}$)

was substracted from the spectra recorded after each addition of reducing agent.[37] In Figure 3.7 are reported the corrected absorption spectra of both rotaxanes *trans*-**4**$^{5+}$ and *trans*-**2**$^{5+}$ during the reduction with $Me_{10}Fc$.

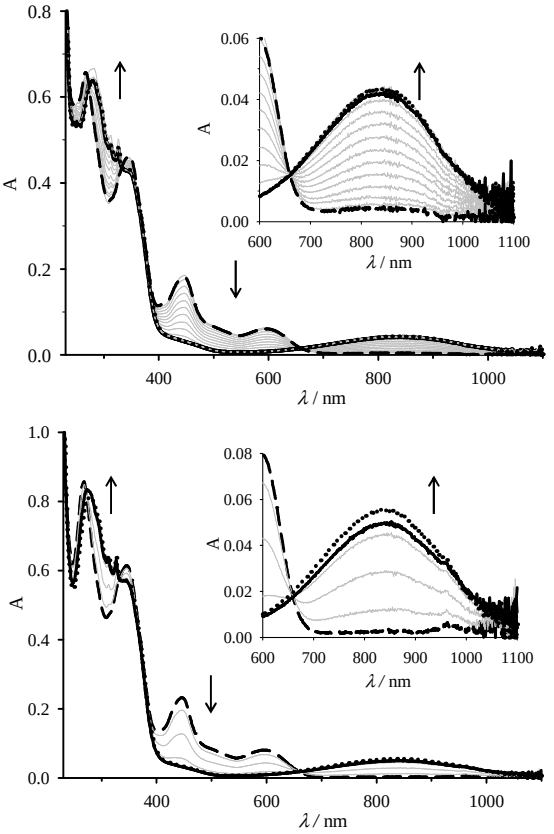

Figure 3.7 Top, absorption variations upon addition of 1eq of $Me_{10}Fc$ to a 2.5 ml 11μM solution of *trans*-**2**$^{5+}$ (- - -) to obtain *trans*-**2**$^{4+}$(—); dotted line (•••) is referred to initial *trans*-**2**$^{4+}$ before oxidation/reduction cycle. Bottom, absorption variations upon addition of 1eq of $Me_{10}Fc$ to a 2.3ml 21μM solution of *trans*-**4**$^{5+}$ (- - -) to obtain *trans*-**4**$^{4+}$(—); dotted line (•••) is referred to initial *trans*-**4**$^{4+}$ before oxidation/reduction cycle. In both figures, inset picture shows theTTF-CBPQT^{4+} charge transfer band region.

The oxidation/reduction cycle performed on *trans*-**2**$^{4+}$ and *trans*-**4**$^{4+}$ shows that the ring shuttling along the axle is quantitative and fully reversible. The presence of AZO unit in the *trans* form does not influence the ring shuttling

3.2.4 SHUTTLING OF CBPQT^{4+} RING AND TRANS-CIS AZOBENZENE PHOTOISOMERIZATION

The experiments reported in the previous paragraph show that the shuttling of the ring along the axle occurs without any interference due to the presence of *trans*-azobenzene unit between the two recognition sites. AZO unit can be photoisomerized *trans* to *cis* and thermally back isomerized *cis* to *trans* without interference due to the presence of the CBPQT^{4+} ring.

In the following paragraph the first part of the redox and light induced switching (Figure 3.2) is reported. Specifically, the azobenzene *trans-cis* photoisomerization was performed after CBPQT^{4+} shuttling (TTF oxidation) and *cis-trans* thermal isomerization was evaluated. The experiment was carried out for both rotaxanes *trans*-**2**$^{4+}$ and *trans*-**4**$^{4+}$ and compared with the dumbbell molecules *trans*-**1** and *trans*-**3**.

Upon addition of 1eq of $Fe(ClO_4)_3$, TTF was oxidized to TTF$^{\bullet+}$ and CBPQT^{4+} shuttling to DNP unit happened quantitatively and immediately (Figure 3.5 and 3.6). Then AZO unit was photoisomerized *trans* to *cis* using 365 nm light and the absorption variation of π–π^* band in the dark, which corresponds to the thermal *cis-trans* isomerization, was monitored. Absorption parameters, photochemical quantum yield and kinetic constants of the investigated compounds are reported in Table 3.2.

Irradiation of *trans*-**2**$^{5+}$ gives a photostationary state with circa 80% of *cis* rotaxane (Figure 3.8) while the irradiation of *trans*-**4**$^{5+}$ gives a PSS with circa 90% of *cis*-**4**$^{5+}$ (Figure 3.9). *Cis* to *trans* isomerization for *cis*-**2**$^{5+}$ is almost one order of magnitude faster than *cis*-**4**$^{5+}$; kinetic constants are 9.74×10^{-4} s^{-1} and 1.172×10^{-4} s^{-1} respectively. These results are consistent with those obtained for the corresponding dumbbell molecule where the *cis* to *trans* isomerization of *cis*-**1**$^{1+}$ is one order of magnitude higher than the one of *cis*-**3**$^{1+}$. No effects are observed in the TTF-CBPQT^{4+} band region during the irradiation period and *cis-trans* thermal isomerization. The region around 320 nm where the sharp features of the DNP unit were initially presents before oxidation, does not show any change. This observation suggests that CBPQT^{4+} ring does not change position during irradiation of the AZO unit and the charge transfer complex between CBPQT^{4+} and DNP is still present even after the thermal back-isomerization

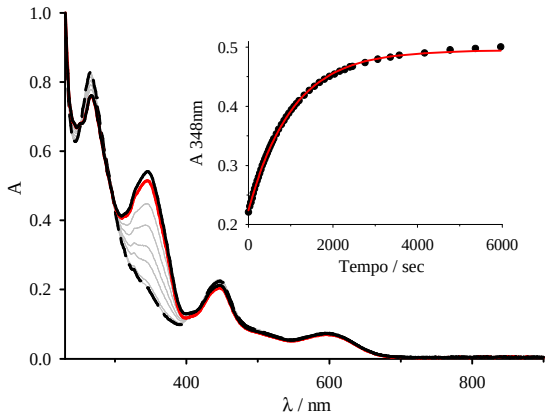

Figure 3.8 Absorption variation during irradiation of 3.0 ml 16.6 μM solution of *trans*-**2**$^{5+}$ and thermal *cis*-*trans* isomerization. *trans*-**2**$^{5+}$ (—), *cis*-**2**$^{5+}$ **(- - -**, PSS ~80% *cis* form) and *trans*-**2**$^{5+}$ after thermal back- isomerization (—). Inset picture: time dependent absorption changes at 348 nm upon leaving the irradiated solution in the dark. The data fitting (red line) according to a first order kinetic equation gives $k_{c\text{-}t}=9.67\times10^{-4}$ s^{-1}

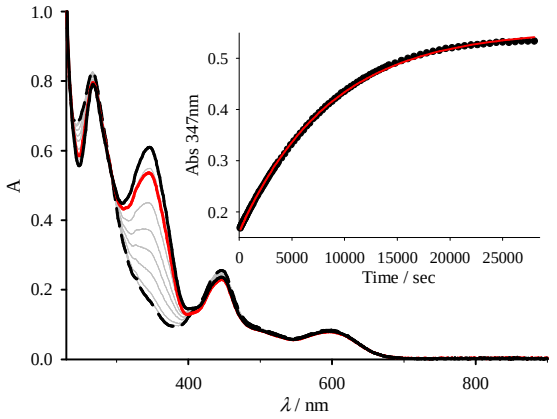

Figure 3.9 Absorption variation during irradiation of 2.5 ml 17.0 μM solution of *trans*-**4**$^{5+}$ and thermal *cis*-*trans* isomerization. *trans*-**4**$^{5+}$ (—), *cis*-**4**$^{5+}$ **(- - -**, PSS ~90% *cis* form) and *trans*-**4**$^{5+}$ after thermal back- isomerization (—). Inset picture: time dependent absorption changes at 348 nm upon leaving the irradiated solution in the dark. The data fitting (red line) according to a first order kinetic equation gives $k_{c\text{-}t}=1.172\times10^{-4}$ s^{-1}

Exhaustive irradiation of both dumbbell molecules, gives different results. In the case of *trans*-**1**$^{1+}$ (Figure 3.10) the resulted photostationary states is rich of circa 75% of the *cis* isomers while in the case of *trans*-**3**$^{1+}$ (Figure 3.11) more than 90% of the initial molecules can be converted to the *cis* form. Kinetics constant measured during thermal *cis* to *trans* isomerization are substantially different. In

the case of *cis*-$\mathbf{1}^{1+}$ the kineric constant (3.50×10^{-3} s^{-1}) is of one order of magnitude bigger than the one obtained for *cis*-$\mathbf{3}^{1+}$ (3.75×10^{-4} s^{-1}). The final spectra after *cis-trans* thermal isomerization (red line) is not perfectly superimposable with the initial one.

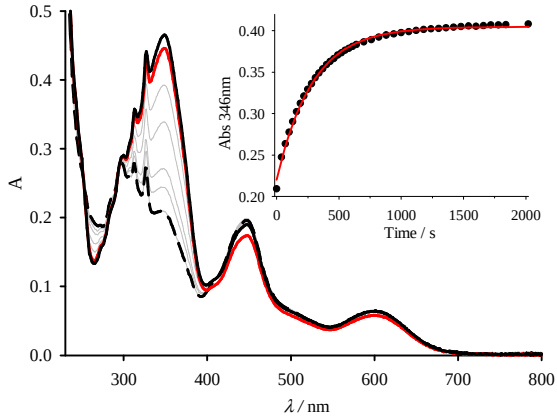

Figure 3.10. Absorption variation during irradiation of 2.5 ml 15 μM solution of *trans*-$\mathbf{1}^{1+}$ and thermal *cis-trans* isomerization. *trans*-$\mathbf{1}^{1+}$ (—), *cis*-$\mathbf{1}^{1+}$ (- - -, PSS~75% *cis* form) and *trans*-$\mathbf{1}^{1+}$ after thermal back- isomerization (—). Inset picture: time dependent absorption changes at 346 nm upon leaving the irradiated solution in the dark. The data fitting (red line) according to a first order kinetic equation gives $k_{c\text{-}t}=3.50\times10^{-3}$ s^{-1}

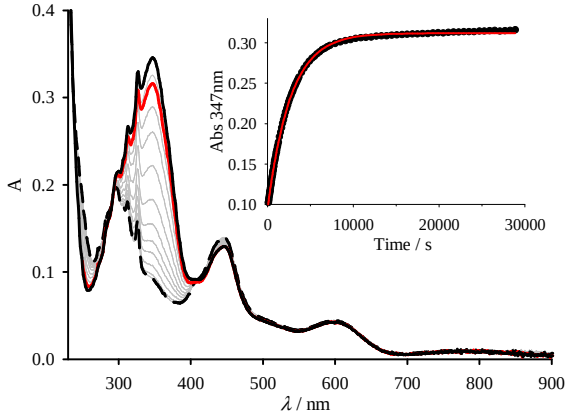

Figure 3.11 Absorption variation during irradiation of 2.25 ml 13.6 μM solution of *trans*-$\mathbf{3}^{1+}$ and thermal *cis-trans* isomerization. *trans*-$\mathbf{3}^{1+}$ (—), *cis*-$\mathbf{3}^{1+}$ (- - -, PSS >90% *cis* form) and *trans*-$\mathbf{3}^{1+}$ after thermal back-isomerization (—). Inset picture: time dependent absorption changes at 347 nm upon leaving the irradiated solution in the dark. The data fitting (red line) according to a first order kinetic equation gives $k_{c\text{-}t}=3.75\times10^{-4}$ s^{-1}

	Absorption		Photochemical isomerization	Thermal isomerization
	λ (nm)	ε (M^{-1} cm^{-1})	Φ	$k_{c\rightarrow t}$ (s^{-1})
trans-**1**$^{1+}$	300 313 348 448 600	19500 23900 31000 12700 3800	0.1[a]	—
cis-**1**$^{1+}$[b]			*c*	3.5×10^{-3}
trans-**2**$^{5+}$	267 345 447 599	47500 33000 12900 4300	0.16[a]	—
cis-**2**$^{5+}$ [b]			*c*	9.7×10^{-4}
trans-**3**$^{1+}$	299 313 326 345	26300 30400 31900 27300	0.19[a]	—
cis-**3**$^{1+}$ [b]			*c*	3.76×10^{-4}
trans-**4**$^{5+}$	282 312 326 350 445 837	33700 27200 26900 23500 1570 2400	0.11 [a]	—
cis-**4**$^{5+}$			*c*	1.172×10^{-4}

Table 3.2:Photophysical and photochemical parameters of the investigated compounds after oxidation with 1 equivalent of $Fe(ClO_4)_3$ in air-equilibrated acetonitrile. [a]*trans→cis* photoisomerization quantum yield; λ_{irr} = 365 nm. [b]Data referred to the photostationary state obtained upon exhaustive 365 nm-irradaition. [c]Not performed

The photochemical *trans-cis* quantum yield of all the compounds where the TTF is oxidixed to the monocationic form, are comparable with those obtained for the initial compounds (Table 3.1). This means that the presence of the $TTF^{\bullet+}$ and the ring on the DNP unit do not influence the azobenzene photoisomerization. Conversely, thermal *cis-trans* isomerization is faster. In the case of *cis*-**1**$^{1+}$ the kinetic constant is almost three order of magnitude faster than *cis*-**1**, while in the case of *cis*-**2**$^{5+}$ is just two order of magnitude. In the case of the *cis*-**3**$^{1+}$ and *cis*-**4**$^{5+}$ the kinetic constant is two order of magnitude faster than the *cis*-**3** and *cis*-**4**$^{4+}$. This speed up is probably due to electronic effects of the $TTF^{\bullet+}$ on the azobenzene unit.[33]

Another reason of this speed up of the *cis-trans* isomerization in the rotaxanes could be the electronic repulsion between the $BIPY^{2+}$ units of the ring and the $TTF^{\bullet+}$. When the azobenzene is in *cis* configuration, the two arms of the rotaxane, one with the ring involved in the charge transfer complex with DNP and the second arm with the $TTF^{\bullet+}$, are closer.[38] This repulsion might have a mechanical effect on the *cis* azobenzene, resulting in a substantially speeding up of the thermal *cis* to *trans* isomerization. This explanation is true in the case of the rotaxanes but not for the dumbbell molecules.

3.2.5 MEMORY SWITCHING CYCLE ON *trans*-2^{4+}

The last paragraph shows the possibility to isomerize the azobenzene unit in the rotaxane with TTF mono-oxidized and ring located on DNP unit. The next step was the reset of all the redox stimulus in order to lock the system in the metastable state (*State B*, Figure 3.2). Reduction using 1eq of $Me_{10}Fc$ affords the fast and quantitative reduction of the $TTF^{\bullet+}$ with the ring trapped on the DNP side and consequently the rotaxane in the *State B* (Figure 3.2). The lifetime of this metastable state depends on the nature of the substituent on the AZO unit.
The results of the "write-lock-erase" experiment for the *trans*-$\mathbf{2}^{4+}$ are summarized in Figure 3.12.

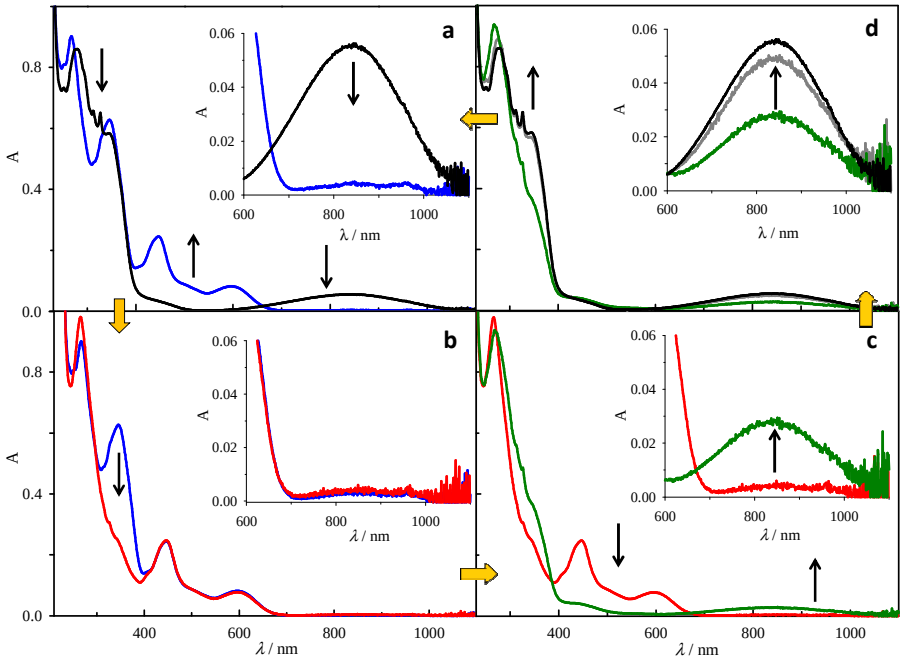

Figure 3.12: Changes in the absorption spectrum observed in MeCN at 295 K for 19 μM solution of *trans*-$\mathbf{2}^{4+}$ (black trace) resulting from the following sequence of operations: a) oxidation with up to 1 equivalent of $Fe(ClO_4)_3$ to obtain *trans*-$\mathbf{2}^{5+}$(blue trace); b) exhaustive irradiation at 365 nm to obtain *cis*-$\mathbf{2}^{5+}$ (red trace); c) reduction with 1 equivalent of $Me_{10}Fc$ to obtain *cis*-$\mathbf{2}^{4+}$ (green trace); d) equilibration in the dark to obtain *trans*-$\mathbf{2}^{4+}$ (grey trace). The absorption bands of the $Me_{10}Fc^{+}$ cation, generated in reaction between $\mathbf{2}^{5+}$ and $Me_{10}Fc$, were arithmetically substracted from the spectra shown as green and grey traces.[37]

The addition of 1 equivalent of Fe^{3+} ions to *trans*-$\mathbf{2}^{4+}$ yields *trans*-$\mathbf{2}^{5+}$ quantitatively, leading (Figure 3.12a) the shuttling of the $CBPQT^{4+}$ ring from $TTF^{\bullet+}$ onto the DNP recognition site, as previously shown. Exhaustive irradiation of this solution at 365 nm causes the *trans*-*cis* isomerization of the TMeAB unit (Figure 3.12b); at the photostationary state we estimate that azobenzene unit gate has been closed in 72% of the rotaxane molecules. Following the successive addition of 1 equivalent of $Me_{10}Fc$ to reduce the *cis*-$\mathbf{2}^{5+}$ back to *cis*-$\mathbf{2}^{4+}$(Figure 3.12c) an analysis of the absorption bands shows that about 53% of the $CBPQT^{4+}$ rings remain trapped on the DNP recognition site, while 47% of the rings have shuttled back to the regenerated neutral TTF site. Such a partial trapping is a result of the fact that the *trans*-*cis* photoisomerization is incomplete (the ring can freely shuttle back to the TTF recognition site in 28% of the rotaxane molecules) and some *cis*-*trans* thermal isomerization can occur while the chemical reduction is being performed. As reported in the previous paragraphs, the thermal *cis*-*trans* isomerization is accelerated substantially when the nearby TTF unit is oxidized and consequently the reduction of *cis*-$\mathbf{2}^{5+}$ has to be performed quickly and efficiently. The absorption spectrum of *trans*-$\mathbf{2}^{4+}$ is regenerated after 30 h in the dark (Figure 3.12d). The TTF-$CBPQT^{4+}$ charge transfer band with maximum at 850 nm, DNP features at around 320 nm and the π–π* band of the *trans*-TMeAB unit at 350 nm are almost restored indicating that azobenzene gate has opened and the $CBPQT^{4+}$ ring has shuttled back to its original position.

The time analysis of the spectral changes in Figure 3.12d provides information about the effectiveness of the kinetic trapping exerted by the *cis*-TMeAB gate.

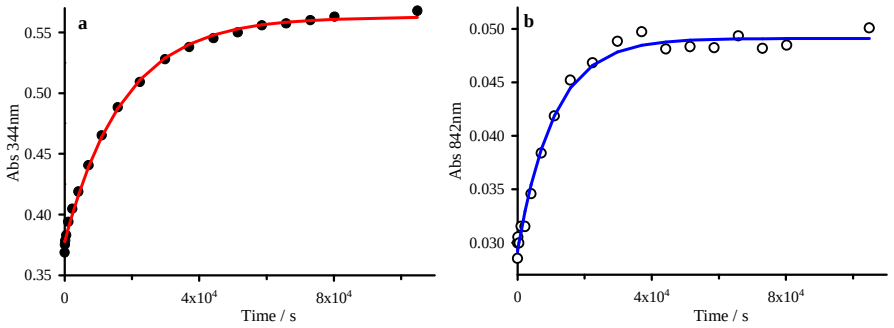

Figure 3.13. Time dependent absorption variation monitored at a) 344 nm (π–π* *trans*-TMeAB band) and b) 842 nm (TTF-CBPQT^{4+} CT absorption band) after fast reduction of *cis*-**2**$^{5+}$.The corresponding absorption spectra are reported in Figure 3.12d.

The rate constants for the recovery of the *trans*-TMeAB absorption band (Figure 3.13a) and TTF-CBPQT^{4+} (Figure 3.13b) charge transfer band are 5.7×10^{-5} s^{-1} and 9.3×10^{-5} s^{-1} respectively. These two constants are comparable and this observation indicates that the two processes happens at the same time scale. This means that in *cis*-**2**$^{4+}$ the CBPQT^{4+} ring cannot shuttle from DNP to TTF site over the *cis*-TMeAB unit and the relaxation rate from the metastable state *State B* to the *State A* (Figure 3.2) is determined by the rate of the thermal opening of the gate (*cis-trans* thermal isomerization of TMeAB). The data remain stored for few hours in the dark at room temperature until the thermal opening of the azobenzene gate occurs.

It is also interesting to note that the rate of thermal *cis* to *trans* conversion of the azobenzene depends on the position of the CBPQT^{4+} ring. If the ring is on the TTF unit, the *trans* azobenzene is regenerated with $k = 7.5\times10^{-6}$ s^{-1} whereas the rate is $k = 5.7\times10^{-5}$ s^{-1} when the ring is on the DNP. The difference is almost one order of magnitude.

We inverted the order of the two inputs by performing fast oxidation of the TTF unit after photochemical closure of the gate with the aim to confirm the memory behavior and investigate the hampering effect of the *cis*-azobenzene gate on the shuttling motion. The results show that the addition of $Fe(ClO_4)_3$ at the photostationary state containing 70% *cis*-**2**$^{4+}$ and 30% *trans*-**2**$^{4+}$ causes immediate and quantitative oxidation of *trans*-**2**$^{4+}$ followed by ring shuttling to the DNP site, whereas *cis*-**2**$^{4+}$ is oxidized on a much slower time scale. It is difficult to establish the position of the CBPQT^{4+} ring after chemical oxidation

of *cis*-**2**$^{4+}$ since the *cis-trans* isomerization occurs on a time scale comparable with that of the chemical oxidation. The results of that experiments are reported in Figure 3.14.

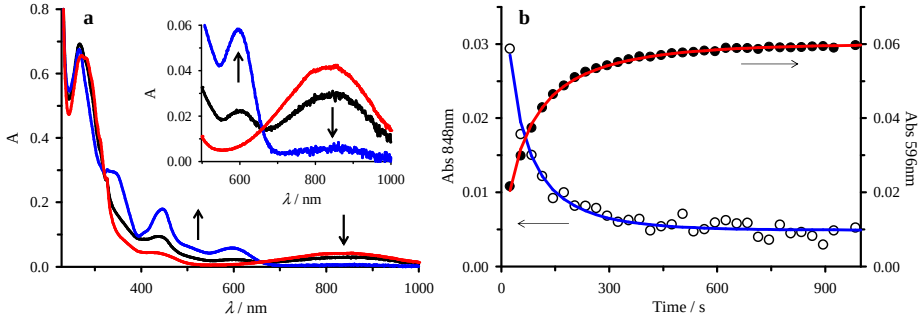

Figure 3.14. a) Absorption spectra of a solution containing ca. 75% *cis*-**2**$^{4+}$ obtained upon exhaustive irradiation of 11 μM *trans*-**2**$^{4+}$ at 365 nm, before (red line) and immediately after the addition of 1 equivalent of $Fe(ClO_4)_3$ (black line). The solid blue line shows the absorption spectrum observed 10 minutes after the addition of the oxidant, when the changes were completed. Inset picture shows the CBPQT^{4+}-TTF CT band region. b) Time dependent absorption changes at 596 nm (TTF$^{\bullet+}$ band, black circles) and 848 nm (CBPQT^{4+}-TTF CT band, white circles). The solid line result from the data fitting according to a second order kinetic equation (k = 2.3×10^3 and 1.4×10^3 $M^{-1}s^{-1}$ for 596 and 848 nm signals respectively)

This reluctance of the TTF unit to be oxidized might came from the fact that the movement of the CBPQT^{4+} ring away from the oxidized TTF unit may be hindered kinetically by the presence of the *cis*-TMeAB unit. The entrapment of the CBPQT^{4+} ring on the TTF side by *cis*-TMeAB unit could hinder the oxidation for both themodynamic (increasing of the potential for the oxidation) and kinetic (molecular encapsulation) reasons.[38] The reluctance of *cis*-**2**$^{4+}$ to become oxidized relative to *trans*-**2**$^{4+}$ can be exploited as a photoinduced write-protection mechanism in which the *trans-cis* isomerization renders the rotaxane less reactive towards chemical oxidation.

3.2.6 MEMORY SWITCHING CYCLE ON *trans*-4^{4+}

Memory switching cycle successfully performed on *trans*-**2**$^{4+}$ and shown in the previous paragraph, was also performed for *trans*-**4**$^{4+}$ rotaxane. The oxidation-irradiation-reduction experiment on *trans*-**4**$^{4+}$ is reported in Figure 3.15.

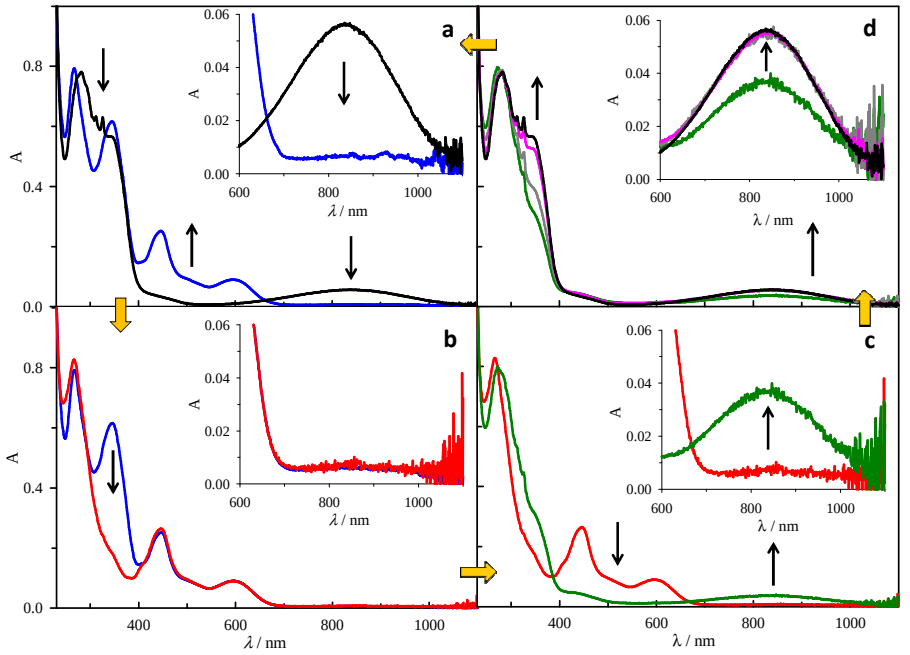

Figure 3.15: Changes in the absorption spectrum observed in MeCN at 295 K for 17 μM solution of *trans*-**4**$^{4+}$ (black trace) resulting from the following sequence of operations: a) oxidation with up to 1 equivalent of $Fe(ClO_4)_3$ to obtain *trans*-**4**$^{5+}$(blue trace); b) exhaustive irradiation at 365 nm to obtain *cis*-**4**$^{5+}$ (red trace); c) reduction with 1 equivalent of $Me_{10}Fc$ to obtain *cis*-**4**$^{4+}$ (green trace); d) equilibration in the dark after 20" (grey trace) and 20 h (pink trace) to obtain *trans*-**4**$^{4+}$. The absorption bands of the $Me_{10}Fc^{+}$ cation, generated in reaction between **4**$^{5+}$ and $Me_{10}Fc$, were arithmetically substracted from the spectra shown as green and grey traces.[37]

The addition of 1 equivalent of $Fe(ClO_4)_3$ to *trans*-**4**$^{4+}$ yields *trans*-**4**$^{5+}$ quantitatively and induces the shuttling of the CBPQT^{4+} ring from TTF$^{\bullet+}$ to the DNP unit (Figure 3.15a). Exhaustive irradiation of this solution at 365 nm causes the *trans-cis* isomerization of the TMeAB unit (Figure 3.15b); at the photostationary state we estimate that the azobenzene unit gate has been closed in 90% of the rotaxane molecules. Following the successive addition of 1.1

equivalents of $Me_{10}Fc$ to reduce the *cis*-**4**$^{5+}$ back to *cis*-**4**$^{4+}$ (Figure 3.15c) an analysis of the CBPQT^{4+}-TTF CT absorption bands shows that about 36% of the CBPQT^{4+} rings remain trapped on the DNP recognition site, while 64% of the rings shuttle back to the regenerated neutral TTF site. The initial intensity of the TTF-CBPQT^{4+} charge transfer band and the DNP features around 320 nm are completely restored 20" after fast reduction (Figure 3.15d) while the TFAB unit is still in the *cis* form. This observation suggests that all the CBPQT^{4+} rings shuttled back to TTF site; *cis*-TFAB gate is not bulky enough to trap the CBPQT^{4+} ring on the DNP side and the memory effect demonstrated in the previous paragraph for **2**$^{4+}$ rotaxane is not present (Figure 3.17).

The time analysis of the spectral changes in Figure 3.15d provides information about the inability of the kinetic trapping of *cis*-TFAB.

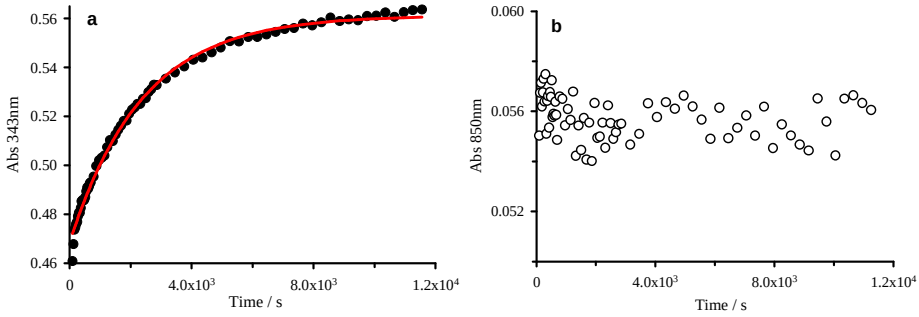

Figure 3.16. Time dependent absorption variation monitored at a) 343 nm (π–π* *trans*-TFAB band) and b) 850 nm (TTF-CBPQT^{4+} CT absorption band) after fast reduction of *cis*-**4**$^{5+}$.The corresponding absorption spectra are reported in Figure 3.15d.

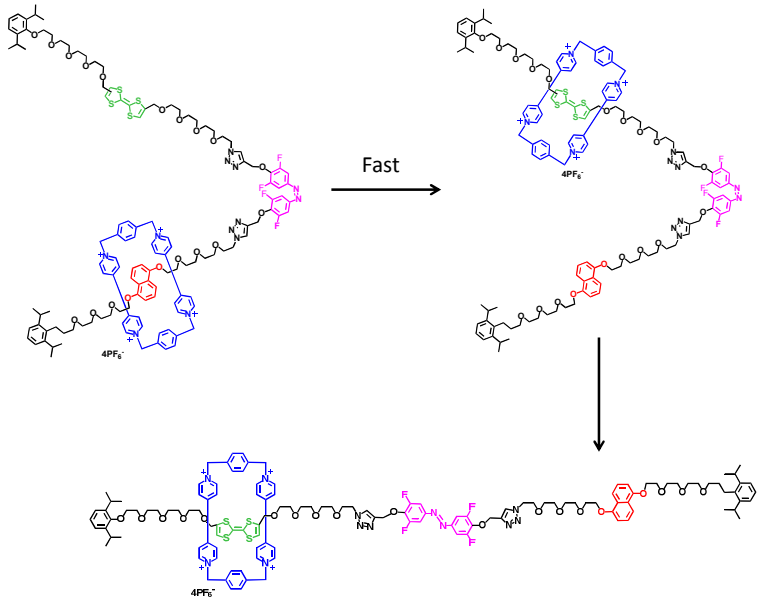

Figure 3.17: Reaction scheme of $\mathbf{4}^{4+}$ reset step after fast reduction of *cis*-$\mathbf{4}^{5+}$.

The rate constant for the recovery of the *trans*-TFAB absorption band (Figure 3.16a) is 4.21×10^{-4} s^{-1}. The time dependent absorption variation monitored on the TTF-CBPQT^{4+} band (Figure 3.16b) shows no variation in the charge transfer band due to the total recovering of the initial intensity 20" after fast reduction. The data remain stored for just few seconds and the total recovering of TTF-CBPQT^{4+} CT band is not correlated with thermal *cis-trans* isomerization of azobenzene unit. That isomerization is substantially accelerated. The kinetic constant is two order of magnitude faster than the one obtained for the rotaxane before oxidation-reduction cycle ($k = 9\times10^{-6}$ s^{-1}).

Fast oxidation of TTF unit after *trans-cis* photoisomerization was performed also for *trans*-$\mathbf{4}^{4+}$. Addition of $Fe(ClO_4)_3$ at the photostationary state containing 90% of *cis*-$\mathbf{4}^{4+}$ and 10% of *trans*-$\mathbf{4}^{4+}$ causes immediate and quantitative oxidation of *trans*-$\mathbf{4}^{4+}$ followed by ring shuttling to the DNP site, whereas *cis*-$\mathbf{4}^{4+}$ is oxidized on a much slower time scale (Figure3.18). Also in that case it is difficult to establish the position of the CBPQT^{4+} ring after chemical oxidation of *cis*-$\mathbf{4}^{4+}$ since the *cis-trans* isomerization occurs on a time scale comparable with that of the chemical oxidation.

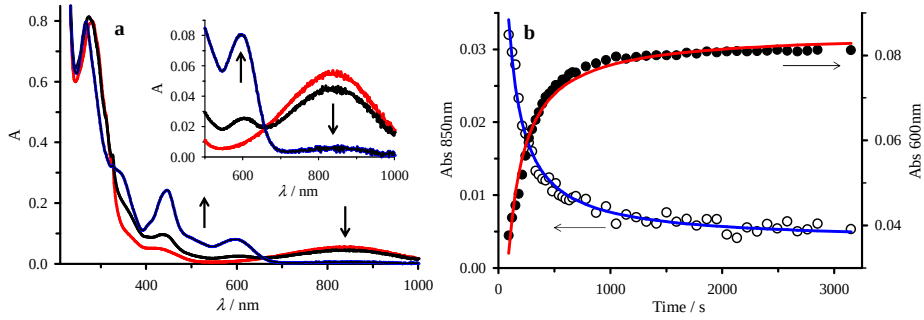

Figure 3.18. a) Absorption spectra of a solution containing ca. 90% *cis*-**4**$^{4+}$ obtained upon exhaustive irradiation of 17 μM *trans*-**4**$^{4+}$ at 365nm, before (red line) and immediately after the addition of 1 equivalent of $Fe(ClO_4)_3$ (black line). The solid blue line shows the absorption spectrum observed 25 minutes after the addition of the oxidant, when change were completed. Inset picture shows the CBPQT^{4+}-TTF CT band region. b) Time dependent absorption changes at 600 nm (TTF$^{\bullet+}$ band, black circles) and 850 nm (CBPQT^{4+}-TTF CT band, white circles). The solid line results from the data fitting according to a second order kinetic equation (k = 1.4×10^3 and 2.0×10^3 M^{-1} s^{-1} for 600 and 850 nm signals respectively)

Despite our experiments show that *cis*-TFAB gate is not bulky enough to prevent the shuttling of the ring from DNP to TTF unit (Figure 3.15), TTF moiety in *cis*-**4**$^{4+}$ cannot be oxidized immediately after addition of one equivalent of $Fe(ClO_4)_3$.

3.3 Conclusion

In this chapter the ability of rotaxane $\mathbf{2}^{4+}$ to operate as bistable memory element[35] under kinetic control, was describes.

The data can be written using an oxidation stimulus and locked using UV light. The oxidation is followed by the shuttling of the $CBPQT^{4+}$ ring from the TTF to the DNP site (writing operation). Photoisomerization of AZO unit enables the closing of the gate and lock the ring on the DNP side (lock operation). The $TTF^{\bullet+}$ is reduced back to the original form without losing the written data for a remarkably long time (circa 3 h). The data remain stored at room temperature in the dark until the thermal isomerization of the azobenzene gate occurs. Light irradiation not only locks the data previously recorded by oxidation but also protects the nonoxidized rotaxanes from accidental writing.

Rotaxane $\mathbf{4}^{4+}$ cannot operate as bistable memory element under kinetic control because the *cis*-azobenzene unit is not bulky enough to lock the ring on the DNP unit after electronic reset. The data can be locked just for few seconds. Also in the case of $\mathbf{4}^{4+}$ light irradiation protects the not-oxidized rotaxanes from accidental writing.

References and Notes

(1) Balzani, V.; Credi, A.; Venturi, M. *Molecular Devices and Machine - Concepts and Perspectives for the Nanoworld*; 2nd ed.; Wiley-VCH Verlag: Weinheim, 2008.

(2) Sauer, M. *Proc. Natl. Acad. Sci.* **2005**, *102*, 9433–9434.

(3) *Molecular Switches*; Feringa, B. L., Ed.; Wiley-VCH Verlag: Weinheim, 2001.

(4) Green, J. E.; Choi, J. W.; Boukai, A.; Bunimovich, Y.; Johnston-Halperin, E.; DeIonno, E.; Luo, Y.; Sheriff, B. a; Xu, K.; Shin, Y. S.; Tseng, H.-R.; Stoddart, J. F.; Heath, J. R. *Nature* **2007**, *445*, 414–417.

(5) Zhang, C.; Du, M.-H.; Cheng, H.-P.; Zhang, X.-G.; Roitberg, A.; Krause, J. *Phys. Rev. Lett.* **2004**, *92*, 158301.

(6) Mativetsky, J. M.; Pace, G.; Elbing, M.; Rampi, M. A.; Mayor, M.; Samorì, P. *J. Am. Chem. Soc.* **2008**, *130*, 9192–9193.

(7) Ward, M. D. *J. Chem. Edu.* **2001**, *78*, 321–328.

(8) Irie, M. *Chem. Rev.* **2000**, *100*, 1685–1716.

(9) Amabilino, D. B.; Stoddart, J. F. *Chem. Rev.* **1995**, *95*, 2725–2828.

(10) Champin, B.; Mobian, P.; Sauvage, J.-P. *Chem. Soc. Rev.* **2007**, *36*, 358–366.

(11) Vickers, M. S.; Beer, P. D. *Chem. Soc. Rev.* **2007**, *36*, 211–225.

(12) Coskun, A.; Spruell, J. M.; Barin, G.; Dichtel, W. R.; Flood, A. H.; Botros, Y. Y.; Stoddart, J. F. *Chem. Soc. Rev.* **2012**, *41*, 4827–4859.
(13) Share, A. I.; Parimal, K.; Flood, A. H. *J. Am. Chem. Soc.* **2010**, *132*, 1665–1675.
(14) Berná, J.; Leigh, D. a; Lubomska, M.; Mendoza, S. M.; Pérez, E. M.; Rudolf, P.; Teobaldi, G.; Zerbetto, F. *Nat. Mater.* **2005**, *4*, 704–710.
(15) Eelkema, R.; Pollard, M. M.; Vicario, J.; Katsonis, N.; Ramon, B. S.; Bastiaansen, C. W. M.; Broer, D. J.; Feringa, B. L. *Nature* **2006**, *440*, 163.
(16) Liu, Y.; Flood, A. H.; Bonvallet, P. a; Vignon, S. a; Northrop, B. H.; Tseng, H.-R.; Jeppesen, J. O.; Huang, T. J.; Brough, B.; Baller, M.; Magonov, S.; Solares, S. D.; Goddard, W. a; Ho, C.-M.; Stoddart, J. F. *J. Am. Chem. Soc.* **2005**, *127*, 9745–9759.
(17) Collin, J.; Dietrich-buchecker, C.; Jimenez-molero, M. C.; Sauvage, J. *Acc. Chem. Res.* **2001**, *34*, 477–487.
(18) Bruns, C. J.; Stoddart, J. F. *Nat. Nanotech.* **2013**, *8*, 9–10.
(19) Dawson, R. E.; Lincoln, S. F.; Easton, C. J. *Chem. Comm.* **2008**, 3980–3982.
(20) Cotí, K. K.; Belowich, M. E.; Liong, M.; Ambrogio, M. W.; Lau, Y. a; Khatib, H. a; Zink, J. I.; Khashab, N. M.; Stoddart, J. F. *Nanoscale* **2009**, *1*, 16–39.
(21) Fahrenbach, A. C.; Warren, S. C.; Incorvati, J. T.; Avestro, A.-J.; Barnes, J. C.; Stoddart, J. F.; Grzybowski, B. a *Adv. Mater.* **2012**, 331–348.
(22) Lewandowski, B.; De Bo, G.; Ward, J. W.; Papmeyer, M.; Kuschel, S.; Aldegunde, M. J.; Gramlich, P. M. E.; Heckmann, D.; Goldup, S. M.; D'Souza, D. M.; Fernandes, A. E.; Leigh, D. A. *Science* **2013**, *339*, 189–193.
(23) Armaroli, N.; Balzani, V.; Collin, J.; Gavin, P.; Sauvage, J.-P.; Ventura, B. *J. Am. Chem. Soc.* **1999**, *121*, 4397–4408.
(24) Ye, T.; Kumar, A. S.; Saha, S.; Takami, T.; Huang, T. J.; Stoddart, J. F.; Weiss, P. S. *ACS Nano* **2010**, *4*, 3697–3701.
(25) Astumian, R. D. *PhysChemChemPhys* **2007**, *9*, 5067–5083.
(26) Kudernac, T.; Ruangsupapichat, N.; Parschau, M.; Maciá, B.; Katsonis, N.; Harutyunyan, S. R.; Ernst, K.-H.; Feringa, B. L. *Nature* **2011**, *479*, 208–211.
(27) Kay, E. R.; Leigh, D. a; Zerbetto, F. *Angew. Chem. Int. Ed.* **2007**, *46*, 72–191.
(28) De Ruiter, G.; Motiei, L.; Choudhury, J.; Oded, N.; Van der Boom, M. E. *Angew. Chem. Int. Ed.* **2010**, *49*, 4780–4783.
(29) Wang, Z.; Elbaz, J.; Remacle, F.; Levine, R. D.; Willner, I. *Proc. Natl. Acad. Sci.* **2010**, *107*, 21996–22001.
(30) Baroncini, M.; Silvi, S.; Venturi, M.; Credi, A. *Chem. Eur. J.* **2010**, *16*, 11580–11587.
(31) Collier, C. P.; Jeppesen, J. O.; Luo, Y.; Perkins, J.; Wong, E. W.; Heath, J. R.; Stoddart, J. F. *J. Am. Chem. Soc.* **2001**, *123*, 12632–12641.
(32) Balzani, V.; Credi, A.; Mattersteig, G.; Matthews, O.; Raymo, F.; Stoddart, J.; Venturi, M.; White, A.; Williams, D. *J. Org. Chem.* **2000**, *65*, 1924–1936.
(33) Durr, H.; Bouas-Laurent, H. *Photochromism, Molecules and Systems*; Elsevier Science Publishers B.V.: Amsterdam, 1990.
(34) Coskun, A.; Friedman, D. C.; Li, H.; Patel, K.; Khatib, H. a; Stoddart, J. F. *J. Am. Chem. Soc.* **2009**, *131*, 2493–2495.
(35) Avellini, T.; Li, H.; Coskun, A.; Barin, G.; Trabolsi, A.; Basuray, A. N.; Dey, S. K.; Credi, A.; Silvi, S.; Stoddart, J. F.; Venturi, M. *Angew. Chem. Int. Ed.* **2012**, *51*, 1611–1615.

(36) Choi, J. W.; Flood, A. H.; Steuerman, D. W.; Nygaard, S.; Braunschweig, A. B.; Moonen, N. N. P.; Laursen, B. W.; Luo, Y.; DeIonno, E.; Peters, A. J.; Jeppesen, J. O.; Xu, K.; Stoddart, J. F.; Heath, J. R. *Chem. Eur. J.* **2006**, *12*, 261–279.

(37) Ferrocinium contribution was evaluated by multiplying the Me10Fc+ epsilon spectra and the concentration corresponding to the Me10Fc addition. The obtained absorpion contribution was substracted from the absorption spectra of rotaxane and $Me_{10}Fc^{+}$mixture.

(38) Saha, S.; Flood, A. H.; Stoddart, J. F.; Impellizzeri, S.; Silvi, S.; Venturi, M.; Credi, A. *J. Am. Chem. Soc.* **2007**, *129*, 12159–12171.

Chapter 4

Acid-base effect on CdSe and CdSe-ZnS quantum dots in organic solution

4.1 Introduction

The achievement of valuable and reproducible spectroscopic properties of colloidal semiconductor nanocrystals (narrow emission, high luminescence quantum yield and photostability) is strictly related to the quality of the material, particularly as far as surface states are concerned.[1] This issue is a consequence of the fact that the surface-to-volume ratio increases as the particle diameter decreases. Surface atoms, that for small QDs are a reasonable fraction, constitute defects in the nanocrystals structure due to the presence of unsaturated valences and dangling bonds.[2] These atoms can be points of attach for external agents (e.g. oxygen and water). The presence of defects prevent the radiative recombination of the charge carriers by enabling non-radiative decay pathways that involve the trapping of the electron and/or hole in the defects.[3] Surface

states affect substantially the redox properties of semiconductor QDs[4] and other phenomena such as photoblinking.[5,6]

Understanding the response of semiconductor QDs to environmental changes is of highest importance for the knowledge of the range of experimental conditions under which these materials are stable. One of the most environmentally and analytically relevant parameters in liquid solution is the proton concentration. The influence of pH on the spectroscopic properties of water soluble CdSe and CdSe-ZnS QDs was addressed on several investigations.[7–10] Although a quenching of the QD is usually observed in acidic conditions,[11,12] some studies have reported an enhancement of the emission of CdTe nanocrystallites in acidic environment.[13,14] The reversibility of the effects of the acid addition on the photophysical properties of the QDs was also investigated. Peng and coworkers carried out detailed studies on the effect of pH on thiol coated cadmium chalcogenide core nanocrystals in aqueous solution, and found that the acid competes with the QDs for the ligands which are Lewis basis. At low pH the ligands detach from the surface of the nanocrystals, which consequently precipitate out. The precipitate can be recovered by deprotonation of the thiol ligands with a base. Dissolution of inorganic nanocrystals was not observed.[7]

The organic ligands that cover the surface of core and core-shell QDs play multiple roles both during and after the synthesis.[8,15] In the synthetic step, ligands control the reactivity of the precursors and the growth rate, thereby determining the final size and the size distribution of the particles. The capping ligands passivate the surface atoms, preventing aggregation and controlling the solubility of the particles. Moreover, the electronic structure of those molecules contributes to the overall electronic and optical profile of the nanoparticles, passivating surface states with consequences on the emission yield.[16] Core-shell QDs, where the core is covered with a layer of another semiconductor material, should have reduced surface trap states. This shell is covered, in its turn, with organic ligands with the purpose to provide solubility and prevent aggregation. Despite this, Rosenthal and co-workers reported that inorganic shell is not uniform and it is likely that in some part of the core surface such layer is very thin or not present at all.[1] Incomplete shell coverage affects the properties of core-shell systems (e.g. the luminescence quantum yield[17]).

In this work we reported a series of experiments aimed at elucidating the effect of acid on the photophysical properties of CdSe core and CdSe-ZnS core-shell semiconductor nanocrystals. We have also addressed the influence of the thickness of the ZnS shell on the changes observed upon addition of acid and studied the reversibility of such effects by successive neutralization with a base. We decided to perform the experiments in organic solvents rather than in water in order to use the as prepared QDs, avoiding successive exchange of the ligand that usually deteriorates the photophysical properties of the nanocrystals. This choice also enabled us to exploit in full the flexibility of currently available solution-based synthetic methodologies to vary the nature of the capping ligands.

4.2 Results and Discussion

All the materials were synthesized according to the procedure reported in Chapter 2, using proper ligand (hexadecylamine or oleic acid) during the shell overcoating (SILAR method). Core-shell **csT** sample was synthesized according to the method reported in literature[18] with minor modifications. Spectroscopic characterization (absorption and emission) was carried out in dilute $CHCl_3$ solution; photophysical properties are gathered in Table 1.

Sample	λ_{abs} / nm[a]	λ_{em} / nm	Φ_{em}[c]	d_{core} / nm	$d_{core-shell}$ / nm
cA	565	580		3.4	-
csA1	589	609	0.15	4.1	6.9
csA2-1	577	588	0.004	3.7	4.4
csA2-3	568	586	0.22	3.7	5.8
csA2-5	566	587	0.21	3.7	7.2
csT	567	592	0.044	3.4	4.8
csO1	616	639	0.055	5.4	8.0
csO2-1	608	633	0.0014	4.3	5
csO2-3	604	624	0.23	4.3	6.4
csO2-5	615[b]	629	0.39	4.3	7.4

Table 1: Spectroscopic data in $CHCl_3$. [a] Maximum of the exciton peak. [b] Estimated. [c] Reference: rhodamine 6G in ethanol solution (Φ = 0.94 in aerated solvent[19])

4.2.1 ACID-BASE EFFECT ON CdSe "Core" QUANTUM DOTS

We have synthesized CdSe QDs core coated with an organic shell of trioctylphosphine oxide (TOPO) and hexadecylamine (HDA), **cA**. The size of the nanocrystals, determined from the absorption spectrum[20] and TEM images, resulted in 3.4nm.

Upon titration of a $CHCl_3$ solution of **cA** with triflic acid (CF_3SO_3H) the luminescence of the quantum dots was completely quenched after addition of 100 equivalents of acid (Figure 4.1a) as previously observed for CdTe QDs.[21] No precipitation was observed, neither after three days.[7] On the other hand we observed a slight decrease and ipsochromic shift of the absorption exctiton peak, consistent with a shrinkage of the nanocrystals. The different behavior with respect to previously investigated systems[7] is probably due to differences in experimental conditions and in particular in the solvent that we chose for our experiments. We performed regular titration in $CHCl_3$ in extreme dilute conditions (10^{-7} - 10^{-8} M), and we followed the changes in the emission spectra until achievement of a plateau of the fluorescence signal. Under these experimental conditions it is possible that the quantum dots reach an equilibrium state which corresponds to the loss of part of the ligands and consequent aggregation (without precipitation).[22] Successive addition of base (tributylamine, TBA) should cause deprotonation of the detached ligands and possibly their reattachement to the surface of the nanocrystals.[7]

Addition of base causes a partial recovery of the luminescence, whose extent depends on the amount of acid present in the solution. We performed two experiments: (i) we added 250 equivalents of acid to a solution of CdSe quantum dots, causing a complete quenching of luminescence and then we titrated with TBA (Figure 4.1b, gray symbols). Under these experimental conditions the luminescence of the nanocrystals was recovered only up to 4% of its original value; (ii) we added 75 equivalents of acid to a solution of CdSe quantum dots, causing a strong but not complete quenching of the luminescence (Figure 4.1b, black symbols). Upon titration of this solution with TBA, the luminescence was restored up to 25% of its original value. These results support the hypothesis of an aggregation of the quantum dots after protonation of the ligands and their subsequent detachment from the surface of the nanocrystals. After addition of a base, the ligands are deprotonated and are able again to bind to the surface of the

quantum dots, thus breaking the aggregates. The efficiency of this process can depend however on the extent of aggregation of the nanocrystals, as suggested by our experiments.

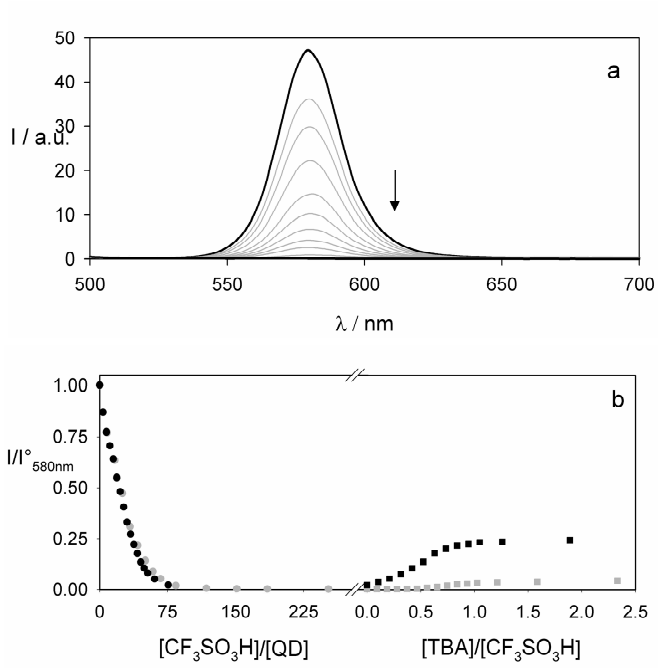

Figure 4.1: (a) Emission spectra of a solution of **cA** 1.9×10^{-7} M upon the titration with CF_3SO_3H. (b) Gray symbols: emission changes at 580 nm upon addition of acid (circles) up to 250 equivalents and successive addition of base (squares); black symbols: emission changes at 580 nm upon addition of acid (circles) up to 75 equivalents and successive addition of base (squares).

4.2.2 ACID-BASE EFFECT ON CdSe-ZnS "Core-Shell" QUANTUM DOTS

Coating the inorganic core with a shell of another inorganic material (ZnS) should passivate and stabilize the nanocrystals, rendering them potentially insensitive to the surrounding. Nevertheless, core-shell quantum dots are covered with a further shell of organic ligands which are Lewis bases and are sensitive to acid and base. We synthesized CdSe-ZnS core-shell quantum dots (cs), coated with TOPO and HDA (**csA1**) and we characterized this material in $CHCl_3$ (Table 1). From the first absorption peak the dimension of the core could

be established;[20] moreover thickness of the shell layer can be control using the synthetic procedures[23] (see Chapter 2). The emission spectrum is characterized by the typical narrow luminescence band, whose maximum depends on the dimension of the core.

In order to investigate the stability of the core-shell quantum dots in presence of acid, we performed titration experiments in $CHCl_3$. Upon addition of CF_3SO_3H, the absorption spectrum of the nanocrystals showed only a slight decrease, whereas the luminescence was strongly quenched (Figure 4.2a): 5000 equivalent of acid caused a 90% decrease of the emission quantum yield of **csA1**. We performed the same titration with CF_3COOH, which is a weaker acid than CF_3SO_3H, and we obtained similar results: the only difference is that more equivalents of acid (20000) were necessary to quenched the 65% of the emission quantum yield of **csA1**. Also in the case of core-shell QDs, it is likely that the effect of the acid is to protonate the organic ligands, causing their detachments from the surface

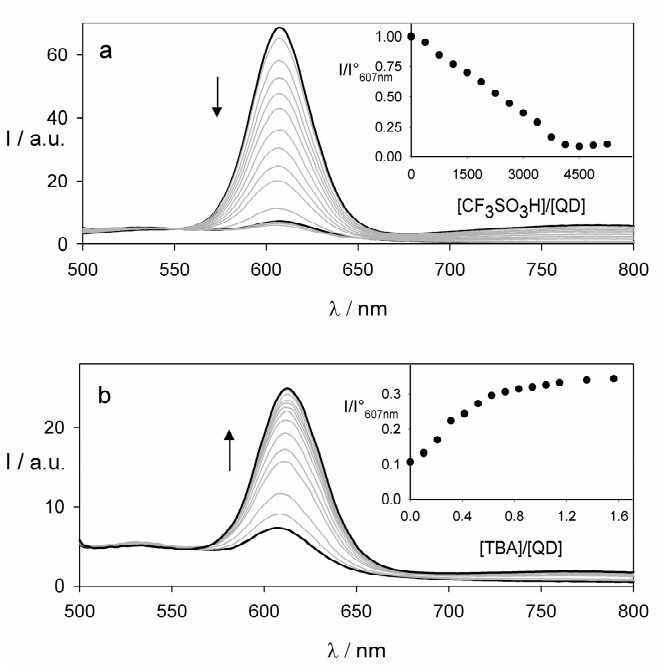

Figure 4.2 Emission spectra of a solution of **csA1** 6×10^{-8} M upon addition of CF_3SO_3H (a) and upon addition of TBA (b). The insets show the emission changes at 607 nm.

The quenching of the luminescence can be due to two reasons. On one hand, as we could interfere also by the spectroscopic properties of our material, the coverage of the core is not perfect, and it is likely that part of the CdSe core is protected from the environment only by organic shell of ligands. As a consequence, protonation of the ligands can cause the exposure of the uncoated core of the QDs with the consequent quenching of the luminescence. Moreover, as for the bare core CdSe, the loss of the ligands can cause aggregation of the nanocrystals, which is also responsible of quenching of the luminescence.[22]

Upon addition of TBA the emission was restores up to 35% of the initial value (Figura 4.2b) and the maximum of the emission band was 3 nm red-shifted. Upon leaving the system at rest for 2 days, the luminescence intensity was enhanced with respect to the original value (Figure 4.3).

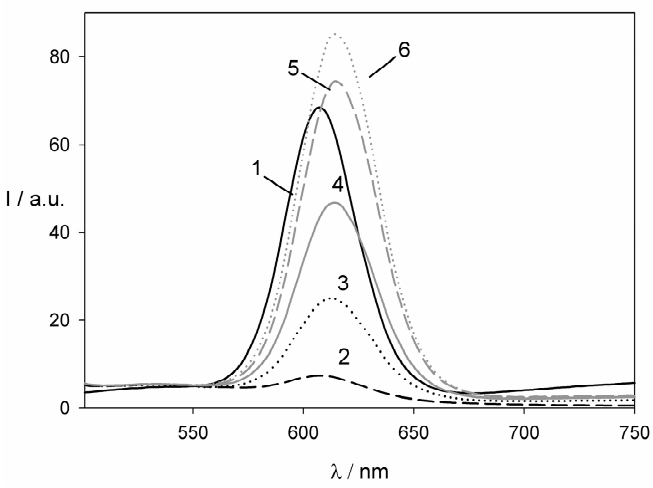

Figure 4.3 Emission spectra of **csA1** (solid black line 1), after addition of 5450 equivalents of CF_3SO_3H (dashed black line 2), after addition of 1.5 equivalents of TBA with respect to CF_3SO_3H (dotted black line 3), after 12 hours (solid gray line 4), after 2 days (dashed gray line 5), after 3 days (dotted gray line 6)

The recovery of the luminescence suggests that upon addition of TBA the protonated free ligands are deprotonated and can bind again on the surface of the quantum dots. At the beginning the luminescence is only partially restored because of kinetic effects: it is likely that the detachment of the protonated ligands causes aggregation of the QDs; after addition of base the deprotonated ligands can bind again on the surface of the nanocrystals, but this process takes

some time because the particles can be aggregated and their surface can be less accessible to the ligands. After 1 day the original emission is restores and upon leaving the system at rest the emission increases above the initial value, possibly for two reasons: (i) the TBA can bind on the surface of the nanocrystals, removing surface defects; (ii) the mild conditions of the ligand detachment/reattachent with respect to the synthetic experimental conditions, can possibly favour an optimized distribution of the ligands on the surface of the quantum dots. The first hypothesis can be ruled out because addition of TBA to a solution of quantum dots does not cause any spectroscopic changes.

Cyclic additions of acid and base to a solution of **csA2-3** (see Chapter 2 for synthesis details) revealed poor reversibility: this observation is consistent with the partial irreversibility of the disgregation process by means of the ligands under these experimental conditions.

Core-shell quantum dots with different organic ligands on the surface were also synthesized, namely CdSe-ZnS coated with TOPO (sample **csT**) and with TOPO and oleate (sample **csO1**). These materials have been investigated in $CHCl_3$; the main spectroscopic properties are gathered in Table 1. We performed on these samples the same acid/base titration experiments performed on **csA1** sample and we observed that upon addition of CF_3SO_3H, the absorption spectrum of the nanocrystals is unaffected (**csT**) or shows only a slight decrease (**csO1**), whereas the luminescence is strongly quenched (Figure 4.4 and 4.5): 700 equivalents cause a 65% decrease of the emission quantum yield of **csT** (Figure 4.4) and 35000 equivalents cause a 90% decrease of the emission quantum yield of **csO1** (Figure 4.5).

Upon addition of TBA the emission is restored, but the two samples show a different behavior (Figures 4.4b and 4.5b): in the case of **csT**, the emission is completely restored and after neutralization of the acid in excess, it is enhanced with respect to the original value (Figura4.4b), whereas **csO1** sample shows only a small recovery of the luminescence (5%) (Figure4.5b).

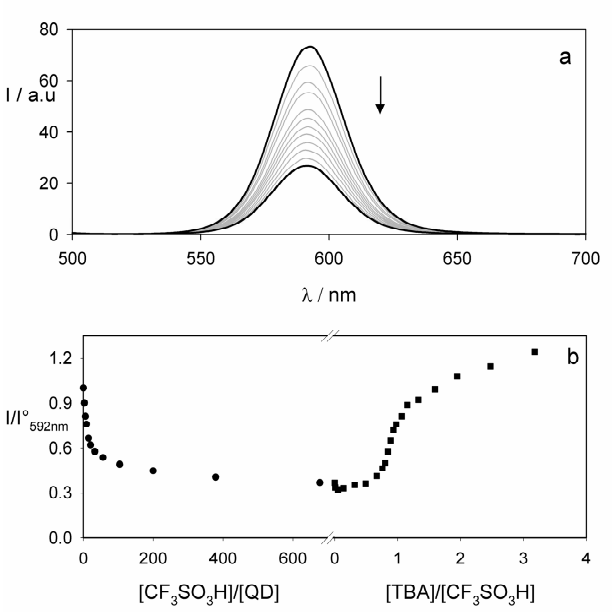

Figure 4.4 (a) Emission spectra of a solution of **csT** 2.2×10^{-7} M upon titration with CF_3SO_3H. (b) Emission changes at 592 nm upon addition of acid (circles) and successively of base (squares)

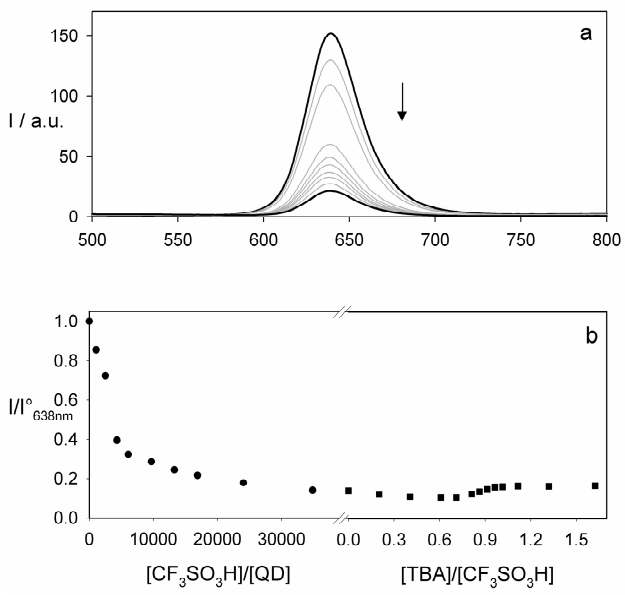

Figure 4.5 (a) Emission spectra of a solution of **csO1** 4×10^{-8} M upon titration with CF_3SO_3H. (b) Emission changes at 638 nm upon addition of acid (circles) and successively of base (squares)

From our experiments and from literature data[7] we can interpret the effect of the acid on the quantum dot as a consequence of the loss of the organic ligands that cover the surface of the nanocrystals. As we already pointed out, the effect on the luminescence can be possibly ascribed to two reasons: (i) the incomplete coating of the core by the inorganic shell, with a consequent exposure of the core to the surrounding environment and/or (ii) the aggregation of the quantum dots.[22]

In order to gain more insight on the effect of the inorganic shell coating, we synthesized three samples of CdSe-ZnS TOPO/HDA (**csA2**) and TOPO/oleate (**csO2**) with inorganic shell of different thickness (see Chapter 2), namely one (**csA2-1** and **csO2-1**), three (**csA2-3** and **csO2-3**) and five (**csA2-5** and **csO2-5**) ZnS monolayers. The samples were characterized in $CHCl_3$ and their spectroscopic properties are gathered in Table 1. Upon titration with acid we observed a quenching of the luminescence, whose efficiency depends on the number of shell monolayers (Figure 4.6): that is, more equivalents of acid are necessary to cause a comparable quenching of the luminescence in the three samples of each series, as the number of the shells increases. This behavior reflects the increase of the dimensions of the nanocrystals (and of the number of organic ligands) on increasing the number of shells. On the other hand, the amount of final quenching does not depend on the thickness of the inorganic shell, thus suggesting that this effect is related to the aggregation of the QDs.

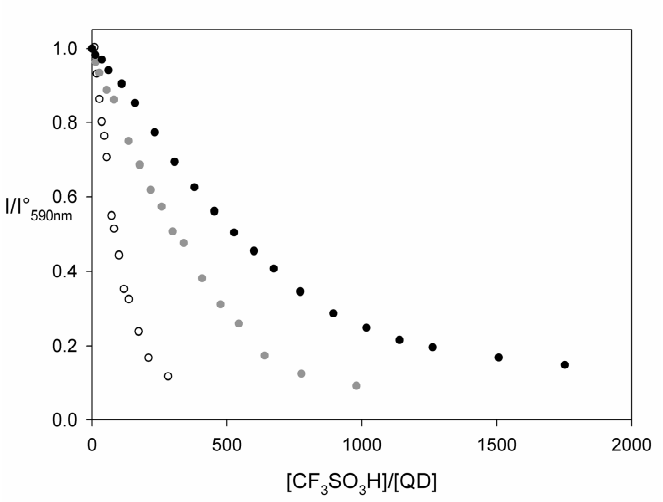

Figure 4.6: Emission changes at 590 nm upon addition of CF_3SO_3H to samples **csA2-1** (white circles), **csA2-3** (gray circles) and **csA2-5** (black circles)

All the samples of the **csO2** series show rather broad emission peaks (FWHM>45nm), indicative of a wide distribution of the dimensions of the nanocrystals. Interestingly, the residual emission peaks at the end of the titration with acid show a red shift of the maximum and a narrower width (Figure 4.7): this result confirms that the quenching effect of the acid is more efficient on the smaller quantum dots.

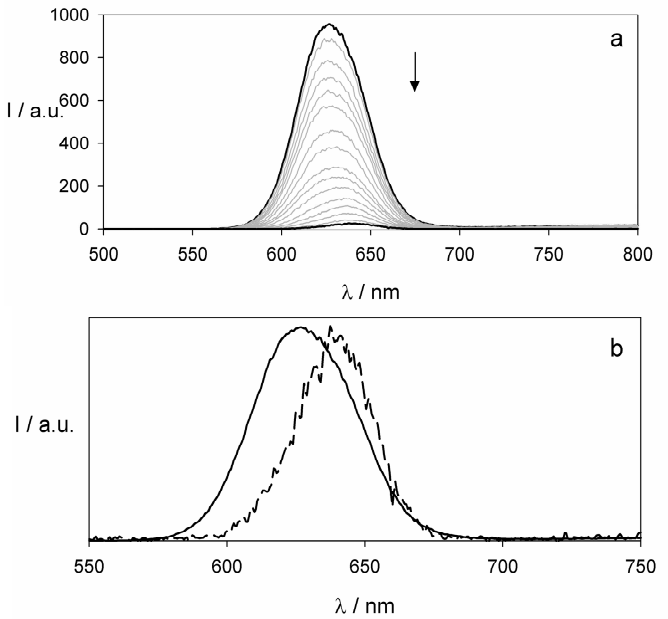

Figure 4.7 (a) Emission spectra of a solution of **csO2-3** 3×10^{-8} M upon titration with CF_3SO_3H. (b) Normalized emission spectra of **csO2-3** before (solid line) and after (dashed line) addition of 2400 equivalents of acid

In order to confirm all our hypothesis we performed TEM experiments on a sample of **csO1** (Figure 4.8a), after addition of CF_3SO_3H (Figure 4.8b) and after successive addition of TBA (Figure 4.8c.). Figure 4.8b show that, after addition of acid, the particles tend to aggregate: a non-homogeneous distribution of the quantum dots on the grid is clearly visible. After addition of base (Figure 4.8c), the nanoparticles are more homogeneously distributed on the surface of the grid, even though still partly aggregated in small clusters (as expected on the basis of the behavior observed in solution for this material).

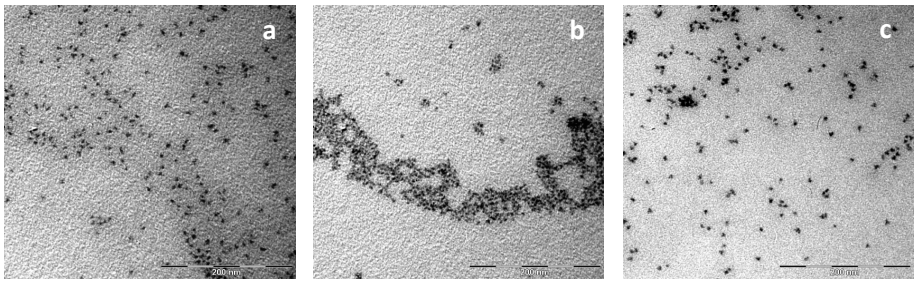

Figure 4.8 TEM images of (a) **csO1**, (b) **csO1** after addition of 166 equivalents of CF_3SO_3H and (c) after successive addition of 1 eq of TBA with respect to the acid.

On sample **csA2-3** we performed three titrations with CF_3SO_3H, under the same conditions, changing only the amount of the acid added at each point of the titration: we observed that, upon increasing the amount of acid added at each point, the luminescence quenching is less efficient. In other words, the same total amount of acid causes a different extent of luminescence quenching, depending on the amount of acid added at each step of the titration (Figure 4.9).

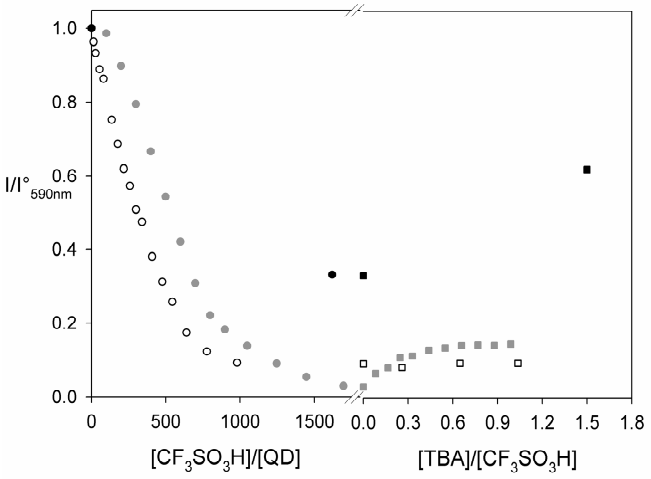

Figure 4.9 Emission changes upon addition of triflic acid (circles) and TBA (squares) in different aliquots to sample **csA2-3**. Black symbols are referred to the titration with large amount of acid at each step; white symbols are referred to the titration with small amount of acid at each addition.

Successive addition of TBA shows that also the luminescence recovery depends on how we performed the titration with the acid. Namely, the luminescence recovery is more efficient (almost 100%) when the acid is added in large aliquotes, whereas it is almost completely inefficient if the acid is added in small aliquots (Figure 4.9). This behavior can possibly depend on the kinetics of the aggregation process that follows the detachment of the ligands: upon addition of acid in small aliquots, the detachment of the ligands causes the formation of small aggregates, that can on their turn aggregate in bigger entities as long as the titration proceeds (Figure 4.10a). On the contrary, upon addition of large amount of acid, the partially uncoated nanocrystals aggregate quickly in smaller aggregates (Figure 4.10b). Therefore also the effect of the base is different: the bigger aggregates are more difficult to disgregate and the luminescence recovery is less efficient. In this sample we did not observed an increase of the luminescence with respect to the original value on addition of TBA, neither after successive addition of native ligands (TOPO, HDA or both).

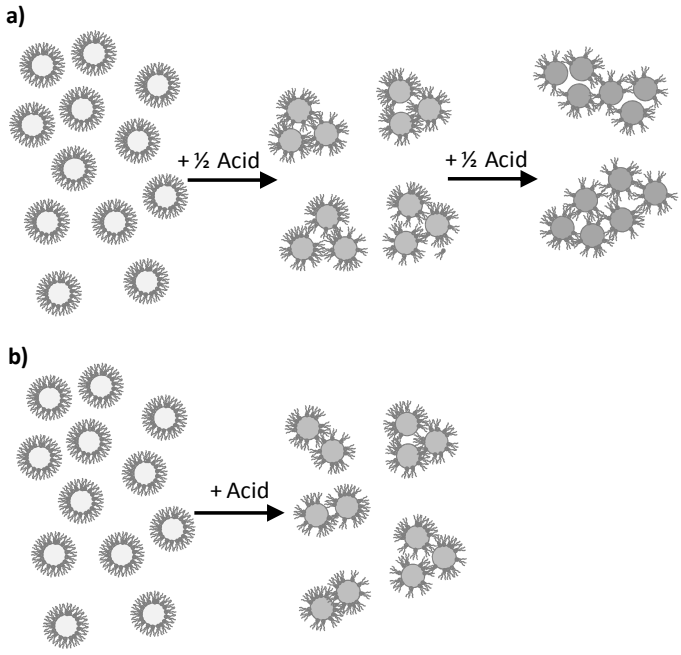

Figure 4.10 Scheme of quantum dots aggregation and quenching after addition of small (a) and large amount of acid (b)

4.3 Conclusion

Inorganic semiconductor nanocrystals are attracting more and more interest for their peculiar spectroscopic properties and also for their stability and insensitivity to their surrounding environment with respect to organic dyes, particularly as far as core-shell systems are concerned. In recent years it is becoming more evident that the surface properties of these materials are very important, because it has been observed that optical properties of quantum dots can depend on their local environment.[24,25]

In this study we explored the behaviour of core-shell quantum dots in acid environment, comparing the same materials originating from different synthesis, material with different organic ligands and materials with different shell thickness. From our results it is evident that the behaviour of the systems is influenced by several parameters, but we can reasonably conclude that core-shell quantum dots are sensitive to acidity of the environment, because of the unavoidable presence of the organic ligands on their surface. This behaviour must be taken into account in designing quantum dot-based systems that are supposed to work in presence of acid or when using quantum dots as scaffolds for pH sensors.

References and Notes

(1) McBride, J.; Treadway, J.; Feldman, L. C.; Pennycook, S. J.; Rosenthal, S. J. *Nano Lett.* **2006**, *6*, 1496–1501.

(2) Wang, X.; Qu, L.; Zhang, J.; Peng, X.; Xiao, M. *Nano Lett.* **2003**, *3*, 1103–1106.

(3) Javaux, C.; Mahler, B.; Dubertret, B.; Shabaev, A.; Rodina, a. V.; Efros, A. L.; Yakovlev, D. R.; Liu, F.; Bayer, M.; Camps, G.; Biadala, L.; Buil, S.; Quelin, X.; Hermier, J.-P. *Nat. Nanotech.* **2013**, *8*, 206–212.

(4) Impellizzeri, S.; Monaco, S.; Yildiz, I.; Amelia, M.; Credi, A.; Raymo, F. M. *J. Phys. Chem. C* **2010**, *114*, 7007–7013.

(5) Chen, Y.; Vela, J.; Htoon, H.; Casson, J. L.; Werder, D. J.; Bussian, D. a; Klimov, V. I.; Hollingsworth, J. a *J. Am. Chem. Soc.* **2008**, *130*, 5026–5027.

(6) Galland, C.; Ghosh, Y.; Steinbrück, A.; Sykora, M.; Hollingsworth, J. a; Klimov, V. I.; Htoon, H. *Nature* **2011**, *479*, 203–207.

(7) Aldana, J.; Lavelle, N.; Wang, Y.; Peng, X. *J. Am. Chem. Soc.* **2005**, *127*, 2496–2504.

(8) Susha, A. S.; Javier, A. M.; Parak, W. J.; Rogach, A. L. *Colloids and Surfaces A* **2006**, *281*, 40–43.

(9) Liu, Y.-S.; Sun, Y.; Vernier, P. T.; Liang, C.-H.; Chong, S. Y. C.; Gundersen, M. a *J. Phys. Chem. C* **2007**, *111*, 2872–2878.
(10) Ruedas-Rama, M. J.; Orte, A.; Hall, E. a H.; Alvarez-Pez, J. M.; Talavera, E. M. *Chem. Comm.* **2011**, *47*, 2898–2900.
(11) Medintz, I. L.; Uyeda, H. T.; Goldman, E. R.; Mattoussi, H. *Nat. Mater.* **2005**, *4*, 435–446.
(12) Mei, B. C.; Susumu, K.; Medintz, I. L.; Delehanty, J. B.; Mountziaris, T. J.; Mattoussi, H. *J. Mater. Chem.* **2008**, *18*, 4949–4958.
(13) Nanoparticles, A. C. *J. Phys. Chem. B* **2003**, *107*, 8–13.
(14) Mandal, A.; Tamai, N. *J. Phys. Chem. C* **2008**, *112*, 8244–8250.
(15) Bullen, C.; Mulvaney, P. *Langmuir* **2006**, *22*, 3007–3013.
(16) Green, M. *J. Mater. Chem.* **2010**, *20*, 5797–5809.
(17) Grabolle, M.; Ziegler, J.; Merkulov, A.; Nann, T.; Resch-Genger, U. *Ann. N. Y. Acad. Sci.* **2008**, *1130*, 235–241.
(18) Tomasulo, M.; Yildiz, I.; Kaanumalle, S. L.; Raymo, F. M. *Langmuir* **2006**, *22*, 10284–10290.
(19) Montalti, M.; Credi, A.; Prodi, L.; Gandolfi, M. T. *Handbook of Photochemistry - Third Edition*; CRC Press: Boca Raton, FL (USA), 2006.
(20) Yu, W. W.; Qu, L.; Guo, W.; Peng, X. *Chem. Mater.* **2003**, *125*, 2854–2860.
(21) Zhang, Y.; Mi, L.; Wang, P.-N.; Ma, J.; Chen, J.-Y. *J. Lumin.* **2008**, *128*, 1948–1951.
(22) Komoto, A.; Maenosono, S.; Yamaguchi, Y. *Langmuir* **2004**, *20*, 8916–6923.
(23) Li, J. J.; Wang, Y. A.; Guo, W.; Keay, J. C.; Mishima, T. D.; Johnson, M. B.; Peng, X. *J. Am. Chem. Soc.* **2003**, *125*, 12567–12575.
(24) Blum, A. S.; Moore, M. H.; Ratna, B. R. *Langmuir* **2008**, *24*, 9194–9197.
(25) Pechstedt, K.; Whittle, T.; Baumberg, J.; Melvin, T. *J. Phys. Chem. C* **2010**, *114*, 12069–12077.

Chapter 5

Photoinduced phase transfer of luminescent quantum dots to polar and aqueous media

5.1 Introduction

The remarkable resistance to chemical and photo-degradation of luminescent CdSe based nanocrystals[1–6] raise the interest to the development of novel fluorescent platforms and markers for biological applications, ranging from sensing and intracellular tracking of protein movements and interaction.[4,5,7–12] An important requirement for integration into biotechnology is the ability to access a stable, water soluble systems that can be manipulated in a wide range of pH, electrolytes and other chemicals; the latter should allow straightforward and controllable coupling to various biomolecules.[4,5,9,10]

Highly luminescence QDs are reproducibly prepared with narrow size distribution and high fluorescence quantum yield by reacting organometallic precursors at high temperature in coordinating solvents.[13–18] These QDs are

capped with hydrophobic molecules (i.e. trioctyl phosphine TOP, trioctyl phosphine oxide TOPO, alkylamine, carboxylic acid with long aliphatic chain and phospinic acid) and do not disperse in aqueous media. Post-synthetic surface modifications are indispensable to render QDs hydrophilic and biocompatible. An established method to prepare water-soluble QDs relies the exchange of native hydrophobic ligands with bifunctional molecules that combine metal chelating anchoring group and an hydrophilic part to promote water compatibility.[8,19–21] The stability of hydrophilic QDs is influenced by the strength of the coordination binding between the anchoring group and the surface of the nanocrystals and the affinity of the hydrophilic part to the buffer media.[9,10]

Ligands presenting multiple thiol anchoring groups like dihydrolipoic acid (DHLA) in DHLA-PEG and bis-DHLA-PEG ligands, greatly enhance the QDs stability over a wide range of biological conditions compared to monothiol-terminated ligands or other weakly coordinating groups.[20,22,23] Reduction of Lipoic Acid (LA) groups is a key step for the effective capping of QDs.[19,24,25] To date the reduction of lipoic acid used for the QDs phase transfer is performed under strong reducing conditions using $NaBH_4$ as reducing agent.[19,24,26] Although effective this process imposes limitations with respect to the functional group tolerance and introduces an additional processing step (reaction and purification of the reduced ligand). Borohydride reduction can alter the integrity of certain functional groups such as azide in LA-PEG-N_3. Careful preparation, storage and handling under inert atmosphere of DHLA-based ligands is required to avoid re-oxidation of bis-thiol to dithiane.[24,26]

Lipoic acid has a well defined absorption peak with maximum around 350 nm. Sander and co-workers reported that excitation on this band produces a relatively long lived triple state ($t\sim 1\mu s$) which can be converted into DHLA with a moderate yield.[27] Based on that data we explored the possibility to perform photochemical LA reduction with a concomitant QDs cap exchange.

In this work we report a novel method consisting in photomediated transfer of CdSe-ZnS *core-shell* QDs to buffer media. More precisely, we demonstrated that oxidized lipoic acid can be used without prior reduction to drive the cap exchange and QD transfer to polar organic solvents and buffer media using UV

light as reducing agent (300 nm < λ < 400 nm). This process involves the photoinduced reduction of LA- to DHLA-based ligand and simultaneous replacement of the TOP/TOPO cap with the reduced ligands, all taking place in situ. This method can be applied for several LA-based ligands. In Figure 5.1 is reported a general scheme of LA photoreduction and cap exchange.

Pure lipoic acid (LA), LA-PEG_{750}-OCH_3 and mixture of LA-PEG_{750}-OCH_3 and LA-PEG_{600}-FN (FN: -NH_2,-COOH, -N_3) have all been successfully used for this photochemically driven phase transfer. The use of the method for the preparation of the hydrophilic QDs simplify the procedure for the reduction of the ligand and successive cap exchange in one-pot, avoiding purification after the reduction step.[21]

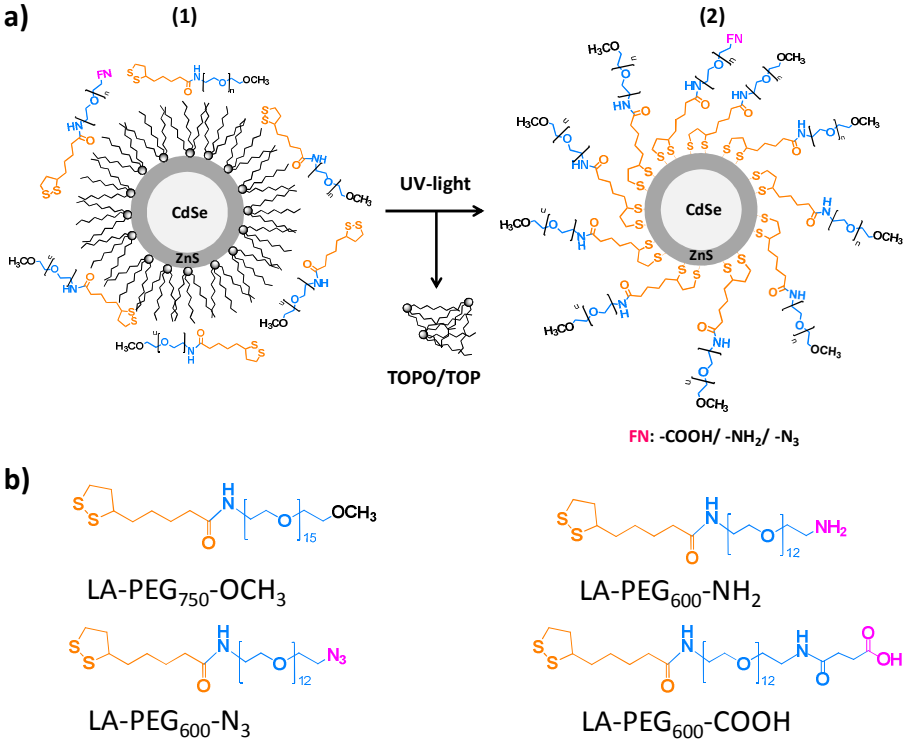

Figure 5.1 (a) Schematic representation of the UV-promoted cap exchange and phase transfer of TOP/TOPO-QDs from hexane to methanol and other polar media including water; *1* is the initial hydrophobic and *2* is the final hydrophilic QDs dispersion. (b) Chemical structure of the ligands used in this study.

The great features of the method to prepare robust functionalized QDs, was tested to collect *in vivo* imaging of brain vasculature of live mice, where well-resolved vessel structures can be visualized for several hours using intravenously injected QDs, combined with two photon fluorescence microscopy.

5.2 Results and Discussion

Ligand synthesis was carried out following previous reports.[20,21] CdSe-ZnS QDs used in that work, were prepared step-wise by reduction of organometallic precursors at high temperature, following the procedures reported in literature.[17,25]

The photo-cap exchange was carried out using two alternative procedures.

(1) The hydrophobic QDs are first precipitated from nonpolar solvents (chloroform, hexane or toluene) as fine powder/paste and mixed with a solution of LA-based ligands in polar solvent and irradiated with UV light.

(2) Irradiation of a biphasic mixture with non polar solvent (hexane) containing the TOP/TOPO capped QDs and the polar solvent immiscible with hexane (methanol) containing the LA-based ligands.

Phase transfer according to route 1 was carried out as following. In a glass vial, 100 μl of 15-20 μM stock solution (1.5-2.0 nmol) of CdSe-ZnS QDs was precipitated with methanol (two times) and mixed as power/paste with 1.5ml of a proper solvent (Table 5.1) containing LA-PEG (0.03-0.1 M) and TMAH (~5 mM). Addition of TMAH shortened the irradiation time and produced water dispersions with negligible red-shift. A magnetic stirring bar was introduced, the vial sealed with rubber septa and the atmosphere was switched to nitrogen by applying 3 or 4 rounds of mild vacuum followed by flushing with nitrogen. The mixture was placed in a photoreactor (LZC-4V, Luzchem Research, Inc., λ_{irr}=350 nm,4.5 mW/cm^2) and irradiated for a certain amount of time, until a clear solution and homogeneous QD dispersion was obtained. The solvent was removed under vacuum and a mixture of ethanol/chloroform was added. Excess of hexane was added to precipitate out QDs with the aim of removing the hydrophobic ligand (TOP/TOPO). The mixture was centrifuged, the supernatant

discarded and the precipitate dried under mild vacuum. Finally, buffer was added to disperse the QDs capped with hydrophilic ligand. The water solution was filtered through 0.45μm syringe filter and 2 cycles of dilution/concentration using a membrane filter Millipore Amicon Ultra 50,000 MW with the aim of removing the excess of the hydrophilic ligand and solubilized TOP/TOPO were preformed. The concentrated solution was dispersed in DI water or buffer (concentration 5-10μM) and stored in refrigerator at 4°C for further analysis. Using this route it is possible to carry out the reaction in a wide range of polar solvents. In our experiments we successfully performed the phase transfer in methanol, ethanol, 1-propanol, 2-propanol, 1-butanol, *tert*-butanol, DMF and acetonitrile. The quality of the final materials are slightly different (Table 5.1).

Solvent	Irradiation time (min)	Abs peak shift (nm)	PL peak shift (nm)
MeOH	20-25	0	1-3
EtOH	20-30	2-3	6-8
1-propanol	15-20	0	1-3
2propanol	100-120	0	5-7
1-butanol	90-100	0	6-8
t-butanol	20-30	4-5	12-15
DMF	55-65	2-3	4-6
MeCN	90-100	2-3	3-5

Table 5.1 Spectroscopic data for QDs (543 nm green emitting) dispersed in water following photoinduced phase transfer with pure LA-PEG_{750}-OCH_3. Luminescence quantum yield was about 0.5-0.7 of the native hydrophobic materials. [a]MeCN comparatively provides water dispersions of QDs with slightly lower quantum yield.

Phase transfer using route 2 was carried out as following. In a typical reaction, 100 µl of 15-20 µM of CdSe-ZnS QDs were precipitated twice with methanol and dispersed in 750 µl of *n*-hexane in a glass vial. 500 µl of a solution containing LA-PEG (pure metoxy or mixture, 100 mM) and TMAH (10 mM) were added. Magnetic bar was inserted and vial sealed with a rubber cap and oxygen removed in the same way of route 1. The vial was irradiated for 20 min.

Following irradiation the hexane layer, initially colored and emissive under UV light, appears colorless and not emissive. Conversely the methanol layer, initially colorless and not emissive, appears colored and emissive. This observation is the proof that photoreduction of LA ligand and subsequent cap exchange happened (Figure 5.2). The solvents were removed under mild vacuum and same purification steps reported above were performed to obtain a concentrated QDs water solution.

Phase transfer using pure lipoic acid can be carried out using both route. After UV irradiation the resulted methanol solution appears turbid. The mixture was dried under vacuum and hexane added to precipitate out the QDs. Water mixed with potassium *tert*-butoxide. (1.5 eq with respect to lipoic acid) was added to QDs powder to obtain a clear solution.[19]

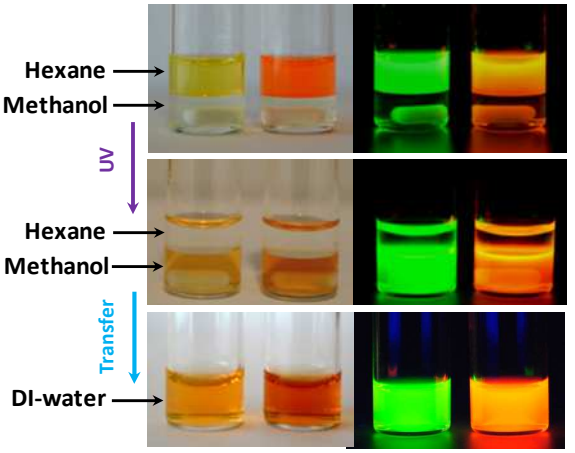

Figure 5.2 Ambient light and fluorescence pictures (hand-held UV-lamp, λ_{ex}=365nm) of vials containing a biphasic mixture of QD hexane solution and LA-PEG methanol solution before (top panel) and after (middle panel) UV irradiation. Bottom panel shows the final QD dispersions in water

The optical and spectroscopic properties of these nanocrystals were tested. Absorption and luminescence spectra of hydrophilic QDs of different size compared with the corresponding TOP/TOPO capped were substantially unchanged. In Figure 5.3 are reported the absorption and luminescence spectra of orange and green emitting CdSe-ZnS QDs dispersed in hexane (TOP/TOPO capped) and DI water (photoreduced LA-PEG_{750}-OCH_3). The luminescence

quantum yield is 50% lower than the hydrophobic one, which is consistent with the literature data for thiol-based ligand exchange.[19,23,24]

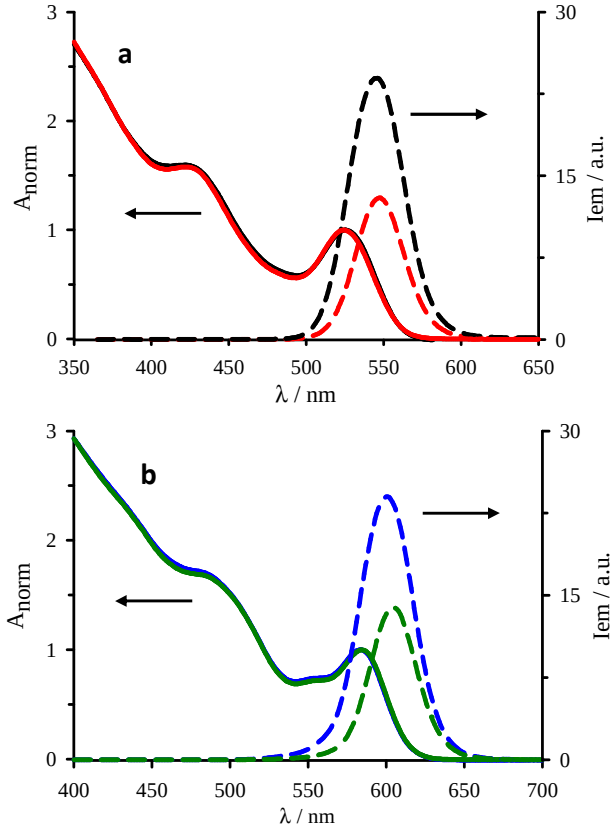

Figure 5.3 Normalized absorption spectra (continous line) and fluorescence emission spectra (dashed line, λ_{ex} = 350 nm, iso-absorption point). a) Green emitting QDs in hexane (TOP/TOPO capped, black-line) and water (photoreduced LA-PEG capped, red line). b) Orange emitting QDs in hexane (TOP/TOPO capped, dark blue-line) and water (photoreduced LA-PEG capped, dark green line).

The addition of TMAH together with the LA-ligand, prior to the irradiation of the mixture, showed a significantly improvement in the phase transfer reaction and final material. More specifically the irradiation time is shortened (from 45 min to 20-25 min) and the emission red-shift between the hydrophobic and hydrophilic QDs is reduced (from 4-7 nm to 1-3 nm).

This new method allow us the preparation of functionalized QDs bearing reactive groups on the surface (e.g. $–NH_2$, –COOH, $–N_3$). The functionalization

consists in the preparation of a mix solution of the functional LA-PEG_{600}-FN and the inert metoxy ligand LA-PEG_{750}-OCH_3 in different molar ratio respect to the total amount of ligands, prior to UV photoreduction. The method produces hydrophilic QDs with the same ratio of functional ligands present in the solution, as already reported for the borohydride reduced ligand.[22] Figure 5.4a shows electrophoresis gel of QDs capped with different ratio of LA-PEG_{750}-OCH_3 and LA-PEG_{600}-NH_2 or LA-PEG_{600}-COOH. The sign and the magnitude of the mobility shift depend on the nature and on the amount of functional ligands used, with large mobility measured for higher fractions of functional ligands.[22] This method was successfully used for the introduction of azide functional groups on the surface of quantum dots. The hydrophilic-functional nanocrystals were prepared in the same way as reported above for amine or carboxy functional QDs. In Figure 5.4b are reported the FTIR spectra of the water soluble QD-N_3 were the typical peak at 2100cm^{-1} of azide is present. This is one of the few examples of direct azide functionalization of semiconductor nanocrystals.[28] The preparation of QD-surface functionalized with azide groups potentially permits the use of chemical coupling based on copper-free strain-promoted azide-alkyne cycloaddition direct onto the nanocrystals.[29]

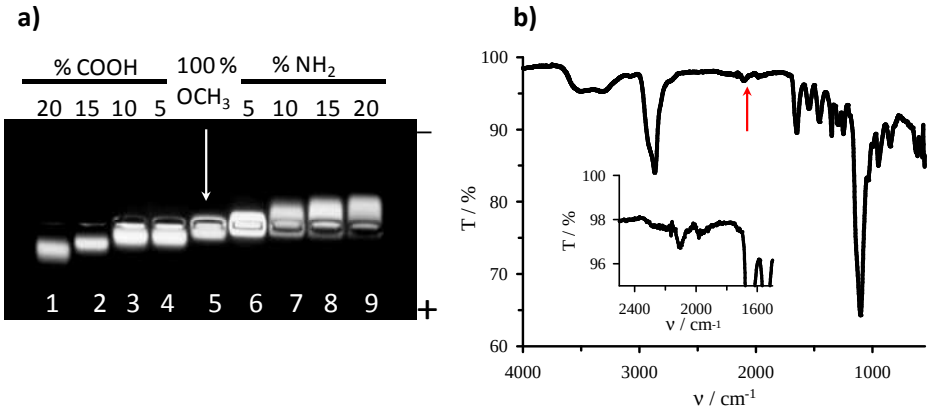

Figure 5.4 (a) Gel electrophoresis image of different QDs suspension bearing a mixture of LA-PEG_{750}-OCH_3/LA-PEG_{600}-NH_2 or LA-PEG_{750}-OCH_3/LA-PEG_{600}-COOH with increasing fraction of end-terminated groups. Lanes 1-4 and 6-9 correspond to QD presenting functional ligands LA-PEG_{600}-COOH and LA-PEG_{600}-NH_2 respectively. A control dispersion of 100% LA-PEG_{750}-OCH_3 is shown in lane 5. (b) FTIR spectra of QDs functionalized with a mixture 85% LA-PEG_{750}-OCH_3 and 15% LA-PEG_{600}-N_3; inset picture shows the azide peak region.

Colloidal stability is a critical point for hydrophilic nanocrystalline materials. We investigated the aggregation property of QD dispersions prepared using the photoinduced phase transfer method and compared with those prepared using $NaBH_4$-reduced ligands.[22] In Figure 5.5a are shown images of several dispersions of green- and orange-emitting QDs in buffer with pH range from 3 to 13 immediately following transfer and after 1 months of storage; DI water is a QD dispersion in just pure de-ionized water. In Figure 5.5b and Figure 5.5c. are also shown pictures of QDs dispersions freshly prepared and after one month of storage containing cell growth media and excess of electrolyte (NaCl 1 M and 2 M), respectively.

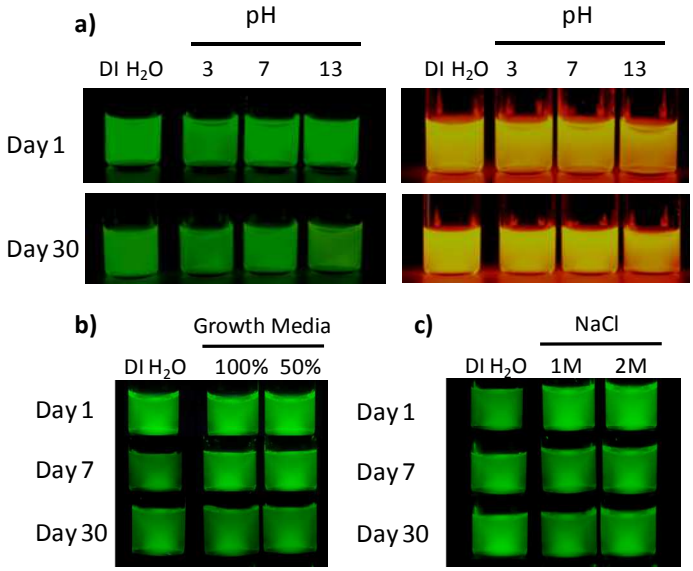

Figure 5.5 (a) Fluorescence pictures of vials containing green (left) and orange (right) emitting QDs (1 μM) dispersed in PBS buffer at varying pH side-by-side with nanocrystals dispersed in pure DI water. (b) Fluorescence pictures of vials containing green-emitting QDs (0.5 μM) dispersed in cell growth media and pure DI water. (c) Fluorescence picture of green-emitting QDs (0.5 μM) dispersed in NaCl solution (1M and 2M) and pure DI water. All the nanocrystals were photocapped with pure LA-PEG_{750}-OCH_3. Day 1 is referred to the freshly prepared samples. The vials were illuminated with hand-held UV lamp (λ=365nm).

An additional stability test (picture not shown) where green-emitting QDs were stored for two months in different pH buffer, electrolyte solution and cell growth media shows a good maintenance of the colloidal properties.[30] These pictures

demonstrated that UV-promoted ligand exchange produces QDs dispersions that are at least as stable as the materials prepared using the conventional DHLA-based route.[20,22]

5.3 Proposed Mechanism

Irradiation in the UV range (300 nm < λ < 400 nm) is a strictly requirement to obtain a stable colloidal suspension in buffer media. Irradiation in the visible range (λ > 400 nm) leads to incomplete phase transfer and the final QDs suspension has poor stability.

In order to investigate the mechanism, UV irradiation of a solution of ligand alone was carried out in 1cm quartz cuvette (Figure 5.6).

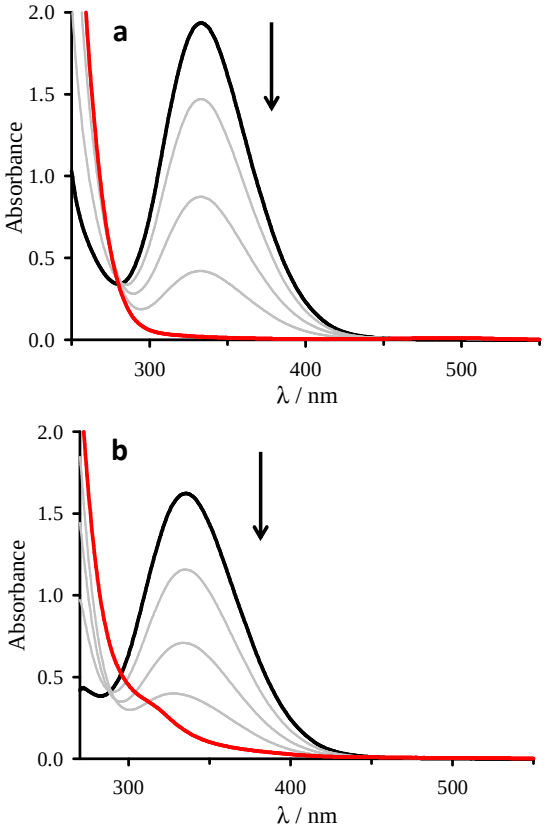

Figure 5.6 Absorption variation during irradiation (λ_{irr}=360 nm, 4.5 mW/cm^2) of 2.2 ml of LA-PEG$_{750}$-OCH$_3$ in (a) methanol (13 mM) and (b) DMF (12 mM). In both cases black line represents the spectra before irradiation and red line after 30 min of irradiation.

Absorption variation during UV irradiation shows the progressive reduction of the band with maximum around 340 nm, indicative of the disappearing of the disulfide bond, as previously reported in literature for lipoic acid in water.[27] This photoreaction can be carried out in different solvents including protic solvents (e.g. methanol, 1-propanol, 2-propanol) and aprotic solvents (e.g. DMF); UV irradiation carried out in an aprotic solvent leads to a slower progression in the absorption peak around 340 nm.

Further evidence of transformation of the disulfide groups to dithiols in the absence of QDs comes from ^{1}H NMR analysis of the ligands following irradiation (Figure 5.7).

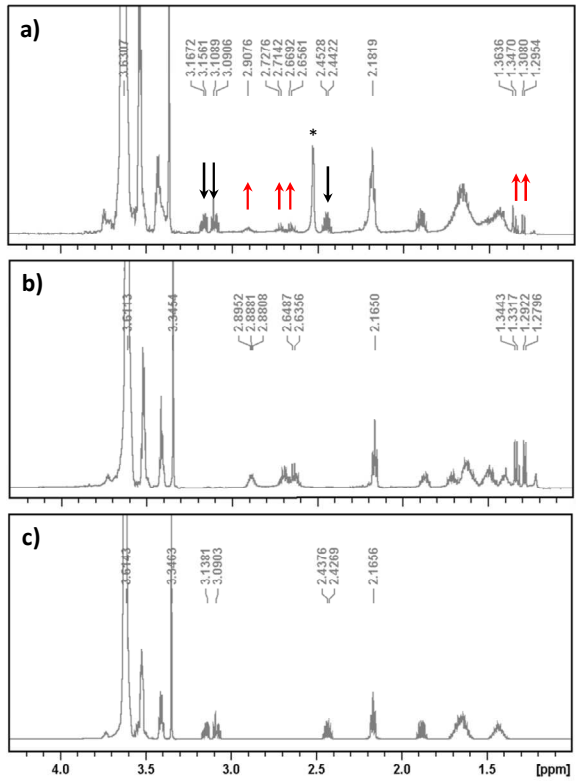

Figure 5.7 ^{1}H NMR spectra collected in $CDCl_3$ from (c) LA-PEG_{750}-OCH_3, (b) $NaBH_4$-reduced LA-PEG_{750}-OCH_3 and (a) UV irradiated (10 min in methanol) LA-PEG_{750}-OCH_3. A mixture of oxidized (LA peaks at 2.4 and 3.0-3.1 ppm, black arrows) and reduced (DHLA peaks at 2.9, 2.7-2.6 ppm and 1.29, 1.36 ppm attributed to thiols, red arrows). The peak at circa 2.5ppm labeled with * comes from impurities.

During irradiation DHLA NMR signals such as the triplet and the doublet at 1.35 and 1.30 ppm and the multiplet at 2.9 and 2.7 ppm appear. The NMR peaks are identical to those obtained for the $NaBH_4$-reduced ligands.[22] These results suggest that LA-based ligands undergo to UV-induced reduction. This process can be potentially accelerated by the presence of QDs. When the semiconductor nanocrystals are in the media they can (1) act as photosensitizers providing excited electrons to enhance the reduction of the ligand (this process may be rather modest because the oxidized ligand is not bound on the QDs surface) and (2) provide a sink for the reaction products because of the preferential binding of the reduced LA to the nanocrystals surface. Since the QD photoexcitation is relatively low due to the low concentration of both QDs and ligand, the driving force for the phase transfer process is probably ascribes to the coupling of the direct ligand reduction and TOP/TOPO cap exchange.

5.4 Fluorescence Imaging of Brian Vasculature of Live Mice

Live animal imaging has demanding requirements for the fluorophore performance and stability. Ideally a fluorescent marker should have high quantum yield, tunable emission, good stability toward degradation and elimination over several hours, well-defined intrinsic partitioning into a particular organ, tissue or cell type and should be amenable to functionalization using facile and diverse chemical methods.
Previous studies shown that CdSe-ZnS are excellent in vivo imaging markers due to the large two photon cross section[6,31] that combined with the use of NIR irradiation two photon fluorescence could allow deep tissue imaging with reduced background.[3]

Quantum dots prepared using the photoinduced phase transfer were successfully used to collect *in vivo* imaging of brain vasculature of mice. Of this material we tested the brightness, the bio-stability and the potential effects on the microbiological environment by imaging the integrity of the QD-labeled brain microvasculature over a period of 24 h. For this application QDs must have limited partitioning into brain tissue, must be small enough to enter brain microcapillarities and must not disrupt the integrity of the blood-brain barrier.

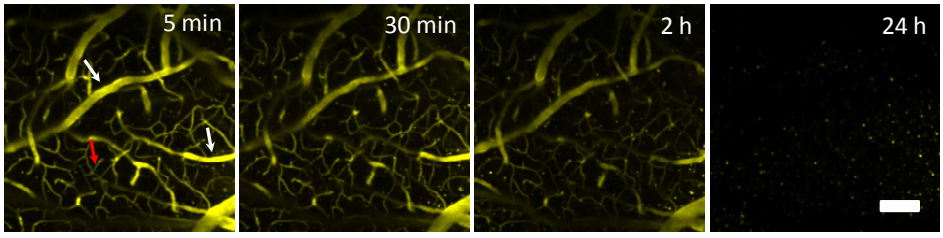

Figure 5.8 Imagines of brain vasculature of cerebral cortex of mice microinjected with QDs phase transferred with pure LA-PEG_{750}-OCH_3. Each panel corresponds to images collected after a given time lapse following QD delivery. Well-resolved structures of the arteriole/venule (white arrow) and capillaries (red arrow) are detected at a depth within 200 μm below the cranial window. No QD aggregation was observed during the imaging time span. The QD signal progressively decreases with time before reaching a background level after 24 h. Scale bar:100 μm.

Two photon fluorescence experiments[30] show well resolved capillary structures with a submicrometer resolution (Figure 5.8). The QDs remained visible in the

blood without any visible self-aggregation or blockage of the microcapillaries up to 2 hours. The signal decreased to background level in 24 h which suggests that no partition into brain tissue happened and QDs were progressively cleared from the blood circulation due to renal filtration.[32] Such long period constitutes a very promising capability as it permits to investigate the integrity of the blood capillaries under different conditions. Moreover the concentration of QDs used to collect these pictures is circa 10% of that used in a previous work to image skin capillaries.[3]

5.5 Conclusion

A new strategy for the effective phase transfer of luminescence nanoparticels was developed. This method involves the use of UV-light to induce the reduction of the di-thiolane ring of the lipoic acid and consequently surface functionalization. Both reactions take place in one-pot without prior reduction of the lipoic acid moiety. Hydrophilic QDs of various size show good colloidal stability and optical properties similar to those with ligands prepared via borohydride reduction.

This method was also successfully applied for the preparation of functional nanocrystals with controllable nature and density of functionality on the surface. The preparation of QD-surface functionalized with azide groups potentially permits the use of chemical coupling based on copper-free strain-promoted azide-alkyne cycloaddition direct onto the nanocrystals. This direct azide functionalization is impossible using the borohydride reagent due to the reduction of the azide functionalities by the reducing agent.

Furthermore we tested the stability of these nanocrystals collecting *in vivo* imaging of brain vasculature of live mice.

References and Notes

(1) Murray, C. B.; Kagan, C. R.; Bawendi, M. G. *Annu. Rev. Mater. Sci.* **2000**, *30*, 545–610.

(2) Talapin, D. V.; Lee, J.-S.; Kovalenko, M. V.; Shevchenko, E. V. *Chem. Rev.* **2010**, *110*, 389–458.

(3) Larson, D. R.; Zipfel, W. R.; Williams, R. M.; Clark, S. W.; Bruchez, M. P.; Wise, F. W.; Webb, W. W. *Science* **2003**, *300*, 1434–1436.

(4) Jaiswal, J. K.; Mattoussi, H.; Mauro, J. M.; Simon, S. M. *Nat. Biotechnol.* **2003**, *21*, 47–51.

(5) Wu, X.; Liu, H.; Liu, J.; Haley, K. N.; Treadway, J. a; Larson, J. P.; Ge, N.; Peale, F.; Bruchez, M. P. *Nat. Biotechnol.* **2003**, *21*, 41–46.

(6) Clapp, A. R.; Pons, T.; Medintz, I. L.; Delehanty, J. B.; Melinger, J. S.; Tiefenbrunn, T.; Dawson, P. E.; Fisher, B. R.; O'Rourke, B.; Mattoussi, H. *Adv. Mater.* **2007**, *19*, 1921–1926.

(7) Bruchez Jr., M.; Moronne, M.; Gin, P.; Weiss, S.; Alivisatos, A. P. *Science* **1998**, *281*, 2013–2016.

(8) Chan, W. C.; Nie, S. M. *Science* **1998**, *281*, 2016–2018.

(9) Medintz, I. L.; Uyeda, H. T.; Goldman, E. R.; Mattoussi, H. *Nat. Mater.* **2005**, *4*, 435–446.
(10) Michalet, X.; Pinaud, F. F.; Bentolila, L. a; Tsay, J. M.; Doose, S.; Li, J. J.; Sundaresan, G.; Wu, a M.; Gambhir, S. S.; Weiss, S. *Science* **2005**, *307*, 538–544.
(11) Zrazhevskiy, P.; Sena, M.; Gao, X. *Chem. Soc. Rev.* **2010**, *39*, 4326–4354.
(12) Pelaz, B.; Jaber, S.; De Aberasturi, D. J.; Wulf, V.; Aida, T.; De la Fuente, J. M.; Feldmann, J.; Gaub, H. E.; Josephson, L.; Kagan, C. R.; Kotov, N. a; Liz-Marzán, L. M.; Mattoussi, H.; Mulvaney, P.; Murray, C. B.; Rogach, A. L.; Weiss, P. S.; Willner, I.; Parak, W. J. *ACS Nano* **2012**, *6*, 8468–8483.
(13) Murray, C. B.; Noms, D. J.; Bawendi, M. G. *J. Am. Chem. Soc.* **1993**, *115*, 8706–8715.
(14) Peng, Z. a; Peng, X. *J. Am. Chem. Soc.* **2001**, *123*, 183–184.
(15) Hines, M. a.; Guyot-Sionnest, P. *J. Phys. Chem.* **1996**, *100*, 468–471.
(16) Peng, X.; Schlamp, M. C.; Kadavanich, A. V; Alivisatos, A. P. *J. Am. Chem. Soc.* **1997**, *119*, 7019–7029.
(17) Dabbousi, B. O.; Mikulec, F. V; Heine, J. R.; Mattoussi, H.; Ober, R.; Jensen, K. F.; Bawendi, M. G. *J. Phys. Chem. B* **1997**, *101*, 9463–9475.
(18) Li, J. J.; Wang, Y. A.; Guo, W.; Keay, J. C.; Mishima, T. D.; Johnson, M. B.; Peng, X. *J. Am. Chem. Soc.* **2003**, *125*, 12567–12575.
(19) Mattoussi, H.; Mauro, J. M.; Goldman, E. R.; Anderson, G. P.; Sundar, V. C.; Mikulec, F. V.; Bawendi, M. G. *J. Am. Chem. Soc.* **2000**, *122*, 12142–12150.
(20) Susumu, K.; Uyeda, H. T.; Medintz, I. L.; Pons, T.; Delehanty, J. B.; Mattoussi, H. *J. Am. Chem. Soc.* **2007**, *129*, 13987–13996.
(21) Susumu, K.; Mei, B. C.; Mattoussi, H. *Nat. Protoc.* **2009**, *4*, 424–436.
(22) Mei, B. C.; Susumu, K.; Medintz, I. L.; Delehanty, J. B.; Mountziaris, T. J.; Mattoussi, H. *J. Mater. Chem.* **2008**, *18*, 4949–4958.
(23) Stewart, M. H.; Susumu, K.; Mei, B. C.; Medintz, I. L.; Delehanty, J. B.; Blanco-Canosa, J. B.; Dawson, P. E.; Mattoussi, H. *J. Am. Chem. Soc.* **2010**, *132*, 9804–9813.
(24) Uyeda, H. T.; Medintz, I. L.; Jaiswal, J. K.; Simon, S. M.; Mattoussi, H. *J. Am. Chem. Soc.* **2005**, *127*, 3870–3878.
(25) Clapp, A. R.; Goldman, E. R.; Mattoussi, H. *Nat. Protoc.* **2006**, *1*, 1258–1266.
(26) Gansalus, I. C.; Barton, L. S.; Gruber, W. *J. Am. Chem. Soc.* **1956**, *78*, 1763–1766.
(27) Bucher, G.; Lu, C.; Sander, W. *ChemPhysChem* **2005**, *6*, 2607–2618.
(28) Zhang, P.; Liu, S.; Gao, D.; Hu, D.; Gong, P.; Sheng, Z.; Deng, J.; Ma, Y.; Cai, L. *J. Am. Chem. Soc.* **2012**, *134*, 8388–8391.
(29) Hao, J.; Huang, L.-L.; Zhang, R.; Wang, H.-Z.; Xie, H.-Y. *Anal. Chem.* **2012**, *84*, 8364–8370.
(30) Palui, G.; Avellini, T.; Zhan, N.; Pan, F.; Gray, D.; Alabugin, I.; Mattoussi, H. *J. Am. Chem. Soc.* **2012**, *134*, 16370–8.
(31) McLaurin, E. J.; Greytak, A. B.; Bawendi, M. G.; Nocera, D. G. *J. Am. Chem. Soc.* **2009**, *131*, 12994–13001.
(32) Choi, H. S.; Liu, W.; Misra, P.; Tanaka, E.; Zimmer, J. P.; Itty Ipe, B.; Bawendi, M. G.; Frangioni, J. V *Nat. Biotechnol.* **2007**, *25*, 1165–1170.

List of Publications

1. Matteo Amelia, Tommaso Avellini, Simone Monaco, Stefania Impellizzeri, Ibrahim Yildiz, Francisco M. Raymo, Alberto Credi

   "Redox properties of CdSe and CdSe-ZnS quantum dots in solution"

   Pure and Applied Chemistry **2011**, *1*, 1-8

2. Tommaso Avellini, Hao Li, Ali Coskun, Gokhan Barin, Ali Trabolsi, Ashish N. Basuray, Sanjeev K. Dey, Alberto Credi, Serena Silvi, J. Fraser Stoddart, Margherita Venturi

   "Photoinduced memory effect in a redox controllable bistable mechanical molecular switch"

   Angewandte Chemie International Edition **2012**, 51, 1611-1615

3. Xin Ji, Goutam Palui, Tommaso Avellini, Hyon Bin Na, Chongyue Yi, Kenneth L. Knappenberger, Jr., Hedi, Mattoussi

   "On the pH-dependent quenching of quantum dot photoluminescence by redox active dopamine"

   Journal of the American Chemical Society **2012**, *134*, 6006-6017

4. Goutam Palui, Tommaso Avellini, Naiqian Zhan, Feng Pan, David Gray, Igor Alabugin, Hedi Mattoussi

   "Photoinduced phase transfer of luminescent quantum dots to polar and aqueous media"

   Journal of the American Chemical Society **2012**, *134*, 16370-16378